Electrodeposition of Nb, Ta, Zr and Cu from Ionic Liquid for Nanocomposites Preparation

LAURA MAIS

Dottorato di Ricerca in Ingegneria Industriale
Università degli Studi di Cagliari
XXVII Ciclo

Electrodeposition of Nb, Ta, Zr and Cu from Ionic Liquid for Nanocomposites Preparation

LAURA MAIS

Supervisor:
Professor Michele MASCIA
University of Cagliari, Italy

Co-supervisors:
Professor Carlos PONCE DE LEON ALBARRAN
University of Southampton, UK

Dottorato di Ricerca in Ingegneria Industriale
Università degli Studi di Cagliari
XXVII Ciclo

Unione europea
Fondo sociale europeo

REGIONE AUTONOMA DELLA SARDEGNA

POR SARDEGNA
obiettivo competitività regionale e occupazione

Laura Mais gratefully acknowledges Sardinia Regional Government for the financial support of her PhD scholarship (P.O.R. Sardegna F.S.E. Operational Programme of the Autonomous Region of Sardinia, European Social Fund 2007-2013 - Axis IV Human Resources, Objective l.3, Line of Activity l.3.1.

This activity is supported by the European Community Framework Programme 7, Multiscale Modelling and Materials by Design of interface-controlled Radiation Damage in Crystalline Materials (RADINTERFACES), under grant agreement n. 263273.

Acknowledgements

First of all, I would like to thank my supervisor, Prof. Michele Mascia, for the possibility of undertaking this PhD, and for his support and advice during these three years at the Department of Mechanical, Chemical Engineering and Materials (DIMCM), University of Cagliari, Italy.

I wish to thank Prof. Annalisa Vacca and Prof. Simonetta Palmas for their support and advices for my research.

I would also like to thank my English supervisor, Prof. Carlos Ponce de Leon Albarran, for his help during my stay at the University of Southampton – Engineering Science (UK).

Thanks to my colleagues at the Department of Mechanical, Chemical Engineering and Materials, for the wonderful time spent together in the office and for being good friends.

Special thanks to Mario for the love and joy he give me during this experience we spent together in our life.

Last, I am grateful to my family, who has always believed in me, and this has permitted me to be what I am, and therefore to reach this important goal.

Contents

Abstract

Multilayer metal materials with nanometric scale are important in modern engineering applications. Composite materials based on metals with different characteristics give rise to new materials with unique properties. Among the others, nanostructured composites constituted by immiscible metals can present interfaces able to control defects produced by high doses of radiation, stress and temperature: their properties can be exploited in nuclear power reactor. Immiscible systems constituted by Cu/Nb or Cu/Ta multilayers exhibit higher thermal stability and improved mechanical properties with respect to bulk Nb, bulk Ta and bulk Cu.

Refractory metals present high melting point, high hardness and high resistance against strong acids and bases. The electrodeposition of these metals presents several limitations: the most important is the very negative deposition potential that makes difficult the deposition of metals such as niobium, tantalum and zirconium. Since both oxygen reduction and hydrogen evolution from water splitting occur at potential values much less cathodic than the metals reduction, at the low potential requested to obtain niobium, tantalum and zirconium in metal form it is necessary the use of electrolytes free of water and oxygen and characterized by high stability in large potential windows. To overcome this limitation, the electrodeposition from molten salts or ionic liquids as solvents have been proposed.

In the present project the electrochemical coating of niobium, tantalum zirconium and copper has been investigated in 1-butyl-1-methylpyrrolidinium bis(trifluoromethylsulfonyl) imide

([BMP][TFSA]) on both boron doped diamond (BDD) and metal substrates in order to determine the reduction path for both single metal and nanometric composites electrodeposition.

Electrochemical experiments have been performed at different temperatures in a glove box, under nitrogen atmosphere. Galvanostatic runs and cyclic voltammograms performed at different scan rates and different potential windows have been carried out in order to determine the behaviour of the systems employed. Potentiostatic experiments were performed at the potential values corresponding to the voltammetric peaks and the samples obtained were analysed by SEM-EDX analyses.

Regarding the electrodeposition of refractory metals nanometric crystallites have been obtained at 125 °C.

Cu/Nb and Cu/Ta composites have been prepared by a dual bath deposition technique; the deposits were constituted by fine crystallites with average sizes in the range 50-100 nm. The elemental maps indicate a different distribution of Cu/Nb and Cu/Ta in the composites obtained with the different substrates.

Chapter 1

Overview of the Thesis

This Chapter starts with the illustration of the motivations which lead us to the development of this Thesis. After that, a summary of the Thesis is given, by showing how it is structured in different Chapters. Finally, a list of publications in journals and conference papers and other activities of the author is presented.

1.1. Motivations

Multilayer metal materials with nanometric size are important in modern engineering applications. Composite materials based on metals with different characteristics give rise to new materials with unique properties. Among the others, nanostructured composites constituted by immiscible metals can present interfaces able to control defects produced by high doses of radiation, stress and temperature: their properties can be exploited in nuclear power reactors, where materials withstanding elevated temperatures and radiation fluxes for long time in a corrosive environment are requested.
Niobium, tantalum and zirconium are so-called refractory metals: they present high melting point, high hardness and high resistance against strong acids and bases.
Thin-film composites of Cu/Nb and Cu/Ta exhibit high thermal stability and mechanical properties; moreover, high radiation damage-resistance of Cu/Nb composites was observed during radiation at room and elevated temperatures. This is of great relevance for materials used in fission and fusion reactors, which may be submitted to higher doses of radiations and may manifest significant damages depending on the types of reactions occurring in the reactor.
Immiscible systems constituted by Cu/Nb or Cu/Ta multilayers exhibit higher thermal stability and improved mechanical properties with respect to bulk Nb, bulk Ta and bulk Cu.

The electrochemistry of refractory metals (IV, V and VI groups) has been widely studied in molten salts to optimize the cathodic deposition process of these metals. Due to their properties, such as high strength and high corrosion resistance, refractory metals are widely used in electronics, optics, sensors, automotive, nuclear and aerospace industries.

Nanoscale composites coatings have been obtained by using several techniques, including electrodeposition, electron-beam evaporation, and magnetron sputtering.

The electrodeposition of refractory metals presents several limitations: the most important is the very negative deposition potential that makes difficult the deposition. Since both oxygen reduction and hydrogen evolution from water splitting occur at potential values much less cathodic than the metals reduction, at the low potential requested to obtain niobium, tantalum and zirconium in metal form it is necessary the use of electrolytes free of water and oxygen and characterized by high stability in large potential windows.

To overcome these limitations, the electrodeposition from molten salts or ionic liquids as solvents have been proposed. Other than industrial processes, such as the Hall-Heroult for alluminium, several case studies are reported in the literature for refractory metals deposition from molten salts. However, despite they have good ionic conductivity and wide potential windows, the main disadvantage is that the metal deposit obtained from these media is dendritic and sometimes powdery. Furthermore, there are severe issues such as corrosion problems in processes with high temperatures. Recently, the use of room temperature ionic liquid (RTIL) has received great attention due to the low operative temperatures and the high potential window of stability: these properties make RTIL ideal solvents in the electrodeposition of refractory metals.

Ionic liquids show good electrical conductivity, high thermal stability and have wide electrochemical windows; their properties allow the direct electrodeposition of crystalline metals and semiconductors at elevated temperatures and, in this context, ionic liquids can be

regarded as the link to molten salts. Ionic liquids give an extension of the area of application of the coatings of refractory metals.

1.2. Activity and results

In the present project the electrochemical deposition of niobium, tantalum and zirconium has been studied using ionic liquids as solvent.

The process has been investigated in 1-butyl-1-methylpyrrolidinium bis(trifluoromethylsulfonyl)imide [BMP][TFSA] on boron doped diamond (BDD) or metal substrates in order to determine the reduction path for either single metal or nanometric composites electrodeposition.

Electrochemical experiments have been performed at different temperatures in a glove box, under nitrogen atmosphere. Galvanostatic runs and cyclic voltammograms performed at different scan rates and different potential windows have been carried out in order to determine the behaviour of the systems. Potentiostatic experiments were performed at the potential values corresponding to the voltammetric peaks and the samples obtained were analysed by SEM-EDX analyses.

Regarding the electrodeposition of refractory metals, nanometric crystallites have been obtained at 125 °C.

Cu/Nb and Cu/Ta composites have been prepared by a dual bath deposition technique; the deposits were constituted by fine crystallites with average sizes in the range 50-100 nm. The elemental maps indicate a different distribution of Cu/Nb and Cu/Ta in the composites obtained with the different substrates.

1.3. Summary

This Thesis is structured in five main chapters subdivided in paragraphs for each topic, in order to allow the reader to better follow the development of the research project. Electrochemical processes and techniques are reported in the Appendix.

A summary of this Thesis is shown in the following list, where a brief description of each chapter is given.

Chapter 2. A general overview of the electrodeposition of refractory metals both in high temperature molten salts and in low temperature molten salts (or ionic liquids) is given, focusing the attention on the properties of ionic liquids. This chapter introduces the reader from the basics of electrodeposition of refractory metals.

Chapter 3. Here, all the procedures to obtain the experimental data used to study the processes investigated are explained as well as all the devices used. The techniques used to characterize the samples obtained are also explained.

Chapter 4. This Chapter shows all the experimental results obtained for refractory metals electrodeposion and for the development of nanocomposites materials, focusing the attention on the use of different substrates as working electrode.

Chapter 5. In this Chapter conclusions are given.

Appendix. This chapter is focused on the electrochemical processes taking place at electrode surface and electrochemical techniques used to investigate the electrochemical behaviour of electrode materials.

1.4. Publications in Journal and Conference Papers

Some of the topics present in this Thesis have been published in international journal papers, national and international congresses/conferences.

International Journal Papers:

A. Vacca, M. Mascia, L. Mais, S. Rizzardini, F. Delogu, S. Palmas, *On the Electrodeposition of Niobium from 1-Butyl-1-Methylpyrrolidinium Bis(trifluoromethylsulfonyl)imide at Conductive Diamond Substrates*, Electrocatalysis (2014) 5:16-22

M. Mascia, A. Vacca, L. Mais, S. Palmas, E. Musu, F. Delogu, *Electrochemical deposition of Cu and Nb from pyrrolidinium based ionic liquid*, Thin Solid Films (2014) 571:325-331

Laura Mais, Michele Mascia, Annalisa Vacca, Simonetta Palmas, Francesco Delogu, *Voltammetric Study on the Behaviour of Refractory Metals in ([BMP][TFSA]) Ionic Liquid*, Chemical Engineering Transactions (2014) 41:97-102

Annalisa Vacca, Michele Mascia, Laura Mais, Francesco Delogu, Simonetta Palmas, Alessandra Pinna, *Electrodeposition of Zirconium from 1-butyl-1-methylpyrrolidinium-bis(trifluoromethylsulfonyl) imide: electrochemical behaviour and reduction pathway*, Materials and Manufacturing Processes, DOI 10.1080/ 10426914.2015.1004698.

Not yet published International Journal Papers:

Laura Mais, Michele Mascia, Annalisa Vacca, Simonetta Palmas, Francesco Delogu, *Electrochemical deposition of Cu/Ta composites*

from pyrrolidinium based ionic liquid [Submitted to "Journal of Applied Electrochemistry"]

National and International Congresses and Conferences:

Laura Mais, Michele Mascia, Annalisa Vacca and Simonetta Palmas, *On the Electrodeposition of Niobium and Copper in a Ionic Liquid for Multilayers Preparation*, ELECTROCHEM 2013, Southampton (UK), September 2013

M. Mascia, A. Vacca, L. Mais, S. Palmas, *On the Electroreduction of Niobium from Ionic Liquid at Different Temperatures*, 64th Annual Meeting of the International Society of Electrochemistry (Mexico), September 2013

M. Mascia, A. Vacca, L. Mais, S. Palmas, *Electrochemical behaviour of Nb, Ta, Zr, and W in pyrrolidinium based ionic liquid*, 64th Annual Meeting of the International Society of Electrochemistry (Mexico), September 2013

M. Mascia, A. Vacca, S. Palmas, L. Mais, S. Rizzardini, F. Delogu, *Electrochemical deposition of Cu and Nb in Pyrrolidinium based Ionic Liquid for Multilayers preparation*, Multilayers'13, Madrid (Spain), October 2013

Laura Mais, Michele Mascia, Annalisa Vacca, Simonetta Palmas, Simone Rizzardini, Francesco Delogu, *On the electroreduction of Tantalum from 1-Butyl-1-Methylpyrrolidinium Bis(trifluoromethylsulfonyl)imide*, XXXV RGERSEQ-1STE^{3}, Burgos (Spain), July 2014

L. Mais, M. Mascia, A. Vacca, S. Palmas, F. Delogu, *Electrodeposition of Nb-Cu and Ta-Cu composites from 1-butyl-1-methylpyrrolidinium bis(trifluoromethylsulfonyl) imide*, 65th

Annual Meeting of the International Society of Electrochemistry, Lausanne (Switzerland), September 2014

L. Mais, M. Mascia, A. Vacca, S. Palmas, F. Delogu, *Voltammetric study on the behaviour of refractory metals in ([BMP][TFSA]) ionic liquid*, 10th European Symposium on Electrochemical Engineering, Chia, Sardinia (Italy), October 2014

In addition to the work presented in this Thesis the author has also participated, during the course of the study, in other research projects:

International Journal Papers:

A. Vacca, M. Mascia, S. Palmas, L. Mais, S. Rizzardini, *On the formation of bromate and chlorate ions during electrolysis with boron doped diamond anode for seawater treatment*, Journal of Chemical Technology and Biotechnology (2013) 88:2244-2251

A.Vacca, M.Mascia, S.Rizzardini, S.Palmas, L.Mais, *Coating of gold substrates with polyaniline through electrografting of aryl diazonium salts*, Electrochimica Acta (2014) 126:81-89

National and International Congresses and Conferences:

M. Mascia, A. Vacca, S. Palmas, A. Da Pozzo, L. Mais, *Trattamento Elettrochimico Per La Rimozione Di Chlorella Vulgaris Con Anodi Di BDD*, GEI-ERA2012, Santa Marina Salina, Messina (Italy), June 2012

S. Palmas, A. Da Pozzo, M. Mascia, A. Vacca, L. Mais, C. Ricci, *Sensibilizzazione Di Nanostrutture Di TiO_2 Con Cumarina,* GEI-ERA2012, Santa Marina Salina, Messina (Italy), June 2012

A. Lallai, L.Mais, *Ruolo del Triton X100 nella biodegradazione del fenantrene,* GRICU 2012, Montesilvano (Italy), September 2012

M. Mascia, A. Vacca, S. Palmas, A. Da Pozzo, L. Mais, *Rimozione di Microalghe Mediante Trattamento Elettrochimico con Anodi di Diamante Conducente*, GRICU 2012, Montesilvano (Italy), September 2012

A. Vacca, M. Mascia, S. Palmas, L. Mais, S. Rizzardini, *Electrochemical preparation of Gold/Polyaniline electrodes through electrografting of diazonium Salts*, GEI2013, Pavia (Italy), September 2013

M. Mascia, A. Vacca, S. Palmas, L. Mais, *Three Dimensional Electrodes For The Removal Of Microalgae From Water*, 9th European Congress of Chemical Engineering, The Hague (The Netherlands), April 2013

Simonetta Palmas, Annalisa Vacca, Michele Mascia, Simone Rizzardini, Laura Mais, Elodia Musu, Esperanza Mena and Javier Llanos, *Synthesis and characterization of ordered TiO_2 nanostructures*, ELECTROCHEM 2013, Southampton (UK), September 2013

P.Ampudia, S.Palmas, A.Vacca, M.Mascia, L.Mais, S.Monasterio, S.Rizzardini, E.Musu, *Systematic investigation on the effect of the synthesis conditions on the performance of nanotubular structured electrodes*, SiO_2 Advanced dielectrics and related devices, X International Symposium, Cagliari (Italy), June 2014

S. Monasterio, F. Dessì, M. Mascia, A. Vacca, S. Palmas, L. Mais, *Electrochemical treatment for the removal of Chlorella Vulgaris*

and Microcystis aeruginosa by using a fixed bed single cell, 65th Annual Meeting of the International Society of Electrochemistry, Lausanne (Switzerland), September 2014

L. Mais, M.J. Martín de Vidales, C. Ponce de León Albarran, *Photoelectrocatalytic oxidation of Methyl Orange with highly ordered TiO_2 nanotubes array*, 10th European Symposium on Electrochemical Engineering, Chia, Sardinia (Italy), October 2014

Chapter 2

Introduction

A general overview of the electrodeposition of refractory metals both in high temperature molten salts and in low temperature molten salts (or ionic liquids) is given, focusing the attention on the properties of ionic liquids. This chapter introduces the reader from the basics of electrodeposition of refractory metals

2.1. Background

Electrodeposition of metals is essential for a variety of industries including electronics, optics, sensors, automotive and aerospace. Due to their physical proprieties such as superconductivity, thermal and mechanical stability, refractory metals are widely used in several application fields. The mechanical properties of refractory metals, such as the excellent corrosion resistance and the nuclear properties of some, make them particular interesting as coatings.

Electrodeposition of metals from a liquid bath containing metal salts is the state of the art in industrial coatings: the technique has shown to be affordable and economically sustainable for very large coatings. Nanoscale composites coatings have been obtained by using several techniques, including electrodeposition [1], electron-beam evaporation, severe plastic deformation [2] and magnetron sputtering [3].

Thin-film composites of Cu/Nb and Cu/Ta exhibit higher thermal stability and mechanical properties with respect to bulk Cu, bulk Nb or bulk Ta. Moreover, high radiation damage-resistance of Cu/Nb composites was observed during radiation at room and elevated temperatures [4] [5].
This is of great relevance for materials used in fission and fusion reactors, which may be submitted to higher doses of radiation and may manifest significant damage depending on the types of reactions occurring in the reactor.

The electrochemical deposition of Cu is currently achieved from aqueous solutions, while the deposition of refractory metals from aqueous media is virtually impossible, due to the wide negative deposition potential. High temperature molten salts are often proposed in literature for electrodeposition of refractory metals although these baths have many technical and economic problems,

such as the loss in the current efficiency, due to the dissolution of metal after its deposition, and corrosion problems at high temperatures. Recently, the use of room temperature ionic liquid (RTIL) has received great attention due to the lower operative temperatures and the high potential window of stability. These properties make RTIL ideal solvents in the electrodeposition of metals.

2.2. Ionic liquids

Since ionic liquids have extraordinary physical properties superior to those of water or organic solvents, they have attracted considerable attention in recent years.

The ionic liquids based on $AlCl_3$ can be regarded as the first generation of ionic liquids. In 1970s and 1980s, Osteryoung *et al.* [6] [7] and Hussey *et al.* [8] [9] carried out extensive research on organic chloride–aluminium chloride ambient temperature ionic liquids and the first major review of room temperature ionic liquids was written by Hussey [10].

The synthesis of air and water stable ionic liquids, which are considered as the second generation of ionic liquids, attracted further interest in the use of ionic liquids in various fields. In 1992, Wilkes and Zaworotko [11] reported the first air and moisture stable ionic liquids based on 1-ethyl-3-methylimidazolium cation with either tetrafluoroborate or hexafluorophosphate as anions. Unlike the chloroaluminate ionic liquids, these ionic liquids could be prepared and safely stored outside of an inert atmosphere. Generally, these ionic liquids are water insensitive, however, the exposure to moisture for a long time can cause some changes in their physical and chemical properties. Ionic liquids based on more hydrophobic anions such as bis-(trifluoromethanesulfonyl) imide and tris-

(trifluoromethanesulfonyl) methide have received extensive attention not only because of their low reactivity with water but also because of their large electrochemical windows [12].
Usually these ionic liquids can be well dried the water contents below 1 ppm under vacuum at temperatures between 100 and 150°C.

Ionic liquids are basically constituted of ions and behave very differently than conventional molecular liquids when they are used as solvents. In contrast to conventional molecular solvents, ionic liquids are usually nonvolatile, non-flammable and less toxic; are good solvents for both organics and inorganics and can be used over a wide temperature range, in fact ionic liquids can be thermally stable up to temperatures of 450 °C [13].
Ionic liquids have reasonably good ionic conductivities compared with those of organic solvents/electrolyte systems (up to ~ 10 mS cm^{-1}); however, at room temperature their conductivities are usually lower than those of concentrated aqueous electrolytes. The conductivity of ionic liquids is inversely linked to their viscosity. Hence, ionic liquids of higher viscosity exhibit lower conductivity. Increasing the temperature increases conductivity and lowers viscosity.

Ionic liquids have been defined to have melting points below 100 °C and most of them are liquid at room temperature. Both cations and anions contribute to the low melting points of ionic liquids. The increase in anion size leads to a decrease in melting point. Cations size and symmetry make an important impact on the melting points of ionic liquids. Large cations and increased asymmetric substitution result in a melting point reduction [14].

Moreover, ionic liquids can have pretty large electrochemical windows, more than 5 V, and hence they give access to elements that cannot be electrodeposited from aqueous or organic solutions.

The electrochemical window is an important property and plays a key role in using ionic liquids in electrodeposition of metals and semiconductors. By definition, the electrochemical window is the electrochemical potential range over which the electrolyte is neither reduced nor oxidized at an electrode. This value determines the electrochemical stability of solvents. As known, the electrodeposition of elements and compounds in water is limited by its low electrochemical window of only about 1.2 V.
In general, the wide electrochemical windows of ionic liquids have opened the door to electrodeposit metals and semiconductors at room temperature which were formerly obtained only from high temperature molten salts. The thermal stability of ionic liquids allows to electrodeposit Ta, Nb, V, Se and presumably many other ones at elevated temperature [14].
Another advantage of ionic liquids is that problems associated with hydrogen ions in conventional protic solvents can be eliminated in ionic liquids because most of the commercially available ionic liquids are aprotic. Therefore ionic liquids, especially air and water stable ones, are considered promising solvents for a wide variety of applications including electrodeposition, batteries, catalysis, separations, and organic synthesis [15].
Nevertheless, they can be used efficiently for the coating of other metals with thin layers of tantalum or aluminium.
In several recent reviews ionic liquids are recommended for electrodeposition [14] [16] [17] [18].

For ionic liquids to be used efficiently, they need not only be economically viable but also simple to handle and recyclable. While it is impractical that ionic liquids will compete with all aqueous solutions in large markets where the current technology works effectively, it is realistic that they should proffer an alternative for the deposition of metals that can only currently be applied using vapour deposition [18].

2.3. Refractory metals

The elements of groups IV, V and VI of the periodic table are called refractory metals due to their high melting points and the refractory nature of their compounds. There are twelve metals with melting points equal to or greater than that of chromium, a temperature which is commonly accepted as the lower melting point limit for defining a refractory metal. Mechanical properties of metals are structure-sensitive; this fact is related to the various types of defects which exist in the crystalline lattice of metals.
They are known for their high melting point, high temperature strength, irradiation damage resistance and excellent corrosion resistance which make them ideal metals for use in the chemical and nuclear industry [19]. In addition, these materials exhibit remarkable resistance to the harshest of chemical environments due to the presence of a tenacious oxide film that forms spontaneously in air.
The nuclear and aerospace industries need materials which can withstand extreme conditions, so that the demand of refractory metals have increased in recent years.

Niobium have high melting point, lower density and low thermal neutron cross-section compared to other refractory metals, which makes niobium useful in atomic reactors. Niobium is highly recommended in nuclear reactors because of its good high temperature creep strength, its resistance to corrosion by liquid sodium-potassium alloys and its outstanding compatibility with nuclear fuels. However, because of the poor oxidation resistance of high temperatures of niobium-base alloys, they must be coated before use in nuclear environments. The corrosion resistance of niobium is similar to, but not quite as good as that of tantalum, being less resistant to very strong acids.

Tantalum has excellent corrosion resistance; this property make it an ideal coating material for components exposed to high temperature

and severe chemical environments [20]. In the nuclear power industry, tantalum is applied in condensers, columns, heat exchangers, helical coils, valve linings and a variety of other components exposed to extremely corrosive fluids [21]. Tantalum thin films exhibit two crystalline phases, body-centered cubic (alpha phase, the bulk structure of tantalum) and a meta-stable tetragonal beta-phase. The structure of deposited thin films is usually the metastable beta-phase or a mixture of the two phases [20].
It has been found that when depositing high quality tantalum films and particularly thicker coatings using molten salts [22], the beta-phase dominates the deposits on most substrates under most processing conditions [23]. The metastable beta-phase converts to the alpha-phase upon heating to 750 ˚C, but annealing of the deposited film to this temperature would adversely affect the properties of a heat treated substrate [24]. For this reason, deposition of tantalum on substrates at high temperatures is not suitable. Therefore, it is preferred to electroplate refractory metals, such as tantalum using ionic liquids, a process that can be carried out at significantly lower temperatures compared to other plating processes.

Zirconium metal has a low absorption cross-section for thermal neutrons, which makes it ideal for nuclear energy uses; this metal has strong corrosion-resistance properties as well as the ability to confine fission fragments and neutrons so that thermal or slow neutrons are not absorbed and wasted, thus improving the efficiency of the nuclear reactor. The use of zirconium in the construction of nuclear fuel elements and other structural components in reactor cores meets many physical and technological requirements essential for the nuclear industry [25].

2.4. Refractory metals deposition in high temperature molten salts

The electrolysis of molten salts permits pure, plastic, nonporous, and coherent layers of refractory metals to be coated on substrates of complex configuration and large size.

The mechanism of the electrodeposition of refractory metals is not yet fully elucidated. Senderoff and Mellors [26] developed a general process for the electrodeposition of eight of the nine refractory metals of groups IV, V and VI as dense coherent deposits by using a solution of the refractory metal in a molten alkali-fluoride eutectic mixture from 680 °C to 800 °C. They concluded that an irreversible metal-producing step is a necessary (though not sufficient) condition for the deposition of coherent deposits from molten salts.

Inman and White [27] have summarized in a review the electrochemistry of refractory metals in molten salts electrolytes. The authors have reported that the recovery of a primary metal is ensured by using, as solvent, a melt having a much larger decomposition voltage than that of the solute and an inert cathode; controlling the electrodeposition of metal by rate processes other than mass transfer, will lead to coherent deposits.

Few years later, Girginov et al. [28] have presented a selective review of the anodic and cathodic processes of Ti, Zr, Nb and Ta from molten salts-based electrolytes in order to investigate the optimization of cathodic deposition of these metals highlighting that the two main types of electrolyte employed in the electrodeposition of refractory metals were chloride and fluoride based.

Despite molten salts have large electrochemical windows, good heat capacity, can attain very high temperatures and conduct electricity, the extreme operating conditions limit the variety of substrates used

for the refractory metals electrodeposition and allow to such technical and economical problems as the loss in the current efficiency and corrosion problems at high temperatures. Thus, the electrodeposition of refractory metals from ionic liquid at low temperatures represents a valid alternative to the use of high-temperature molten salts.

The first result on the electrodeposition of coherent, dense deposits of refractory metals using mixtures of alkali metal fluorides have been reported by Mellors and Senderoff [29]. To obtain deposits of niobium they used eutectic composition of KF-LiF and KF-NaF as a solvent and NbF_5 as a source of Nb at temperature of about 775 °C obtaining columnar structure of electrodeposits.

The metallic Nb obtained from electrodeposition processes carried out by employing molten LiF-KF-K_2NbF_7 baths at temperatures between 650 °C and 850 °C exhibited the necessary purity for its use in the preparation of superconducting tapes, in the nuclear technology and in metallurgy [30].

The influence of temperature on Nb plating using LiCl-KCl and NaCl-KCl melts was studied by Gillersberg *et al*: at temperatures below 550 °C no coherent layer was obtained, at temperatures between 550 °C and 650 °C the Nb layers were highly heterogeneous, and characterized by many undesired inclusions. Finally, at a temperature of 750 °C homogeneous layers of metallic Nb were deposited [31].

The Ta(V) reduction has been studied in a wide range of melts, such as chlorine or fluorine melts.

In FLINAK-K_2TaF_7 Polyakova *et al.* [32] have studied the nature of the tantalum reduction process at 710 °C using various working electrodes, such as molybdenum, platinum and silver; the authors affirm that the cyclic voltammograms shape were not reproducible

and electrochemically TaF_7^{2-} is reduced to tantalum metal in a single quasi-reversible five-electron step.

In LiF-NaF-K_2TaF_7 with low oxygen contents on Ag electrode, Chamelot *et al.* [33] recorded a single peak in the reduction sense associated with one reoxidation peak on the reverse scan. The reduction peak reveals the one-step reaction involving pentavalent and zerovalen tantalum at 800 °C.

In chloride electrolytes [28] suggest that the electrodeposition of microcrystalline Ta took place in a narrow potential range in chloride melts and confirmed a single step mechanism in NaCl-KCl-K_2TaF_7 melts.

The effect of fluoride ions on the reduction of zirconium has been studied by Guang-Sen *et al.* [34] in fluoride-chloride melts: the voltammetric behaviour of zirconium at 973 K and 1033 K in equimolar KCl-NaCl with $ZrCl_4$ on a platinum electrode showed that the electroreduction process of Zr is reversible. According to the number of electrons exchanged, the authors established that the process has double two-electron steps: Zr(IV)/Zr(II) and Zr(II)/Zr. The cathodic reduction of Zr(IV), in the same electrolytic bath, was also studied with different concentrations of KF: a new peak appeared when small amount of KF ($X_{F^-}/X_{Zr^{4+}}$= 1.07) were added into equimolar KCl-NaCl melts with $ZrCl_4$. The currents at peaks related to Zr(IV)/Zr(II) and Zr(II)/Zr reduction decreased as the ratio ($X_{F^-}/X_{Zr^{4+}}$) in the melts increased. The authors have concluded that the new peak recorded in the presence of KF represents the main reduction of Zr when the ratio $X_{F^-}/X_{Zr^{4+}} \geq 6$.

Kawase and Ito [35] have studied the voltammetric behaviour on Ni electrode in the solution obtained after the anodic dissolution of Zr in the LiCl-KCl eutectic. Cyclic voltammograms reveal that Zr(II) and Zr(IV) can exist in molten salts between 450 and 550 °C and the ratio of Zr(II)/Zr(IV) increases with increasing temperature. At 450 °C

only one cathodic peak related to Zr(IV)/Zr(II) is observed, while at 550 °C two cathodic peaks, related to the reduction of Zr(IV)/Zr(II) and Zr(II)/Zr, are observed.

The electroreduction process of Zr(IV) was studied by Chen *et al.* [36] at molybdenum electrode in LiCl-KCl-K_2ZrF_6 molten salts at 923 K; the authors highlighted that Zr(IV) was reduced to Zr metal by a two-step mechanism corresponding to the Zr(IV)/Zr(II) and Zr(II)/Zr transitions. Furthermore, the cathodic peaks are not dependent on the sweep rate so it has been concluded that the reduction process of Zr(II)/Zr and Zr(IV)/Zr(II) are both reversible (or quasi-reversible).

Analogous behaviour has been reported by Wu *et al.* [37] that studied the electrochemical reduction of Zr(IV) on Pt electrode at 1023 K in NaCl-KCl-K_2ZrF_6 molten salt; two cathodic reduction peaks related to Zr(IV)/Zr(II) and Zr(II)/Zr steps were observed in the potential range from 0 to –1.6 V vs. Ag/AgCl. The authors thus observed a two-electron transfer process involving the formation of Zr(II).

On the other hand, Groult *et al.* [38] studied the electrochemical behaviour of Zr(IV) in potassium-free fused alkali fluorides in the temperature range of 773-1123 K by using either tungsten or molybdenum electrodes, and observed a single well-defined oxido-reduction wave, and concluded that the reduction of Zr(IV) is a single four-electron reversible step controlled by diffusion process.

A detailed electrochemical study of the molten LiF-CaF_2-ZrF_4 system is provided in the 810-920 °C temperature range by Gibilaro *et al.* [39] on an inert Ta electrode. The authors have reported that at 840 °C a single peak is observed in the cathodic run associated with a stripping peak; the reduction mechanism was a one step process exchanging four electrons and controlled by the Zr ions diffusion in the molten salt.

2.5. Refractory metals deposition in ionic liquids

Few data on the electrochemistry of refractory metals in ionic liquids can be found in literature.

The electrodeposition of Nb from low temperature ionic liquids was investigated by Babushkina *et al.* [40]; the authors obtained a relatively detailed picture of the electrochemical behaviour of $NbCl_5$ in 1-butyl-1-methylpyrrolidinium chloride by using electrochemical studies and Raman spectroscopic measurements. Several similarities were found with the behaviour obtained for fused alkali metal solvents, so that the authors concluded that high temperature molten salts and ionic liquids may be considered as "two sides of the same coin". However, metallic Nb deposits were not obtained under the adopted conditions.

Zein El Abedin *et al.* [41] have shown the differences on the electrochemical behaviour of [BMP][TFSA] ionic liquid with different concentrations of TaF_5 either in presence or absence of LiF on platinum electrode; cyclic voltammograms clearly indicate that three reduction peaks appear in the presence of LiF while only two reduction peaks, correlated to the electrolytic reduction of Ta(V) to Ta(III) and to the reduction of Ta(III) to Ta(0), have been recorded without LiF addition.

The two-step reduction mechanism of Ta(V) was confirmed few years later by Borisenko *et al.* [21] that studied the electrochemical behaviour of TaF_5 in $[Py_{1,4}]$TFSA on Au(111) at 25 °C.

The electrochemical behaviour of Ta(V) chloride and oxochloride species has been also studied by Babushkina and Ekres [42] in $Pyr_{14}Cl$ ionic liquid: the authors reported that the mechanism of the electrochemical reduction of Ta(V) depends strongly on the composition of the electrolytic bath.

Few data on the electrochemistry of Zr(IV) using room temperature ionic liquids as solvent has been hitherto reported in the literature. Tsuda *et al.* obtained Al-Zr alloys working with aluminium chloride-1-ethyl-3-methylimidazolium chloride molten salt at 353 K [43]; however, the reduction process was complicated by the formation of insoluble $ZrCl_3$.

More recently Compton *et al.* studied the electrochemistry of $ZrCl_4$ in N-Butyl-N-methylpyrrolidinium- bis(trifluoromethylsulfonyl) imide at 25°C [44]: as in the case of chloroaluminate molten salts, the reduction of zirconium in pyrrolidinium-based ionic liquid was complicated by the formation of Zr(III). Moreover, the authors highlighted the interesting use of $ZrCl_4$ as dry agent for ionic liquid due to the formation of insoluble $ZrCl_2O$ by hydrolysis of zirconium chloride in the presence of water in the solvent.

Chapter 3

Materials and methods

Here, all the procedures to obtain the experimental data used to study the processes investigated is explained as well as all the devices used. The techniques used to characterize the samples obtained are also explained.

3.1. Experimental methods

3.1.1. Materials and Chemicals

The air and water stable ionic liquid 1-butyl-1-methylpyrrolidinium bis(trifluoromethylsulfonyl)imide [BMP][TFSA], NaF (99.99 %), LiF (99.99 %), NbF_5 (98 %), TaF_5 (98 %) and ZrF_4 (99.9 %) were purchased from Aldrich.

The purity of the ionic liquid given by the supplier is ≥ 98.5 %. The presence of impurities in commercial ionic liquids (even in ultrapure quality) can alter the deposition process in initial stages, leading to misinterpretation of the surface processes [21]. Prior to use, ionic liquid was dried at 125 °C for 24 h under stirring in order to remove water content and stored in a nitrogen filled glove box (Sicco).

Different substrates, such as silicon coated with boron doped diamond (Si/BDD, electrode area 0.7 cm^2) purchased from Neocoat (Switzerland), niobium foils (thickness 0.25 mm, 99.8%, Aldrich), tantalum foils (thickness 0.25 mm, 99.9%, Aldrich), polycrystalline gold foils (thickness 0.25 mm, 99.9%, Aldrich) and copper foils (thickness 0.25 mm, 99.98%, Aldrich) were used as working electrode materials (electrode area 0.6 cm^2). The high electrochemical stability of diamond electrodes, compared to conventional electrode materials, under several conditions makes these materials of particular interest. Boron doped diamond electrodes have some other advantages such as high electrochemical reproducibility and high thermal stability.

Prior to use metallic working electrodes were cleaned for 10 minutes in an ultrasonic bath in acetone. A platinum sheet and a platinum wire were used as counter and quasi reference-electrodes, respectively. From an electrochemical point of view a Pt quasi-reference electrode is definitely not a perfect one, but it has the advantage that avoids all type of contamination.

3.1.2. Electrochemical set-up

All electrochemical experiments were performed at fixed temperature ranging from R.T. to 200 °C in the nitrogen filled glove box as shown in Figure 1.

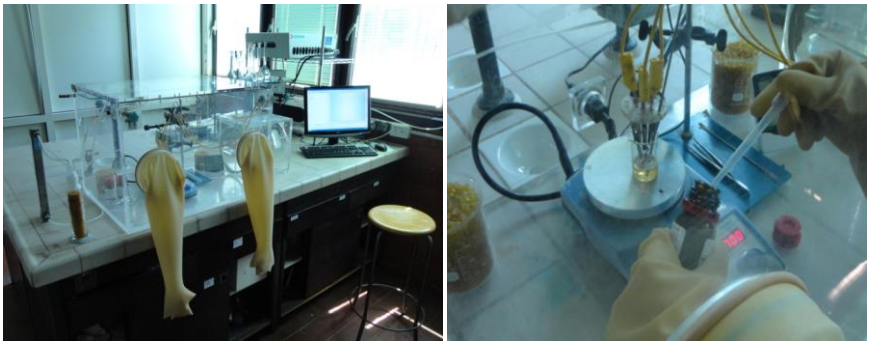

Figure 1: *Nitrogen filled glove box in which all experiments were performed.*

The typical three electrode cell consisted of a pyrex cylindrical beaker equipped with a counter electrode with an area of 0.8 cm^2 immersed in solution, a quasi-reference electrode with an area of 0.15 cm^2 immersed in solution and a working electrode (surface area dependent on the substrate used).

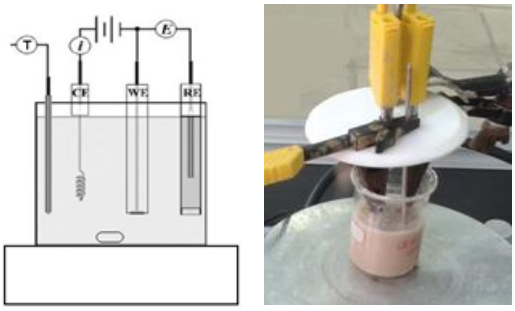

Figure 2: *The three electrode cell used for all electrochemical experiments.*

The solutions were prepared by adding either NaF or LiF to the ionic liquid up to a concentration of 0.25 M and stirred until dissolved

maintaining the resulting electrolytic bath at 125 °C for 24 h. The solution containing either sodium fluoride or lithium fluoride salts was characterized by cyclic voltammetries before the addition of metal salts. NbF_5, TaF_5 and ZrF_4 were dissolved in a concentration of 0.25 M and the electrolytic bath was maintained at 125 °C for 24 h under stirring and again characterized by cyclic voltammetries. It was observed that the metal salts were not completely dissolved in the liquid and a partial residue of the salt was seen at the bottom of the solution. Copper ions were introduced in [BMP][TFSA] ionic liquid containing LiF (0.25 M) by oxidation of a copper sheet (Aldrich, 99.98%) in a divided cell a fixed potential of 0.1 V vs. Pt. During the copper dissolution the solution was maintained at 125°C and magnetically stirred.

3.2. Electrochemistry

3.2.1. Cyclic voltammetry

Electrochemical measurements were carried out using a Metrohm Autolab 302N potentiostat-galvanostat controlled by NOVA software (Metrohm, Switzerland).

Cyclic voltammetries were started from the open circuit potential (OCP) in the negative direction at different potential windows, different scan rates and different temperatures. In order to avoid ion concentration gradients in the electrolyte, the ionic solution was magnetically stirred prior to each scan.

Figure 3: *Metrohm Autolab 302N potentiostat-galvanostat controlled by NOVA software (Metrohm, Switzerland).*

3.2.2. Pre-electrolysis process

Cyclic voltammetry was performed on the dried ionic liquid to study its electrochemical behaviour. In order to reduce residual water active in solution, potentiostatic experiments were performed by using a titanium grid coated with platinum electrode fixing the potential at -2 V for 7000 s. The ionic liquid treatment was conducted inside the glove box under nitrogen atmosphere. A cyclic scan was then performed to compare the electrochemical behaviour before and after the potential hold in the liquid.

3.2.3. Electrodeposition process

Upon purification of the ionic liquid, indicated by extremely low currents in the *i-t* curve, either LiF (0.25 M) or NaF (0.25 M) were added to the ionic liquid and stirred until dissolved at 125 ˚C. Then 0.25 M of metal salt was added into the solution and stirred until mostly dissolved. The solution was then left in the glove box overnight to settle and allow any further dissolution of the powders to occur.

Potentiostatic experiments were performed at different potential values, determined in the cathodic scan of the voltammogram, to test the deposition conditions; the potential was kept at fixed value under stirring. Potentiostatic scans were repeated at different potentials

until deposition was observed. After the electrodeposition tests the samples were washed in isopropanol and boiled in distilled water for 15 minutes to remove the residual ionic liquid.

3.3. Surface and structure analysis

Different analytical techniques, such as scanning electron microscopy, energy dispersive X-ray analysis and X-ray diffraction were used to analyse the electrodeposited layers on the substrate.

3.3.1. Scanning electron microscopy

A high resolution Scanning Electron Microscopy (SEM) equipped with Energy Dispersive X-Ray (EDX) detector (Zeiss, Germany) was employed to investigate the surface morphology of the deposited films and to obtain information on the elements present on the deposited layers.

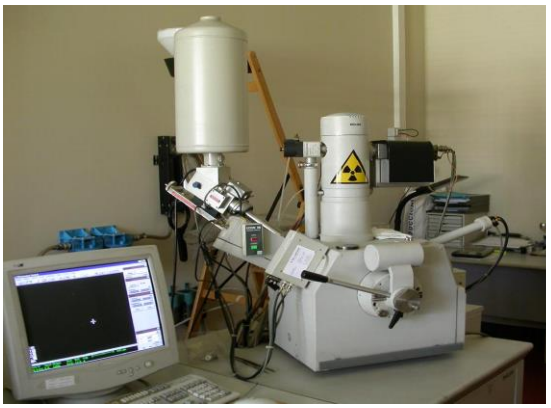

Figure 4: *Scanning Electron Microscopy (SEM) equipped with Energy Dispersive X-Ray (EDX) detector (Zeiss, Germany).*

The EDX analyses were performed usually for every sample at four magnifications. Point analyses were also performed for some representative layers. Focused ion beam (FIB) was used to very precise cross-sections of a sample for subsequent imaging via SEM.

3.3.2. X-Ray diffraction

XRD patterns were collected with a Miniflex II Rigaku diffractometer, equipped with Cu Kα radiation, over a range of scattering angle 2θ from 20° to 70°. Discrete angular displacements of 0.01° and acquisition times of 1 min were used. The XRD patterns were analysed according to the Rietveld method.
The best fitting of the experimental XRD profiles with a set of mathematical functions provided information on the relative amounts of the deposited phases, as well as on their microstructure [45]. The average size of the coherent diffraction domains and their average total strain content were estimated under the assumption of isotropic size and strain content [45].

Chapter 4

Results and discussion

This Chapter shows all the experimental results obtained for refractory metals electrodeposition and for the development of nanocomposites materials, focusing the attention on the use of different substrates as working electrode.

4.1. Introduction

Electrochemical conditions and purity of ionic liquid are key factors in controlling the electrodeposition of refractory metals. The pre-electrolysis treatment implemented in order to remove the water impurities from the liquid is discussed below. Than the electrochemical conditions investigated for electrodeposition of metals and the microstructure analysis of the electrodeposited layers are presented.

4.1.1. Treatment of Ionic Liquid

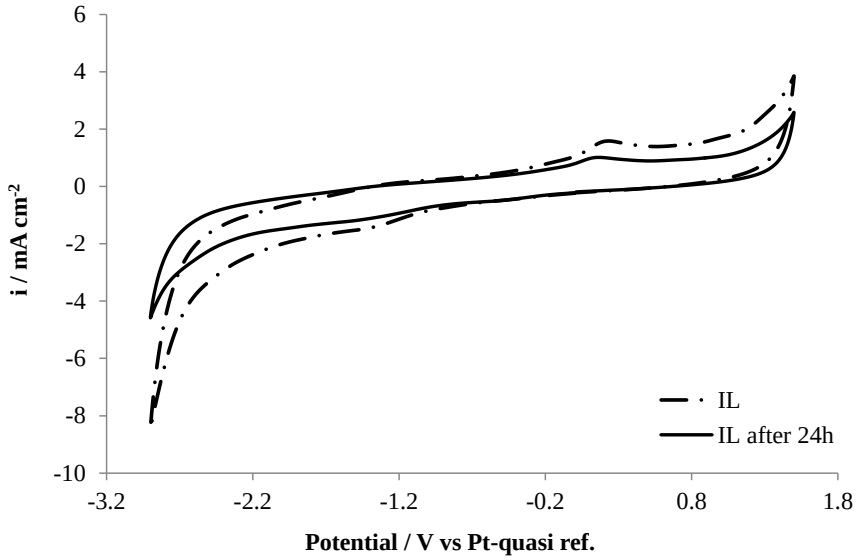

Figure 5: *Cyclic voltammetries of pure ionic liquid recorded on BDD electrode before and after heat treatment at 125°C (scan rate 100 mV/s).*

Impurities in ionic liquids can strongly alter the deposition process in initial stages leading to the misinterpretation of the surface processes. Consequently, the as-received low-purity ionic liquid, 1-butyl-1-methyl-pyrrolidinium bis(trifluoromethylsulfonyl)imide was

purified before to start the investigation of the behaviour of the system.

Figure 5 shows the voltammetric behaviour of pure ionic liquid at 125 °C, as-received and after 24 h at 125 °C; BDD was used as cathode. The ionic liquid exhibits a wide electrochemical window of stability (4.5 V) where the degradation of the anion and cation constituting the ionic liquid does not occur.
The anodic peak centred at about 0.5 V could be related to the presence of impurities: halides or monovalent ions (K^+, Na^+) are often detected in commercial ionic liquids, even of ultrapure quality [21]; moreover, it is difficult to completely avoid contamination of moisture and oxygen. By extending the potential range from -3.2 to 2.5 V an increase in the current density was observed in the cathodic and anodic limits probably due to the irreversible reduction of the [BMP] and the [TFSA] oxidation: under these extreme conditions the original white colour of the ionic liquid changed to dark-brown.

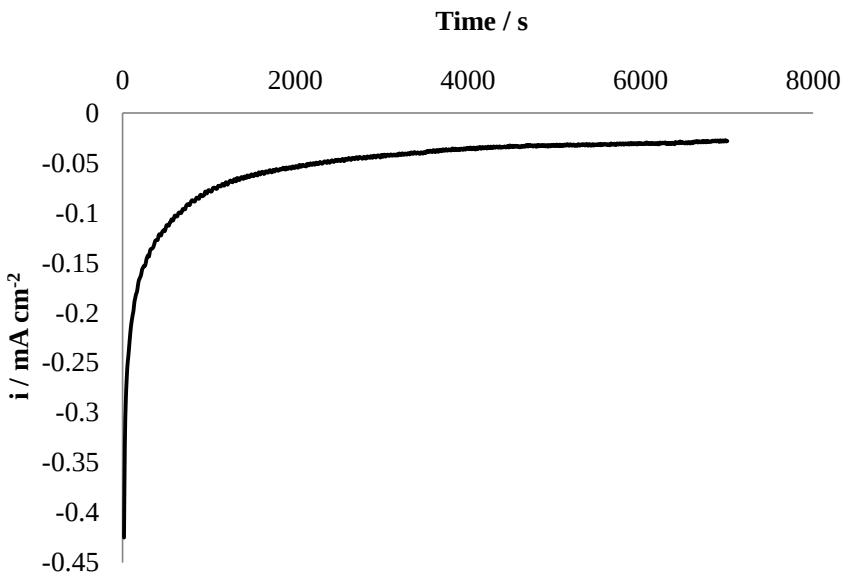

Figure 6: *Decreasing trend of end current densities during the electrolysis process indicating that impurities are being extracted from the liquid.*

Since one of the known impurities was water, the as-received ionic liquid was dried inside the glove box under nitrogen atmosphere to remove as much water as possible from the ionic liquid. The corresponding curve after drying the ionic liquid, submitted to an electrolysis process for 7000 s, is shown in Figure 6.

Theoretically pure ionic liquid should have no current running through it, resulting in a linear curve as it is free of impurities. However, from Figure 7 it is possible to observe that the ionic liquid purchased for this present study has an end current density of approximately 0.8 $mA \cdot cm^{-2}$, indicating that the ionic liquid is not pure, containing some impurities. A significant increase in current density can be seen through the ionic liquid, which is probably due to water reduction or impurities. The exact impurities in the ionic liquid are unknown.

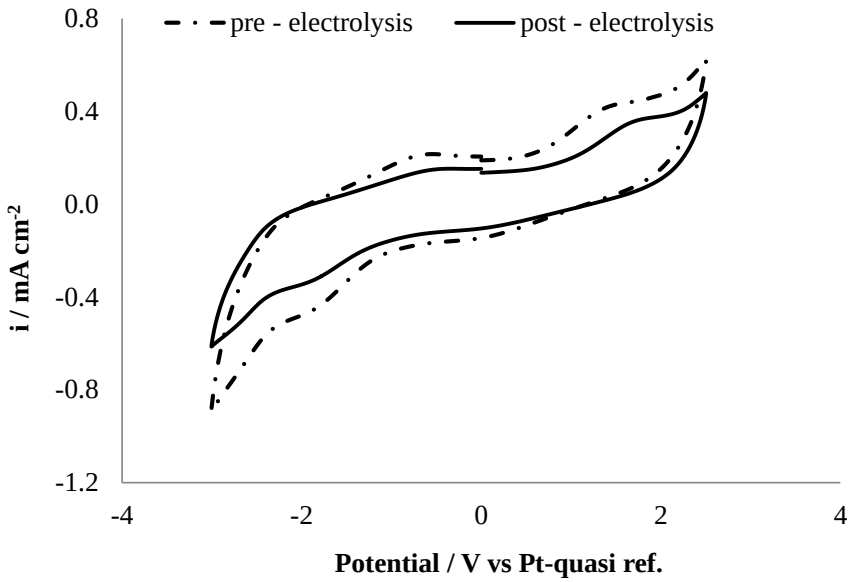

Figure 7: *Cyclic voltammetry before and after pre-electrolysis process (scan rate 100 mV/s).*

Cyclic voltammetries were recorded before and after the electrochemical treatment to determine the purity level of the as-received ionic liquid.

Figure 7 shows that the current density decreases after the electrolysis process highlighting the reduction of residual water active in solution. It is evident that there is some current flowing through the ionic liquid, however not as high as the current observed in the as-received ionic liquid. This suggests that the water was not entirely removed and the difficulty of drying the liquid.

4.2. Electrochemical deposition of niobium

After purification, either NaF or LiF were added to the IL up to a concentration of 0.25 M.

Using high temperature molten salts as electrolyte it was found that the addition of fluorides of alkali melts, such as NaF and LiF to the electrolytic bath facilitates the electrodeposition of refractory metals and improves the quality of the deposit obtained [41].

4.2.1. Boron doped diamond substrate

Figure 8 shows the cyclic voltammograms at different temperatures of [BMP][TFSA] containing 0.25 M LiF and 0.25 M NbF_5 at BDD electrode at a scan rate of 100 mV/s. The electrode potential was swept initially from the OCP to more negative potentials. The voltammograms exhibit a different behaviour with increased temperature: the peak potentials of the cathodic peaks slightly move to less negative values. The peak currents of the cathodic and anodic branch significantly increase with rising temperature; the mobility of

the electroactive species towards the electrode surface increases leading to increasing the reduction and oxidation reaction rate [41].

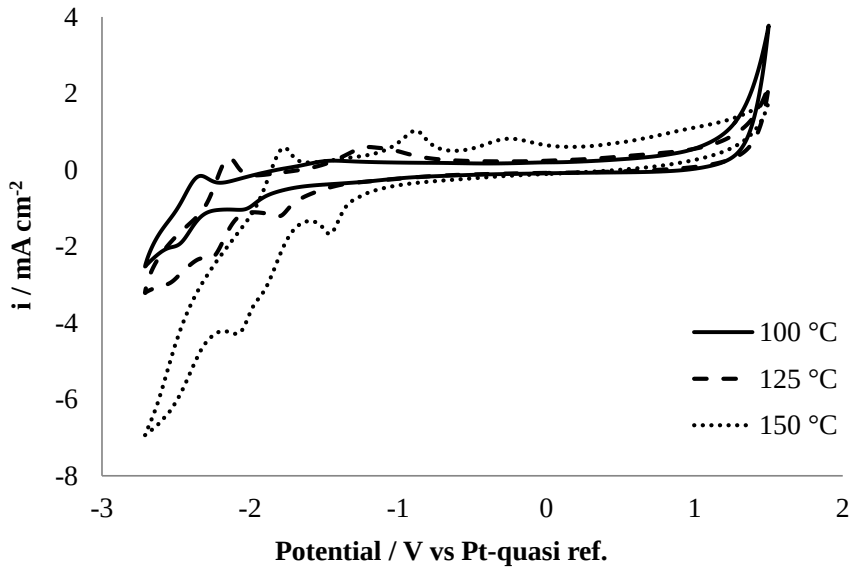

Figure 8: *Cyclic voltammograms of 0.25 M NbF_5 and 0.25 M LiF in [BMP][TFSA] ionic liquid at different temperatures (scan rate 100 mV/s).*

An increase of the temperature above 150 °C leads to significant change of the kinetics of the electrochemical processes, but can also provoke the destruction of the structure of ionic liquid [42]. Subsequent experimental tests have been conducted at 125 °C: this is a good compromise to have high conductivity and solubility of metal salts and to avoid extreme operating conditions.

Figure 9 shows the cyclic voltammograms of ionic liquid containing 0.25 M NaF and 0.25 M NbF_5 at BDD electrode at different scan rates. The electrode potential was scanned from the open circuit potential in the negative direction down to -2.8 V while the anodic scan was up to 1.5 V. Three reduction waves can be observed in the cathodic scan at -1.1 V, -1.7 V and -2.2 V, while in the backward scan two less defined oxidation waves appear at -1.6 V and 0.5 V.

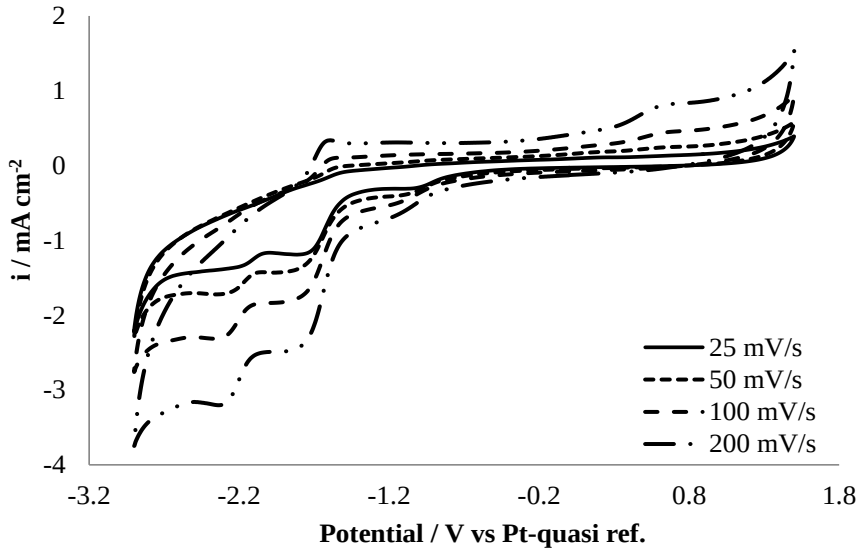

Figure 9: *Cyclic voltammograms at different scan rates of [BMP][TFSA] containing 0.25 M NbF_5 and 0.25 M NaF at BDD electrode at 125 °C.*

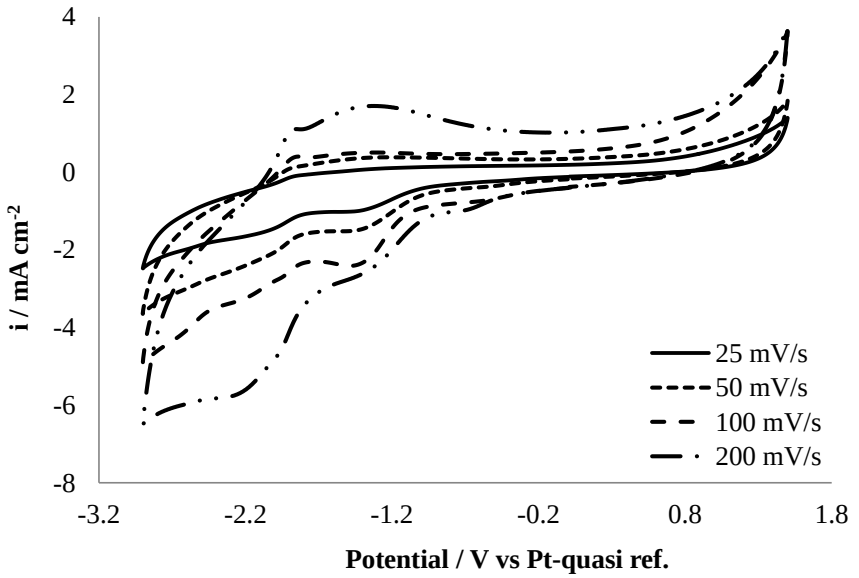

Figure 10: *Cyclic voltammograms at different scan rates of [BMP][TFSA] containing 0.25 M NbF_5 and 0.25 M LiF at BDD electrode at 125 °C.*

Analogous features were observed in the cathodic scan by using LiF instead of NaF (see Figure 10): the first and the second cathodic peaks are shifted to -0.68 V and -1.3 V respectively, while the third cathodic peak remains centred at -2.2 V. In the reverse scan two not well resolved peaks are present, which can be better analysed by decreasing the cathodic stop potential in the cyclic voltammetries.
As can be seen from Figure 11, if the reduction scan is stopped at -2.3 V the oxidation peak at -1.9 V is still present while stopping the cathodic scan at -2.0 V, it does not appear in the voltammogram but only the oxidation peak at around -1.1 V is observed.

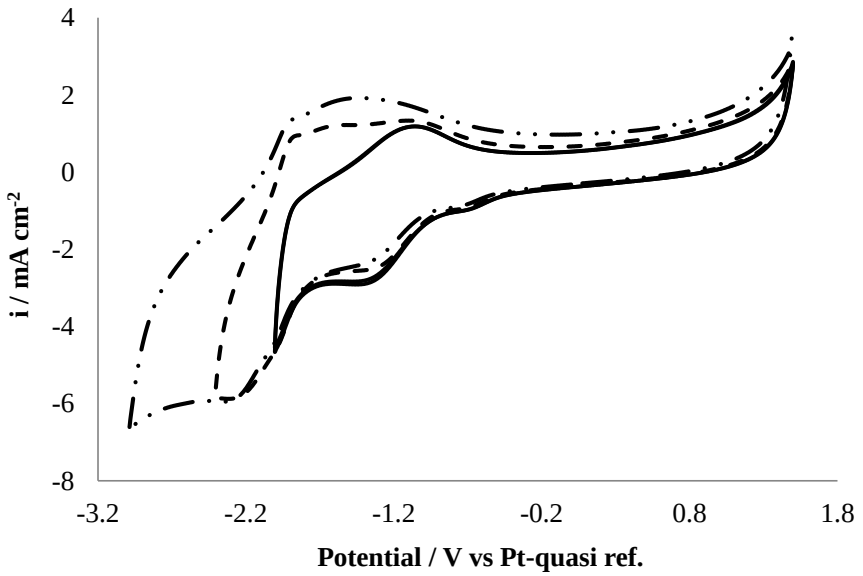

Figure 11: *Cyclic voltammograms of [BMP][TFSA] containing 0.25 M NbF_5 and 0.25 M LiF at BDD electrode at 125° C obtained at different stop potentials (scan rate 200 mV/s).*

A three steps mechanism can be than proposed for Nb(V) electroreduction.

The Nb(V) reduction has been widely studied in molten salts with different eutectic compositions. Kuznetsov [46] evidenced a three

step reduction involving Nb(V), Nb(IV) and Nb(II) at temperature below 630 °C using LiCl-KCl-$NbCl_5$ as electrolytic bath: the formation of Nb(II) allowed to the formation of insoluble subhalide cluster compounds which affected the metal deposition. Different composition of the melt and temperature of the bath can lead to metal deposition: the formation of Nb(II) was suppressed by working at temperature higher than 650 °C, while introducing fluoride ions had a beneficial effect on the quality of the Nb deposit and stabilized the higher oxidation states.
A two-step mechanism Nb(V) <=> Nb(IV) <=> Nb(0) was proposed in NaCl-KCl-K_2NbF_7 mixture along with the formation of a thin film of Nb carbide (NbC and Nb_2C) when carbon based electrodes were used [47]. Nb has a strong affinity for carbon, which acts as a depolarizer for the reduction reaction, so that the formation of a first layer of carbides with thickness of few atoms cannot be avoided [45]. Babushkina *et al.* studied the voltammetric behaviour of Nb(V) in 1-butyl-1-methyl-pyrrolidinium chloride at low temperatures with Raman spectroscopy: although metallic Nb has not been obtained, the authors demonstrated many similarities with the behaviour obtained in high temperature molten salts. In particular, the different steps of reduction involving Nb(V), Nb(IV) and Nb(III) chloride complexes were analogous to these observed during Nb reduction in chloride molten salts [40].

In order to individuate the reduction steps and the possible mechanism of Nb(V) deposition at BDD electrodes, a set of potentiostatic experiments was performed fixing the potential at the peak values determined in the cathodic scan of the cyclic voltammetries, and it was imposed for 1 h under stirring conditions. Figure 12 shows the SEM micrograph for the sample obtained fixing the potential at -1.5 V along with the corresponding EDX analysis; a black deposit was visible also with the naked eye; SEM pictures of this sample reveal the presence of a layer on the BDD surface.

A deposit was not observed at -2.4 V and only traces of Nb were detectable by EDX. At higher magnifications (Figure 13), a smooth layer is well visible; the cracks can be attributed to the internal or residual stress usually present in an electrodeposition process.

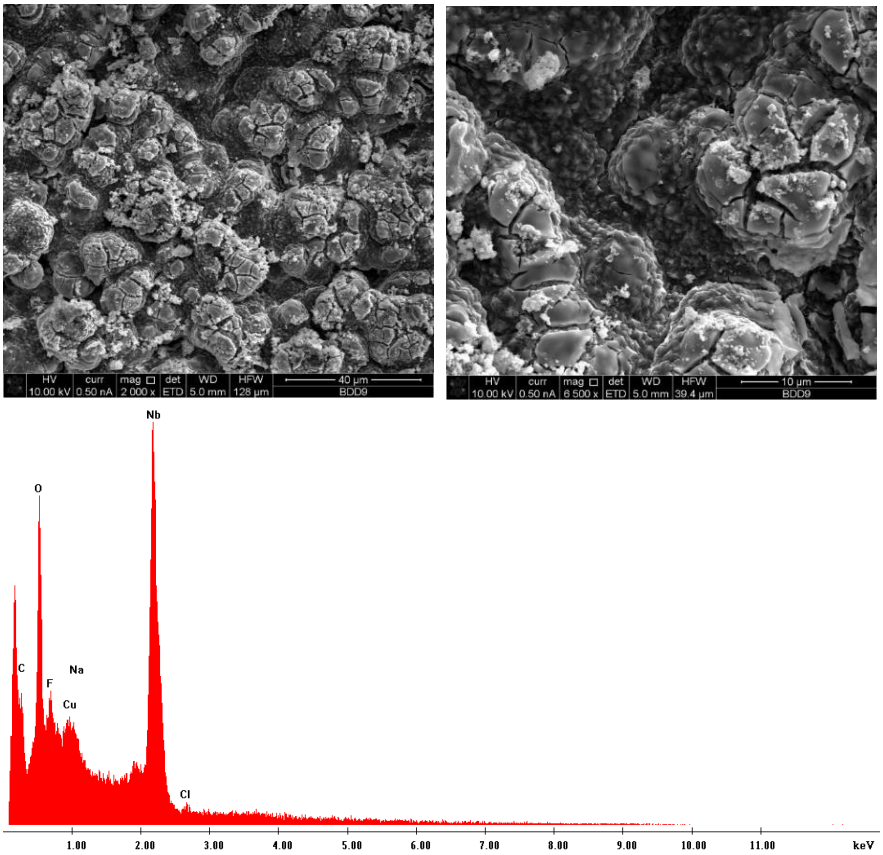

Figure 12: *SEM micrograph and EDX profile of the electrodeposit formed potentiostatically on BDD in [BMP][TFSA] containing 0.25 M NbF_5 and 0.25 M LiF at potential of -1.5 V for 1 h at 125° C.*

The EDX analyses show the presence of elemental Nb along with F, O and C; in some cases also sulphur was detected. One assumption is that sulphur and some of the oxygen may result from the ionic liquid trapped in the crackle layer during the growth of the deposit.

Figure 14 shows the FIB cross section of a sample obtained under potentiostatic conditions at -1.5 V for 10 minutes. An almost regular coating was obtained, with a thickness of about 50 nm, which is in agreement with the theoretical values calculated from the charge passed in the potentiostatic experiment.

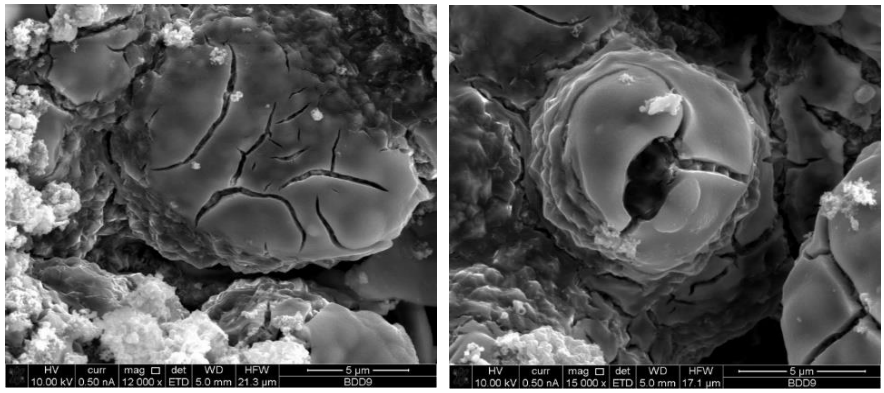

Figure 13: *SEM micrograph of the electrodeposit formed potentiostatically on BDD in [BMP][TFSA] containing 0.25 M NbF_5 and 0.25 M LiF at potential of -1.5 V for 1 h at 125° C.*

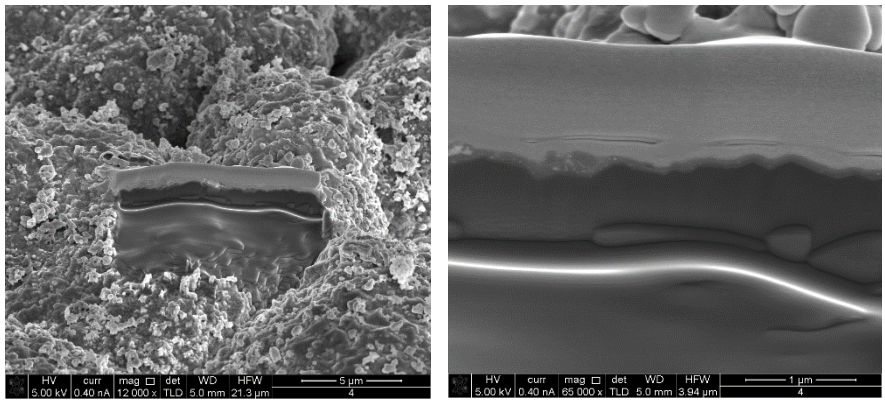

Figure 14*: SEM micrograph of the focused ion beam (FIB) cross section of the electrodeposit formed potentiostatically on BDD in [BMP][TFSA] containing 0.25 M NbF_5 and 0.25 M LiF at potential of -1.5 V for 10 minutes at 125° C.*

Element	Atomic % concentration
C	61
O	12
F	6
Nb	21
Total	100

Table 1: *Semi quantitative EDX elemental analysis of the Nb electrodeposit obtained at -1.5 V for 3600 s.*

The deposit obtained at -1.5 V was then characterized by XRD. The specimens were prepared by imposing the potential for 15 h, in order to obtain layer thick enough to be detected at wide angles.
A representative XRD pattern is shown in Figure 15 together with the best-fitted Rietveld integral profile.

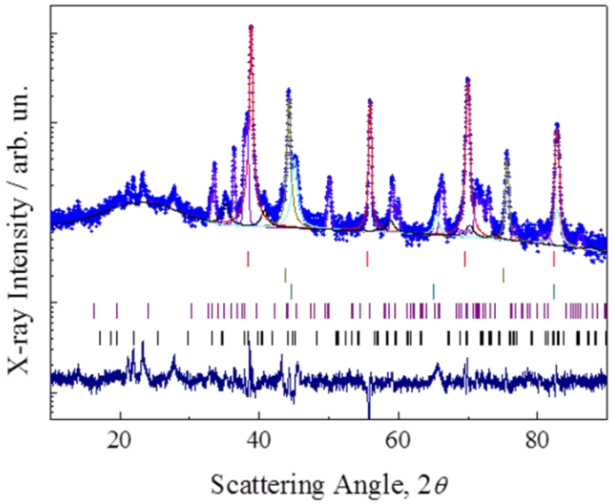

Figure 15: *XRD pattern of layer deposited over the BDD substrate as a function of the scattering angle 2θ. The Rietveld integral profiles belonging to the different detected phases are shown together with the indexing information (vertical bars below the XRD pattern).*

The background line is also shown for reference. The experimental data have been elaborated to enhance the visibility of XRD peaks at wide angles. In particular, the scattered intensity *I(Q)* is multiplied

by the scattering wave vector Q, defined as $4\pi \sin\theta/\lambda$, where λ is the X-ray wave length. The logarithm of the product is plotted as a function of the scattering angle 2θ. It can be seen that metallic Nb is the dominant crystalline phase over the background mostly due to the B-doped C diamond phase used as the conductive substrate during the electrochemical deposition process. Secondary XRD reflections can be ascribed to the formation of the stable carbide phase Nb_2C, and to the unusual one Nb_6C_5. It can be reliably concluded that almost the 85% of deposited Nb is in its metallic form.

Taking these information into account it is possible to describe the reduction of Nb(V) at BDD electrode from [BMP][TFSA]. Since deposit was not obtained at -0.68 V, the first reduction peak observed in the voltammetries can be attributed to the partial reduction of Nb(V) to Nb(IV), Nb(III) or Nb(II). In pyrrolinidinium chloride ionic liquid with addition of $NbCl_5$, the formation of Nb(IV) and Nb(III) chloride complex has been evidenced in the literature [40]. On the other hand in melt salts the kind of anion determines the composition of the first coordination sphere, stabilizing the higher oxidation state when fluoride ions are involved: spectrochemical investigations showed that in NaCl-KCl-K_2NbF_7 the Nb is mainly engaged in fluorocomplexes such as NbF_7^{2-} and NbF_7^{3-} [45] [48] [49].

In the present work the electrochemical reduction has been made in the presence of either NaF or LiF, so that fluorocomplex with Nb(IV) may be formed as first step. Nevertheless, the presence of carbides as Nb_2C and Nb_6C_5 detected by X-ray diffraction are indicative of the possible formation of Nb(II) and other non-stoichiometric forms. The subsequent reduction peak centred at -1.3 V can be attributed to the formation of Nb(0) since metallic Nb has been obtained by potentiostatic deposition at -1.5 V. The anodic peak observed in reverse scans at -1.1 V can be associated to the incomplete stripping of the electrodeposit. However, the ratio of anodic to cathodic charge is lower than one, revealing some irreversibility of this system.

Stripping seems to be kinetically hindered, which is a common phenomenon in air and water stable ionic liquids [41]. Using LiF instead of NaF the shift of the first and second reduction peaks can be observed; this behaviour may be related to the role of cations of the second coordination sphere, with a behaviour similar to that observed in tantalum deposition from [BMP][TFSA]. The positive effect of LiF on the quality of deposit was attributed to the ionic polarizability of Li^+ which can weaken the Ta–F bonds leading to a facilitation of Ta deposition [50]. At the potential related to the third reduction wave, deposit on the surface of BDD was not observed. A similar behaviour was already observed during electrodeposition of Ta from [BMP][TFSA] for which three reduction steps were identified in the presence of LiF: the first and second steps were related to the formation of metallic tantalum, while the third one was connected to the formation of subhalides which can partially undergo to further reduction to Ta [41] [51]. The formation of subhalides was attributed to the accumulation of fluoride ions which were liberated during the reduction steps: this accumulation increases the kinetics of the formation of F-Ta complexes, favouring their formation with respect to the reduction of Ta, although the latter process is thermodynamically favoured, occurring at higher potential values. Analogous phenomena may explain the electrochemical behaviour of Nb observed in the present work: if the reduction of NbF_5 is too fast, as in the case of high applied overpotential, F^- cannot diffuse fast enough so that it accumulates near the surface, promoting the formation of F-Nb complexes rather than the metallic Nb.

4.2.2. Polycrystalline gold substrate

Cyclic voltammograms of ionic liquid containing LiF and NbF_5 on polycrystalline gold at 125°C have been recorded at different scan rates (Figure 16) and different potential windows (Figure 17).

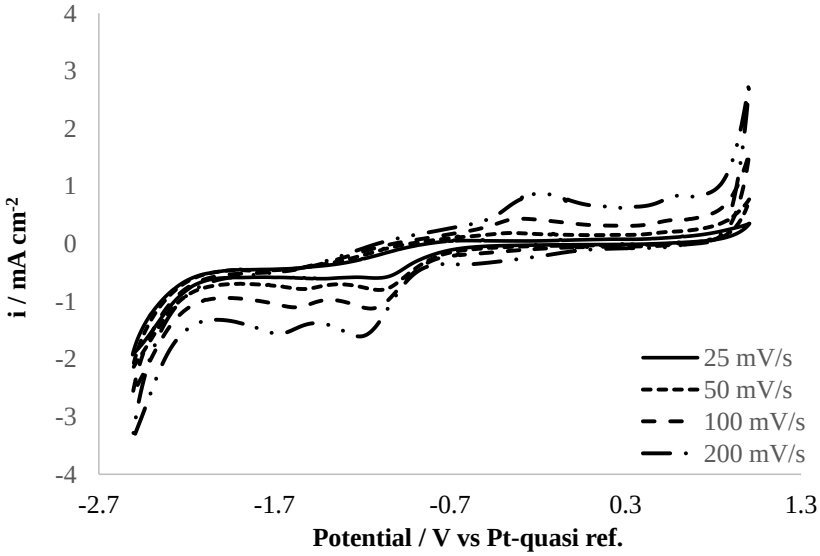

Figure 16: *Cyclic voltammograms of [BMP][TFSA] containing 0.25 M NbF_5 and 0.25 M LiF at polycrystalline gold electrode at 125° C .*

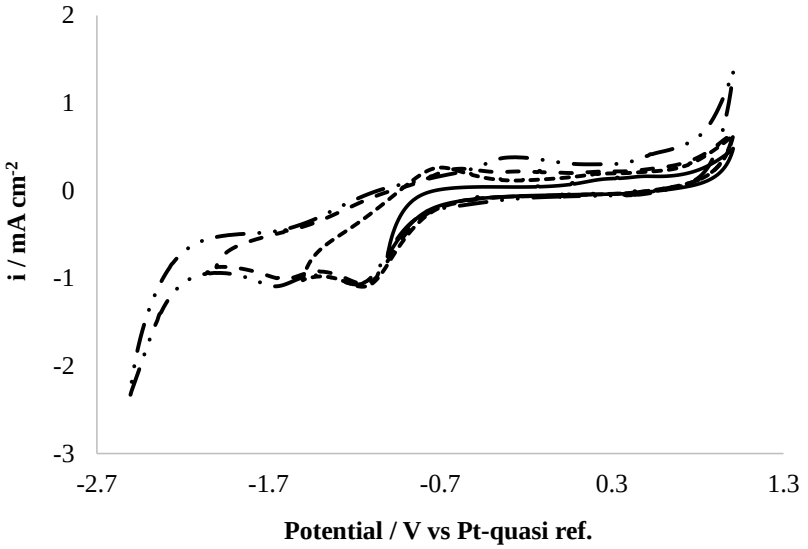

Figure 17: *Cyclic voltammograms of [BMP][TFSA] containing 0.25 M NbF_5 and 0.25 M LiF at polycrystalline gold electrode at 125° C (scan rate 100 mV/s).*

The electrode potential was scanned from the OCP in the negative direction down to -2.5 V while the anodic scan was up to 1 V.
Two reduction waves can be observed in the cathodic scan at -1.2 V and -1.6 V, while in the backward scan one oxidation peak and one less defined oxidation wave appear at -0.2 V and 0.5 V, respectively.

A two-step mechanism can be proposed:

Nb(V) <=> Nb(III) <=> Nb(0)

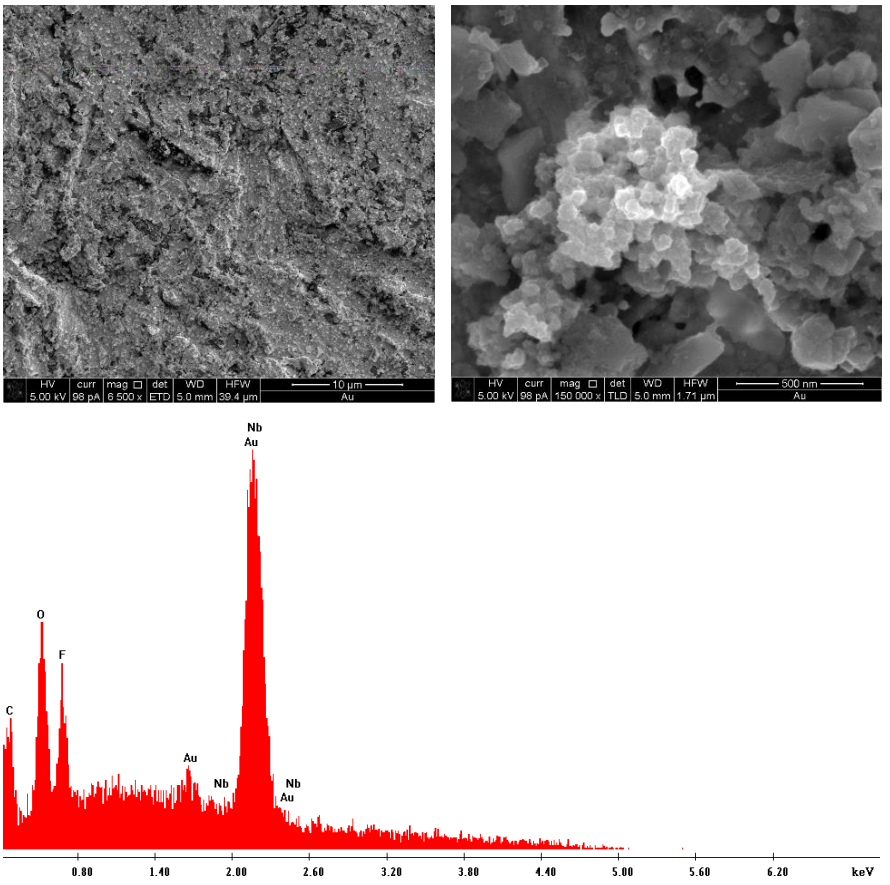

Figure 18: *SEM micrographs and EDX profile of the electrodeposit formed potentiostatically on gold electrode in [BMP][TFSA] containing 0.25 M NbF_5 and 0.25 M LiF at potential of -1.6 V for 1 h at 125° C.*

In order to get more information on the electrode process, the solution was electrolyzed by holding the potential at -1.6 V resulting in a very thin layer of a brown/black deposit on the working electrode.
The process at -1.2 V might be due to reduction of Nb(V) to Nb(III) and to subvalent Nb species.

Agglomerated fine spherical structures with nanometric sizes are seen in the SEM images (Figure 18); furthermore the EDX analysis indicate the presence of some fluorine and oxygen in addition to Nb in the deposit afterthorough washing: this may be due to trapped electrolyte or due to the formation of subvalent NbF_x films.

4.2.3. Copper substrate

The electrochemical behaviour of Nb was studied also using copper substrates in [BMP][TFSA] containing 0.25 M NbF_5 and 0.25 M LiF: Figure 19 shows the voltammetric behaviour at different values of scan rates.
The potential was scanned in the cathodic direction starting from the OCP. Two reduction peaks are clearly evident at -0.5 V and -1.5 V, indicating that the reduction of Nb(V) involves at least two electrochemical steps under the conditions adopted in this work. In the reverse scan two oxidation waves can be observed, although less evident than the corresponding cathodic peaks. Also small waves at -0.8 V and -1.8 V seem to appear at higher scan rate, but they cannot be attributed to reactions involving Nb ions, as it can be observed in the voltammograms obtained with the electrolyte prior the addition of NbF_5 (Figure 20), in which these peaks are evident.

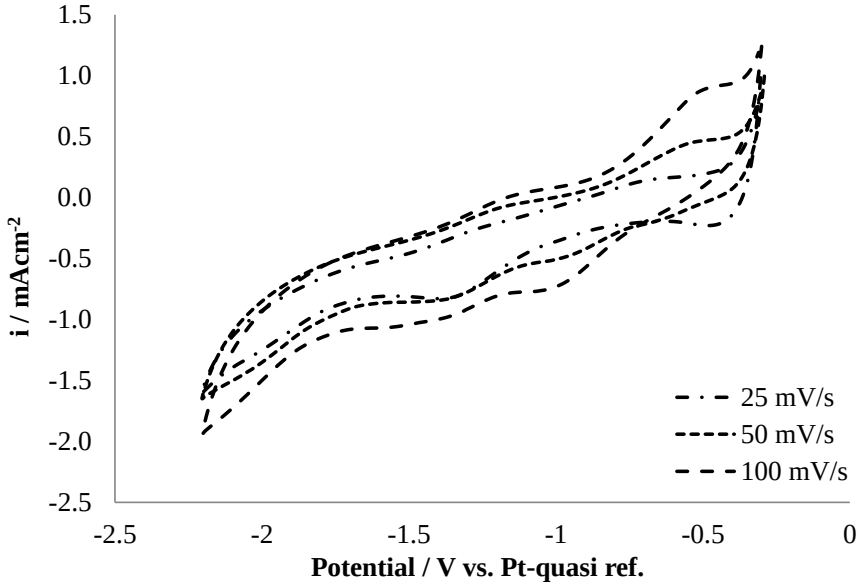

Figure 19: *Cyclic voltammograms of [BMP][TFSA] containing 0.25 M NbF_5 and 0.25 M LiF at copper electrode at 125° C.*

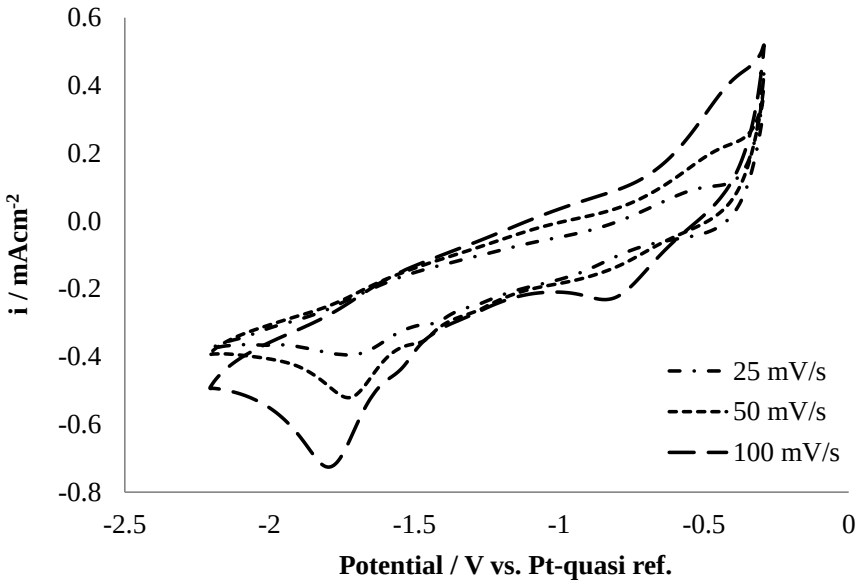

Figure 20: *Cyclic voltammogram of [BMP][TFSA] and 0.25 M LiF at copper electrode at 125° C.*

Two waves appear at -0.5 V and -1.5 V confirming a two steps reaction path Nb(V) => Nb(IV) => Nb(0); it is in agreement with the results reported in the literature. To confirm this mechanism, a set of potentiostatic experiments was performed; the potential was set at the peak values determined in the cathodic scan of the voltammograms and it was imposed for 1 h under stirring conditions.

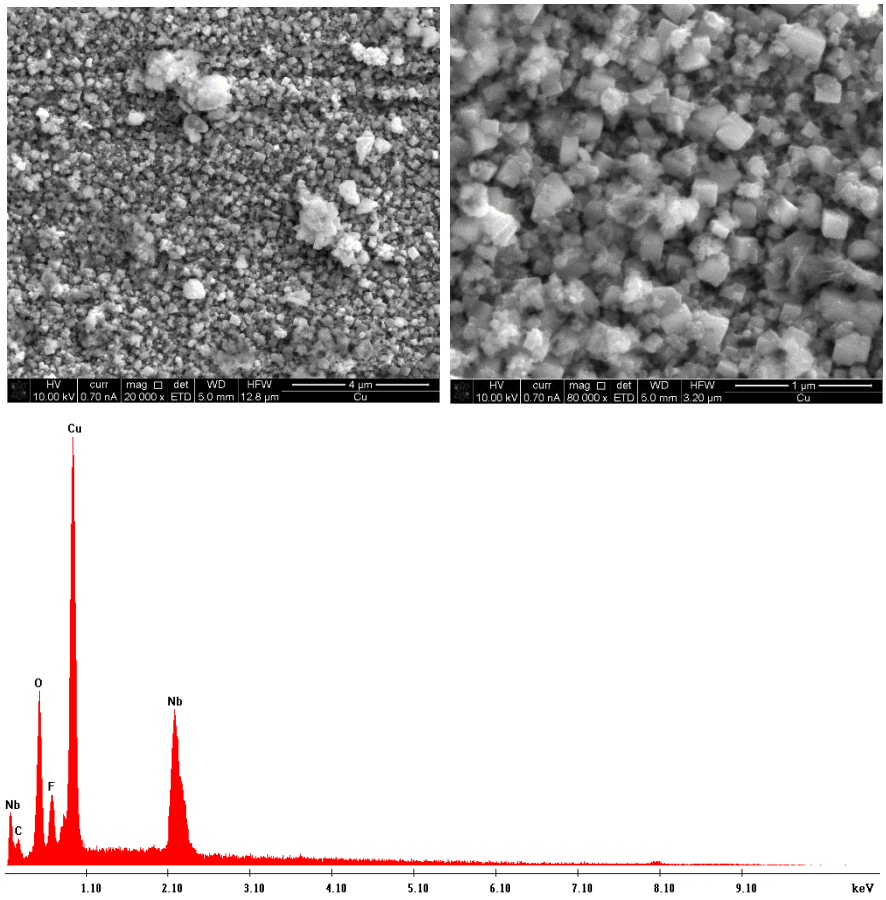

Figure 21: *SEM micrographs and EDX profile of the electrodeposit formed potentiostatically on copper electrode in [BMP][TFSA] containing 0.25 M NbF_5 and 0.25 M LiF at potential of -1.5 V for 1 h at 125° C.*

The copper sheets were then characterised: the SEM and EDX analyses of the samples obtained at -0.5 V, which corresponds to the potential of the first cathodic peak, reveal that elemental Nb is not present on the surface.
Figure 21 shows the SEM micrographs for a sample obtained potentiostatically at -1.5 V along with the corresponding EDX analyses. A deposit is evident in the SEM pictures, while EDX spectra reveal the presence of Nb. The SEM picture at higher magnification of the deposit obtained at -1.5 V shows a particle structure, with dimension in the range 50-100 nm.
Applying a potential more negative than -1.8 V, appreciable deposit is not evidenced by SEM while EDX only detects traces of Nb.

4.3. Electrochemical deposition of tantalum

4.3.1. Boron doped diamond substrate

Figure 22 shows the cyclic voltammograms of [BMP][TFSA] containing 0.25 M LiF and 0.25 M TaF_5 recorded at BDD electrode at different temperatures.
Scans were initially swept from the OCP towards the cathodic direction at a rate of 100 mV s^{-1}. The cyclic voltammograms exhibit a different behaviour with increasing temperature: the current density increases significantly in the range from 75 °C to 175 °C. This behaviour may be related to the rise of the electrochemically active species which leads to an increase of the redox reaction rates [41].
Two cathodic processes appear in the forward scan at -0.9 V and -1.8 V demonstrating that the electrochemical reduction of tantalum apparently involves two steps, while in the reverse scan one oxidation peak can be observed at 0.5 V. Extending the potential range, an increase in the current densities at the cathodic and anodic limits is observed; under these conditions the clear solution of [BMP][TFSA] containing LiF changed to dark brown.

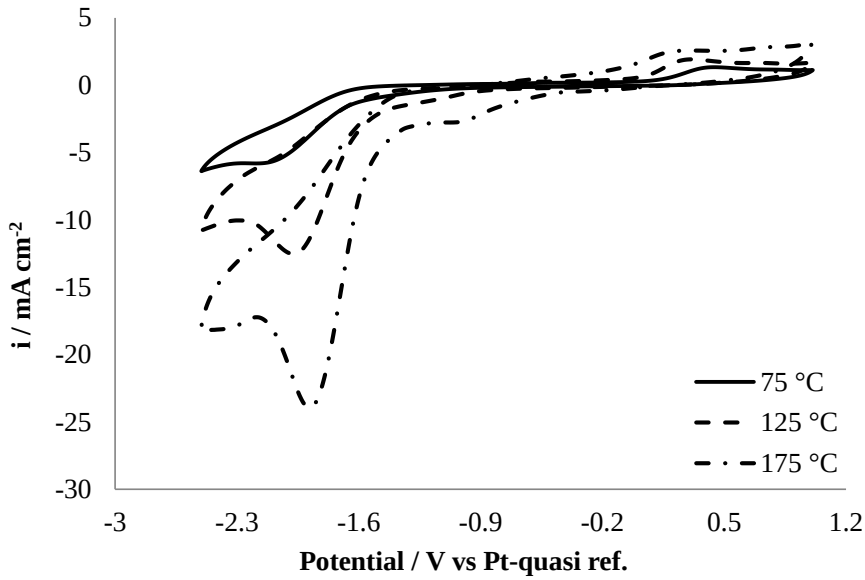

Figure 22: *Cyclic voltammograms of 0.25 M TaF_5 and 0.25 LiF in [BMP][TFSA] ionic liquid at different temperatures (scan rate 100 mV/s).*

The Ta(V) reduction has been studied in a wide range of melts, such as chlorine or fluorine melts.

In FLINAK-K_2TaF_7 Polyakova *et al.* [32] have studied the nature of the tantalum reduction process at 710 °C using various working electrodes, such as molybdenum, platinum and silver; the authors affirm that the cyclic voltammograms shape were not reproducible and electrochemically TaF_7^{2-} is reduced to tantalum metal in a single quasi-reversible five-electron step.

In LiF-NaF-K_2TaF_7 with low oxygen contents on Ag electrode, Chamelot *et al.* [33] recorded a single peak in the reduction sense associated with one reoxidation peak on the reverse scan. The reduction peak reveals the one-step reaction involving pentavalent and zerovalen tantalum at 800 °C.

In chloride electrolytes Girginov *et al.* [28] have suggested that the electrodeposition of microcrystalline Ta took place in a narrow potential range and confirmed a single step mechanism in NaCl-KCl-K_2TaF_7 melts. Zein El Abedin *et al.* [41] have shown the differences

on the electrochemical behaviour of [BMP][TFSA] ionic liquid with different concentrations of TaF_5 either in presence or absence of LiF at platinum electrode; cyclic voltammograms clearly indicate that three reduction peaks appear in the presence of LiF while only two reduction peaks, correlated to the electrolytic reduction of Ta(V) to Ta(III) and to the reduction of Ta(III) to Ta(0), have been recorded without LiF addition. The two-step reduction mechanism of Ta(V) was confirmed few years later by Borisenko *et al.* [21] that studied the electrochemical behaviour of TaF_5 in $[Py_{1,4}]$TFSA on Au(111) at 25 °C. The electrochemical behaviour of tantalum(V) chloride and oxochloride species has been also studied by Babushkina and Ekres [42] in $Pyr_{14}Cl$ ionic liquid: the authors reported that the mechanism of the electrochemical reduction of tantalum(V) depends strongly on the composition of the electrolytic bath.

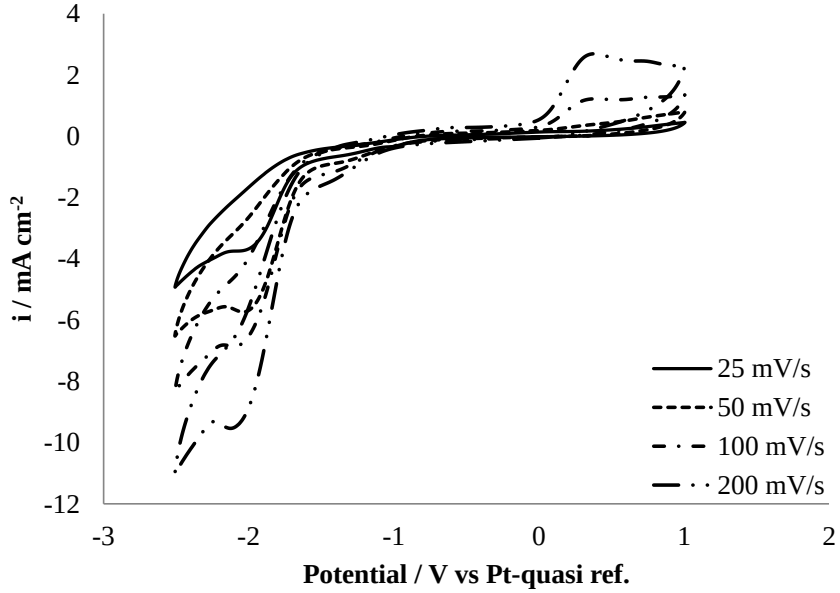

Figure 23: *Cyclic voltammograms of [BMP][TFSA] containing 0.25 M TaF_5 and 0.25 M LiF at BDD electrode at 125° C.*

Analysing the results obtained in the present work (Figure 23) the first cathodic wave recorded at -0.9 V may be attributed to the electrochemical reduction of Ta(V) to Ta(III), as TaF_3 is known to be

stable [21]. The second reduction peak at -1.8 V may be attributed to the electroreduction of Ta(III) to Ta as at this electrode potential the formation of a black deposit on the electrode surface is well visible at naked eye. In the reverse scan two less-defined oxidation waves can be observed; however, the ratio of anodic to cathodic charge is lower than one, revealing that the reoxidation of the deposit is not fully reversible.

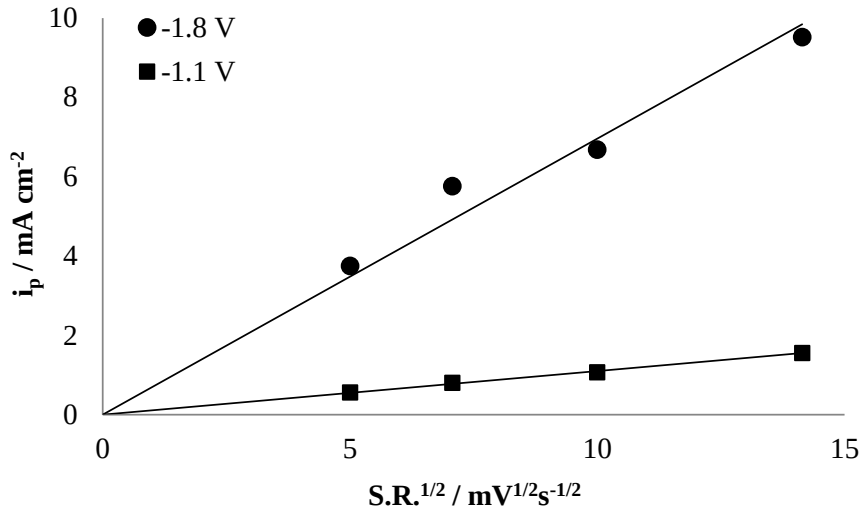

Figure 24: *Values of current density measured at the peak values of -1.1 V and -1.8 V identified in the voltammograms obtained with BDD electrode as a function of the square roots of the scan rates.*

Plotting the current peaks as a function of the square roots of the scan rates (Figure 24) a linear dependence is observed: this behaviour is in agreement with the Randles-Sevčik equation (Equation 1), for a planar diffusion controlled case [52], indicating that the reduction process is mainly controlled by diffusion of the electroactive species to the electrode surface.

$$i_p = -0.4463 \frac{n^{3/2} F^{3/2}}{R^{1/2} T^{1/2}} D^{1/2} c_O^{\infty} \nu^{1/2}$$ Equation 1

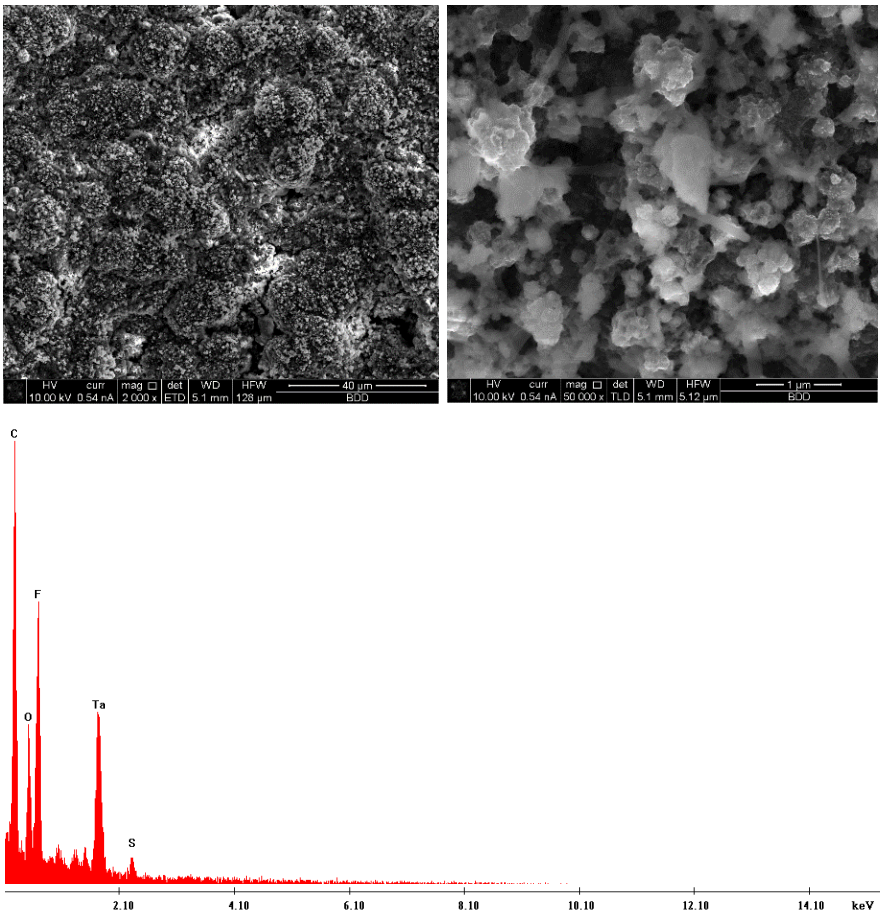

Figure 25: *SEM micrograph and EDX profile of the electrodeposit formed potentiostatically on BDD in [BMP][TFSA] containing 0.25 M TaF_5 and 0.25 M LiF at potential of -1.8 V for 1 h at 125° C.*

Only when a potential of -1.8 V is applied, a dark-brown solid was obtained which was characterised by SEM and EDX analyses (Figure 25). The results indicate a not completely uniform layer with crystallites of size ranging from 50 to 100 nm. EDX profile reveals

the presence of Ta on the BDD surface; traces of F, O, C and S were also detected probably originated from some trapped ionic liquid.

Element	Atomic % concentration
C	9.59
O	10.04
F	28.93
Ta	51.44
Total	100

Table 2: *Semi quantitative EDX elemental analysis of the Ta electrodeposit obtained at -1.8 V for 3600 s.*

4.3.2. Polycrystalline gold substrate

Figure 26 shows the cyclic voltammograms of ionic liquid containing LiF (0.25 M) and TaF_5 (0.25 M) on polycrystalline gold at 125°C.

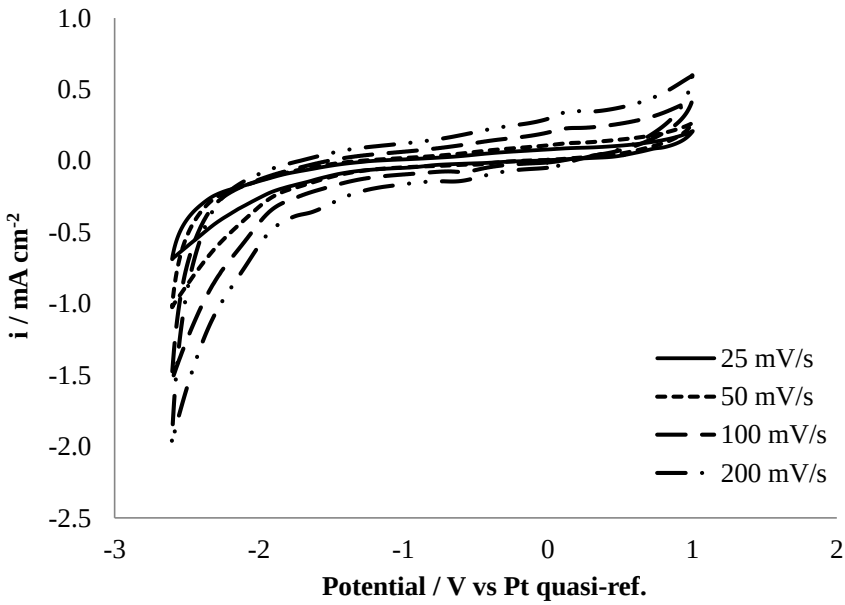

Figure 26: *Cyclic voltammograms of [BMP][TFSA] containing 0.25 M TaF_5 and 0.25 M LiF at polycrystalline gold electrode at 125° C.*

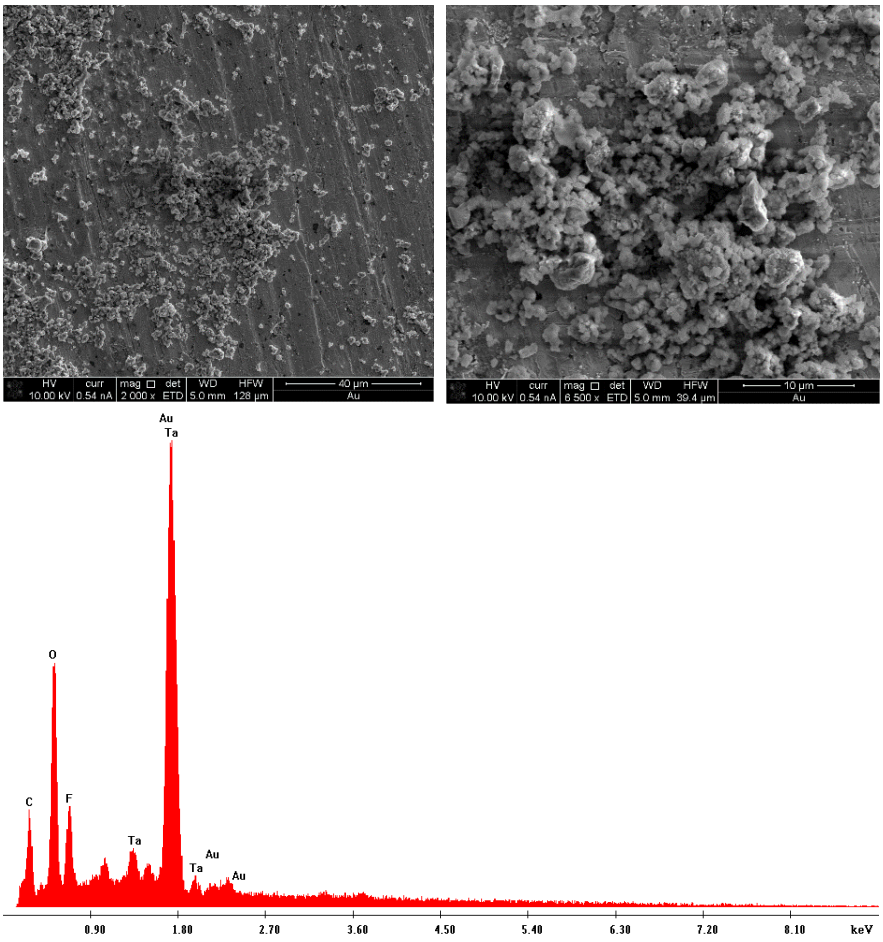

Figure 27: *SEM micrograph and EDX profile of the electrodeposit formed potentiostatically on gold electrode in [BMP][TFSA] containing 0.25 M TaF_5 and 0.25 M LiF at potential of -1.8 V for 1 h at 125° C.*

The electrode potential was scanned from the OCP at different scan rates. The cyclic voltammograms exhibit two cathodic processes in the forward scan at -0.5 V and -1.7 V, while in the backward scan one oxidation peak appears. Analysing the results obtained in the present work and taking into account the previous results showed for BDD electrode, the first cathodic wave recorded at -0.5 V may be attributed to electrochemical reduction of Ta(V) to Ta(III), while the

second reduction peak at -1.7 V may be attributed to the electrolytic reduction of Ta(III) to Ta as at this electrode potential the formation of a black deposit on the electrode surface is well visible at naked eye. The anodic peak recorded on the backward scan is due to the dissolution of the electrodeposit which, however, does not seem to be complete.

The SEM micrograph of such a deposit made at 125°C at -1.8 V for 1 h is presented in Figure 27. As can be seen the electrodeposit contains mainly particles and it is mainly constituted by Ta, but also by C, O and F resulting from the remaining ionic liquid at the electrode surface as revealed from the EDX profile.

4.3.3. Copper substrate

The behaviour of Ta(V) at copper electrode is presented in Figure 28: two well-defined peaks at -0.8 V and -1.7 V have been recorded in the ciclyc voltammograms. In the reverse scan a single oxidation wave at -0.4 V is present. Also at copper electrode the peak current densities (i_p) related to the cathodic reactions of tantalum show a linear dependence on the square root of the scan rates which confirms the diffusion controlled nature of the process (Figure 29).

Also in this case, if the potential is kept at -1.8 V for 1 h, a black deposit with a thin shining layer is obtained so that the second reduction peak might be attributed to the reduction from Ta(III) to Ta. The anodic peak that appears at -0.4 V may be attributed to the partial stripping of the electrodeposit. However, the ratio of anodic to cathodic current is much lower than 1, indicating some irreversibility of the system.

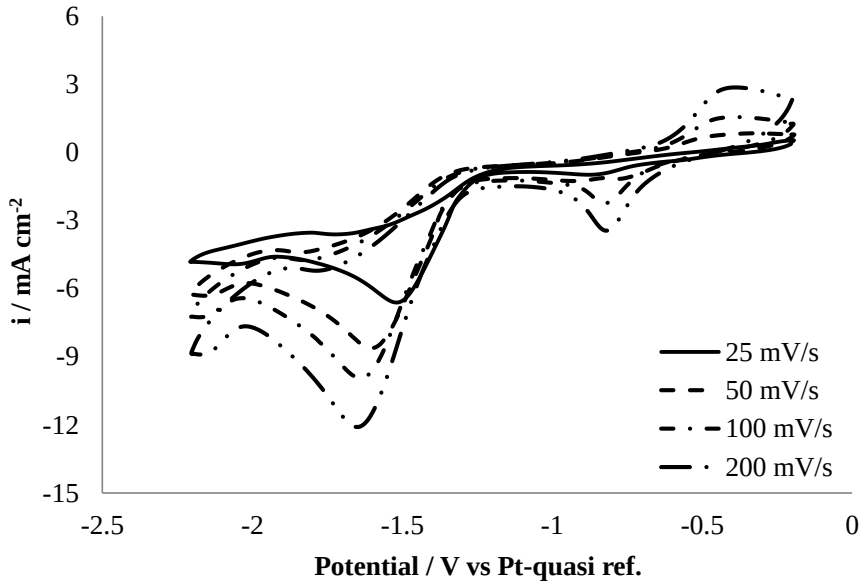

Figure 28: *Cyclic voltammograms of [BMP][TFSA] containing 0.25 M TaF_5 and 0.25 M LiF at copper electrode at 125° C.*

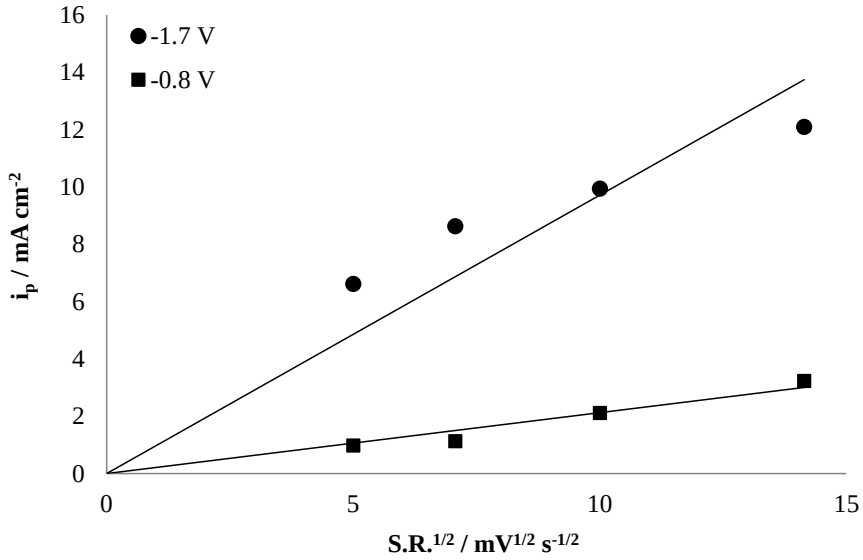

Figure 29: *Values of current density measured at the peak values of -0.8 V and -1.7 V identified in the voltammograms obtained with copper electrode as a function of the square roots of the scan rates.*

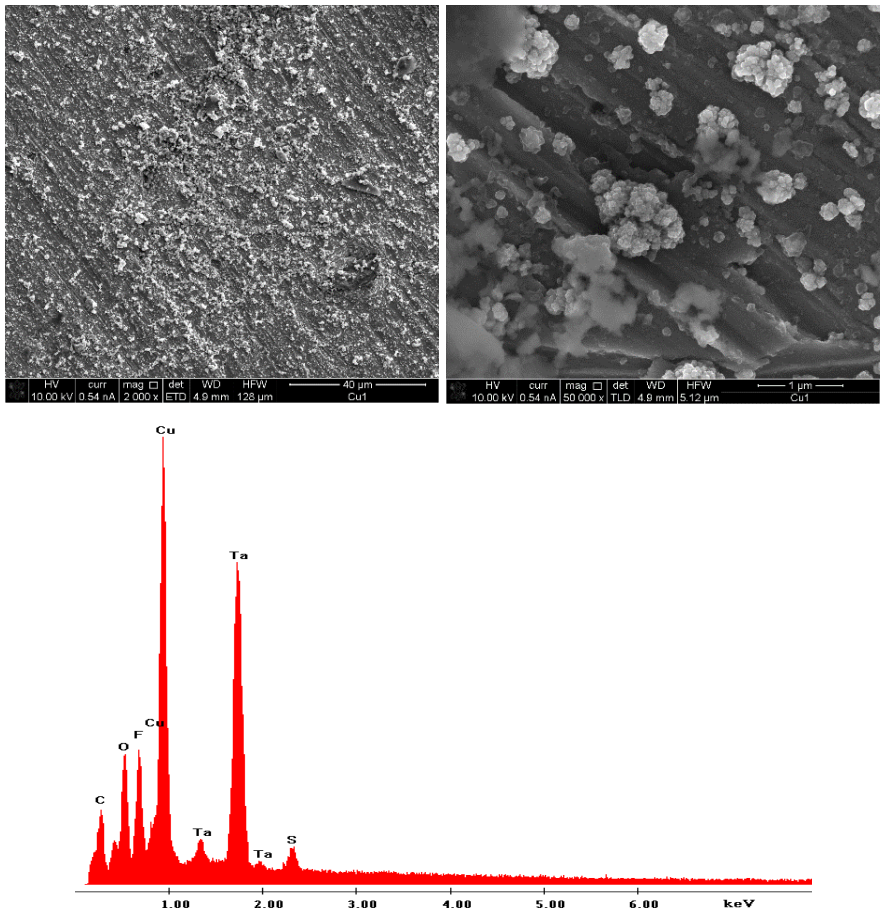

Figure 30: *SEM micrograph and EDX profile of the electrodeposit formed potentiostatically on copper electrode in [BMP][TFSA] containing 0.25 M TaF_5 and 0.25 M LiF at potential of -1.8 V for 1 h at 125° C.*

Figure 30 shows the SEM and EDX results of a deposit obtained on copper surface fixing the potential at -1.8 V for 1 h at 125 °C under stirring conditions. EDX analysis shows the presence of fluorine, oxygen and carbon besides tantalum, resulting from the ionic liquid trapped in the layer during the growth of the deposit; very rarely sulphur was detected. As can be seen, the layer is quite rough and not completely uniform; high resolution micrograph shows the growth of some particles in the range of some ten nanometers.

In order to determine the possible reaction path for tantalum electrodeposition a set of chronopotentiometry experiments have been performed at copper electrode at 125 °C under different applied current intensities (Figure 31).

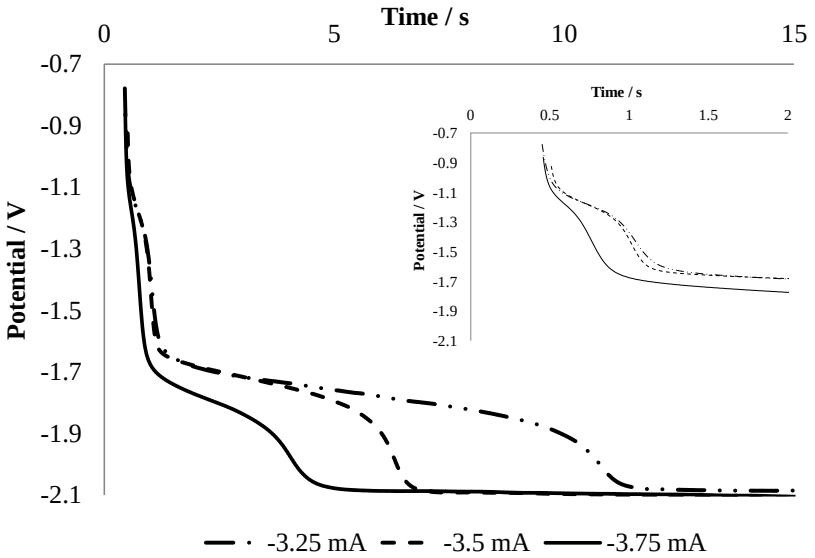

Figure 31: *Trend with time of potential measured during galvanostatic experiments at different values of imposed current density. Inset shows a magnification of the first 2 seconds of galvanostatic experiments.*

Two plateaux can be observed at -1.2 V and -1.8 V confirming that the electroreduction of Ta(V) is a diffusion controlled process in two-steps. The number of electrons exchanged in each step can be determined by analysing the transition times (τ_1 and τ_2) that correspond to the observed potential plateaux. By using the Sand equation [53] for a two steps in-series electrochemical reaction, it is possible to correlate the first transition time (τ_1) with the imposed current, the diffusivity and the concentration of the starting ion and the number of exchanged electrons (n_1). The second transition time (τ_2) depends on the same parameters of the first, but it is correlated with the number of electrons exchanged in the second step (n_2), and

with diffusivity and concentration of the electroactive species formed in the first step. The specific case of two steps in-series reactions diffusion controlled has been studied by Berzins and Delahay [53], which provided the following equation which correlates τ_1 and τ_2:

$$\tau_2 = \tau_1 \left[2 \left(\frac{n_2}{n_1} \right) + \left(\frac{n_2}{n_1} \right)^2 \right] \qquad \text{Equation 2}$$

Table 3 reports the values of transition times obtained at copper electrode under different applied current densities. The average τ_2/τ_1 approaches 5.25 which is in agreement with the theoretical value obtainable with Equation 2 for n_1=2 and n_2=3. Taking these information into account, a possible reaction path for tantalum reduction is:

Ta(V) => Ta (III) => Ta

i (mA cm^{-2})	**τ_1 (s)**	**τ_2 (s)**	**τ_2/τ_1**
-5.41	1.28	8.50	6.64
-5.83	1.00	5.28	5.28
-6.25	0.78	3.52	4.52

Table 3: *Values of transition times under different applied current densities*

4.4. Electrochemical deposition of zirconium

4.4.1. Boron doped diamond substrate

Cyclic voltammetries have been performed at 125°C in 0.25 M LiF and 0.25 M ZrF_4 [BMP][TFSA] (Figure 32); the potential was scanned in the cathodic direction, starting from the OCP.

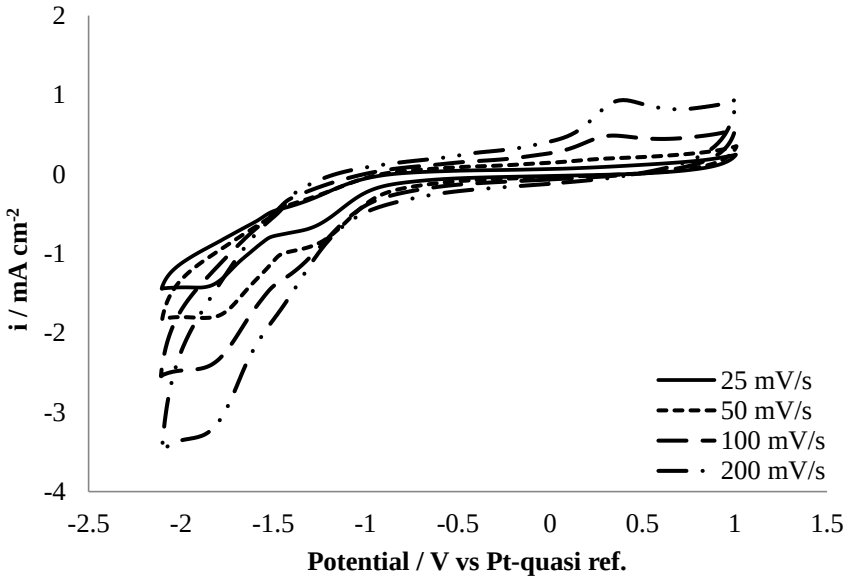

Figure 32: *Cyclic voltammograms of [BMP][TFSA] containing 0.25 M ZrF_4 and 0.25 M LiF at BDD electrode at 125° C.*

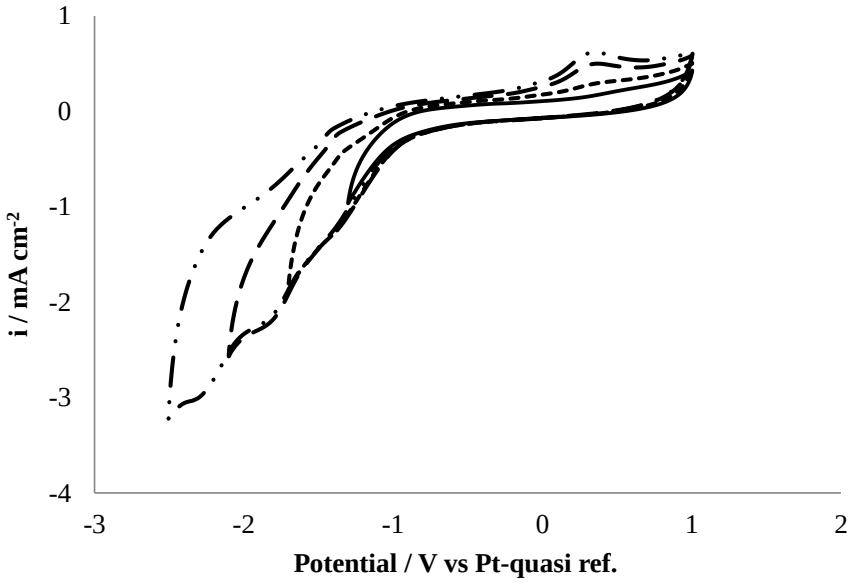

Figure 33: *Cyclic voltammograms of [BMP][TFSA] containing 0.25 M ZrF4 and 0.25 M LiF at BDD electrode at 125° C (scan rate 100 mV/s).*

Figure 33 shows the voltammograms at 100 mV s^{-1} with different potential ranges. As can be seen, two reduction waves appear at -1.3 V and -1.85 V and two oxidation waves can be observed at -1.3 V and 0.5 V. Under the operative conditions adopted in this work, the reduction of Zr(IV) in [BMP][TFSA] seems to occur in a two-step mechanism. However, the attribution of peaks is not straightforward.

The electrochemical behaviour of ionic liquids at different materials has been already observed by other authors, but not completely understood [21].
The effect of fluoride ions on the reduction of zirconium has been studied by Guang-Sen *et al.* [34] in fluoride-chloride melts: the voltammetric behaviour of zirconium at 973 K and 1033 K in equimolar KCl-NaCl with $ZrCl_4$ on a platinum electrode showed that the electroreduction process of Zr is reversible. According to the number of electrons exchanged, the authors established that the process has double two-electron steps: Zr(IV)/Zr(II) and Zr(II)/Zr. The cathodic reduction of Zr(IV), in the same electrolytic bath, was also studied with different concentrations of KF: a new peak appeared when small amount of KF ($X_{F^-}/X_{Zr^{4+}} = 1.07$) was added into equimolar KCl-NaCl melts with $ZrCl_4$. The currents at peaks related to Zr(IV)/Zr(II) and Zr(II)/Zr reduction decreased as the ratio ($X_{F^-}/X_{Zr^{4+}}$) in the melts increased. The authors have concluded that the new peak recorded in the presence of KF represents the main reduction of Zr when the ratio $X_{F^-}/X_{Zr^{4+}} \geq 6$.
Kawase and Ito [35] have studied the voltammetric behaviour at Ni electrode in the solution obtained after the anodic dissolution of Zr in the LiCl-KCl eutectic. Cyclic voltammograms reveal that Zr(II) and Zr(IV) can exist in molten salts between 450 and 550 °C and the ratio of Zr(II)/Zr(IV) increases with increasing temperature. At 450 °C only one cathodic peak related to Zr(IV)/Zr(II) is observed, while at 550 °C two cathodic peaks, related to the reduction of Zr(IV)/Zr(II) and Zr(II)/Zr, are observed.

The electroreduction process of Zr(IV) was studied by Chen *et al.* [36] at molybdenum electrode in LiCl-KCl-K_2ZrF_6 molten salts at 923 K; the authors highlighted that Zr(IV) was reduced to Zr metal by a two-step mechanism corresponding to the Zr(IV)/Zr(II) and Zr(II)/Zr transitions. Furthermore, the cathodic peaks are not dependent on the sweep rate so it has been concluded that the reduction processes of Zr(II)/Zr and Zr(IV)/Zr(II) are both reversible (or quasi-reversible).

Analogous behaviour has been reported by Wu *et al.* [37] that studied the electrochemical reduction of Zr(IV) on Pt electrode at 1023 K in NaCl-KCl-K_2ZrF_6 molten salt; two cathodic reduction peaks related to Zr(IV)/Zr(II) and Zr(II)/Zr steps were observed in the potential range between 0 and -1.6 V vs. Ag/AgCl. The authors thus observed a two-electron transfer process involving the formation of Zr(II).

On the other hand, Groult *et al.* [38] studied the electrochemical behaviour of Zr(IV) in potassium-free fused alkali fluorides in the temperature range between 773 and 1123 K by using either tungsten or molybdenum electrodes, and observed a single well-defined oxido-reduction wave, and concluded that the reduction of Zr(IV) is a single four-electron reversible step controlled by diffusion process.

A detailed electrochemical study of the molten LiF-CaF_2-ZrF_4 system is provided in the 810-920 °C temperature range by Gibilaro *et al.* [39] on an inert Ta electrode. The authors have reported that at 840 °C a single peak is observed in the cathodic run associated with a stripping peak; the reduction mechanism was a one step process exchanging 4 electrons and controlled by the Zr ions diffusion in the molten salt.

Moreover, the electrolyte may originate voltammetric responses: Randstrom *et al.* attributed to traces of oxygen and water in the nitrogen atmosphere the presence of peaks in the voltammograms [54] [55].

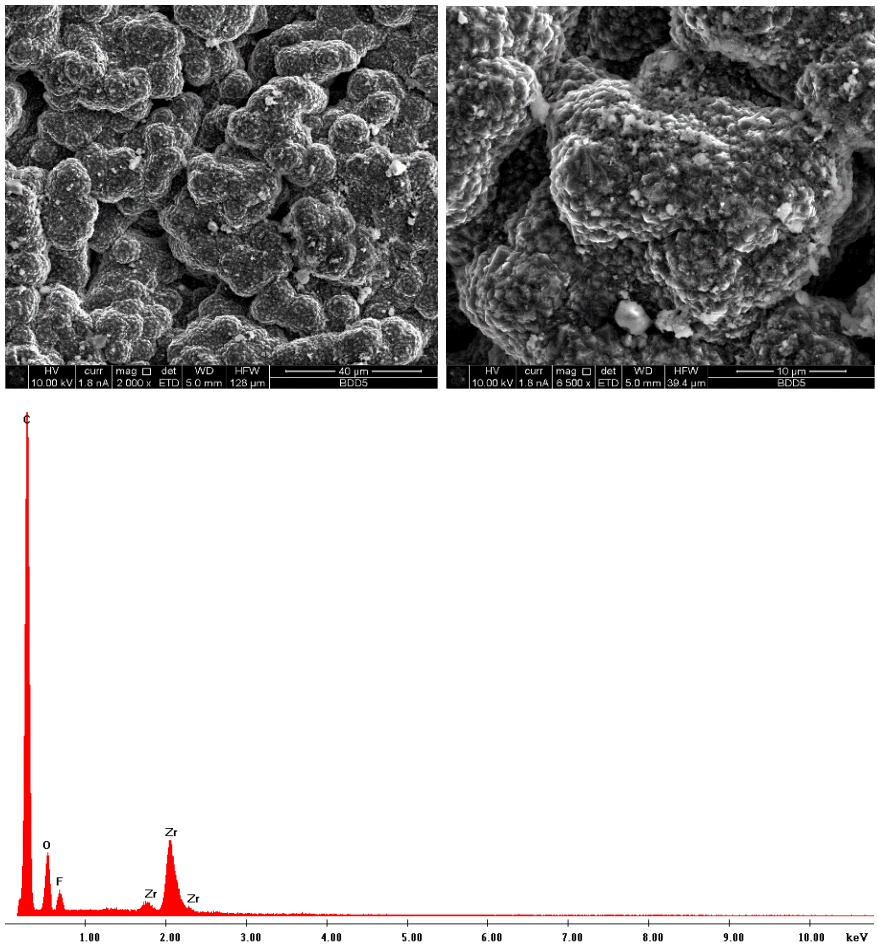

Figure 34: *SEM micrographs and EDX profile of the deposit obtained at -1.85 V for 1 h at 125° C on BDD in [BMP][TFSA] containing 0.25 M ZrF_4 and 0.25 M LiF.*

In order to study the possible reduction mechanism for Zr(IV), different potentiostatic experiments were performed setting the potential at the peak values determined in the cathodic scan of the cyclic voltammetries, for 1 h under stirring conditions.

The samples obtained were characterized by SEM-EDX. SEM and EDX analyses revealed that Zr is not present on the surface of

samples obtained at potential corresponding to the first cathodic peak. At potential values corresponding to -1.85 V, the SEM pattern (Figure 34) shows the presence of a solid deposit: EDX analyses reveal the presence of Zr along with F, which may derive from ionic liquid trapped in the deposit.

In order to determine if the deposit obtained on the BDD surface is constituted by metallic zirconium, X-ray diffraction (XRD) have been performed: Figure 35 shows an example of XRD spectra. The XRD pattern in the angular range 25-75°, shows diffraction peaks marked with black stars, that correspond to the hexagonal structure of zirconium with a space group P63/mmc (ICSD# 05-0665).

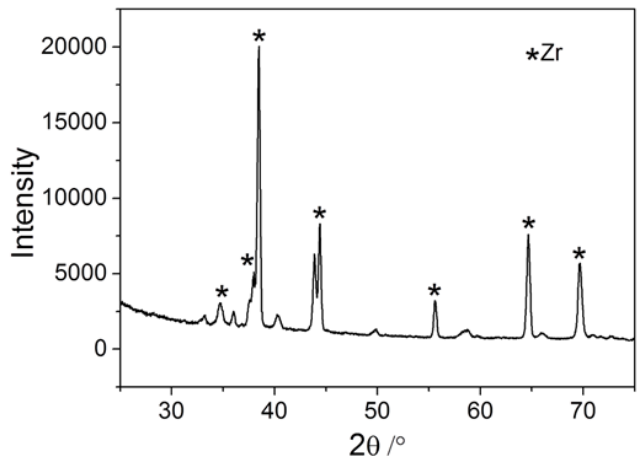

Figure 35: *XRD pattern of the deposit obtained at -1.85 V for 1 h at 125 °C on BDD as a function of the scattering angle 2θ.*

The slight shift with respect to the value reported in the ICSD may derive from lattice distortion, originated by the fluorides arising from unreacted ZrF_4 [56].
The deposit obtained at -1.85 V is then constituted by metallic Zr, and as showed by SEM analyses, is characterised by fine crystallites with average sizes in the range 50-100 nm.

Under the conditions adopted in this work, the reduction of Zr involves two electrochemical steps:

Zr(IV) => Zr(II) => Zr

4.4.2. Polycrystalline gold substrate

The electrochemical behaviour of Zr(IV) was investigated also at polycrystalline gold as substrate.

When ionic liquid contains only 0.25 M of LiF small peaks were present, with current densities lower than 0.5 mA cm^{-2} (Inset Figure 36). In the solution containing both LiF and ZrF_4 two well defined cathodic peaks at -1.0 V and -1.4 V appear at noble metal electrode; in the backward scan only one defined oxidation peak at -0.38 V and a shoulder are evident (Figure 36).

The voltammetric study clearly shows two electrochemical steps involved in the Zr(IV) reduction: the attribution of the peaks has been done on the basis of chronopotentiometries and surface analyses, which are discussed below.

As can be seen from Figure 37, if the reduction scan is stopped at -1.4 V the oxidation peak at -0.38 V is still present while it does not appear in the voltammogram stopping the cathodic scan at -0.8 V.

A two-steps mechanism was also observed in molten salts in which Zr(IV), Zr(II) and Zr(0) have been found [57] [58] as intermediates and final products. However, depending on temperature and composition of the bath, also the direct reduction to Zr(0), involving four electrons was found as possible reaction mechanism [34] [38] [39]. In pyrrolinidinium based ionic liquid at room temperature, also Zr(III) has been individuated during the reduction process [44].

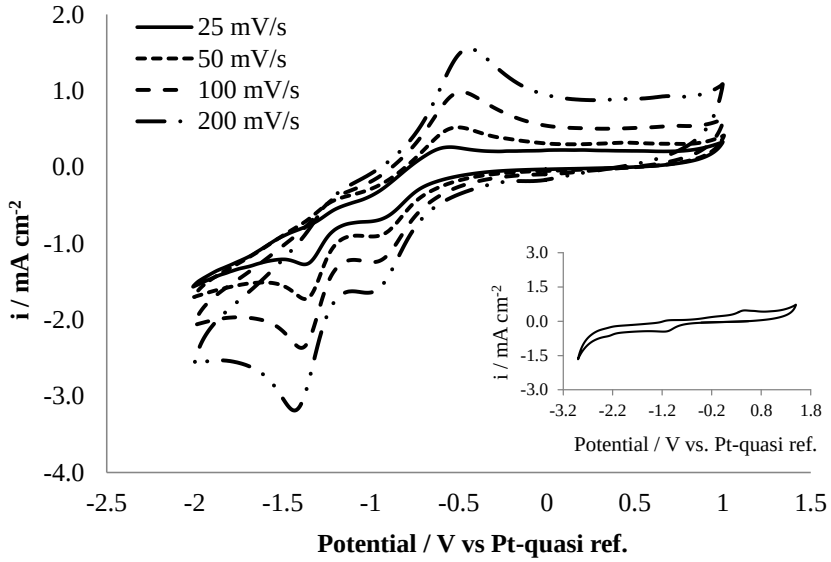

Figure 36: *Cyclic voltammograms of [BMP][TFSA] containing 0.25 M ZrF_4 and 0.25 M LiF at polycrystalline gold electrode at 125° C (Inset shows cyclic voltammogram of [BMP][TFSA] containing 0.25 M LiF at 125 °C, scan rate 100 mV/s).*

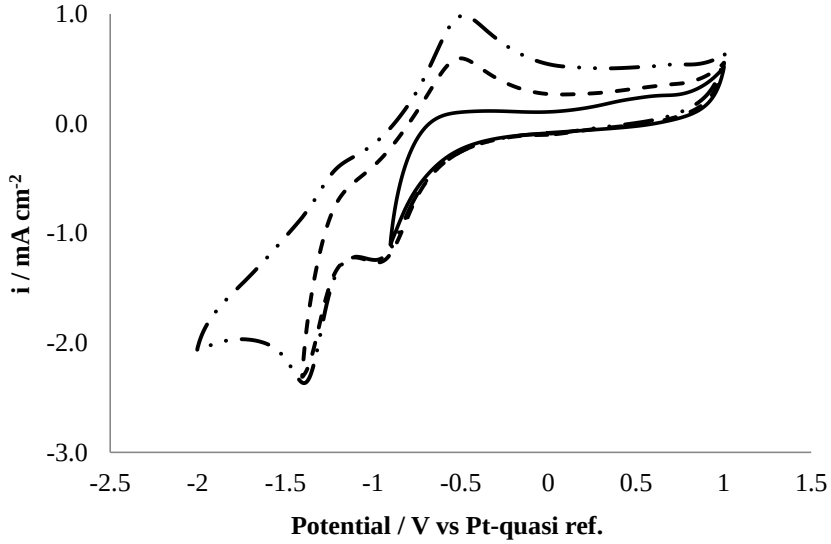

Figure 37: *Cyclic voltammograms of [BMP][TFSA] containing 0.25 M ZrF_4 and 0.25 M LiF on polycrystalline gold electrode at 125° C (scan rate 100 mV/s).*

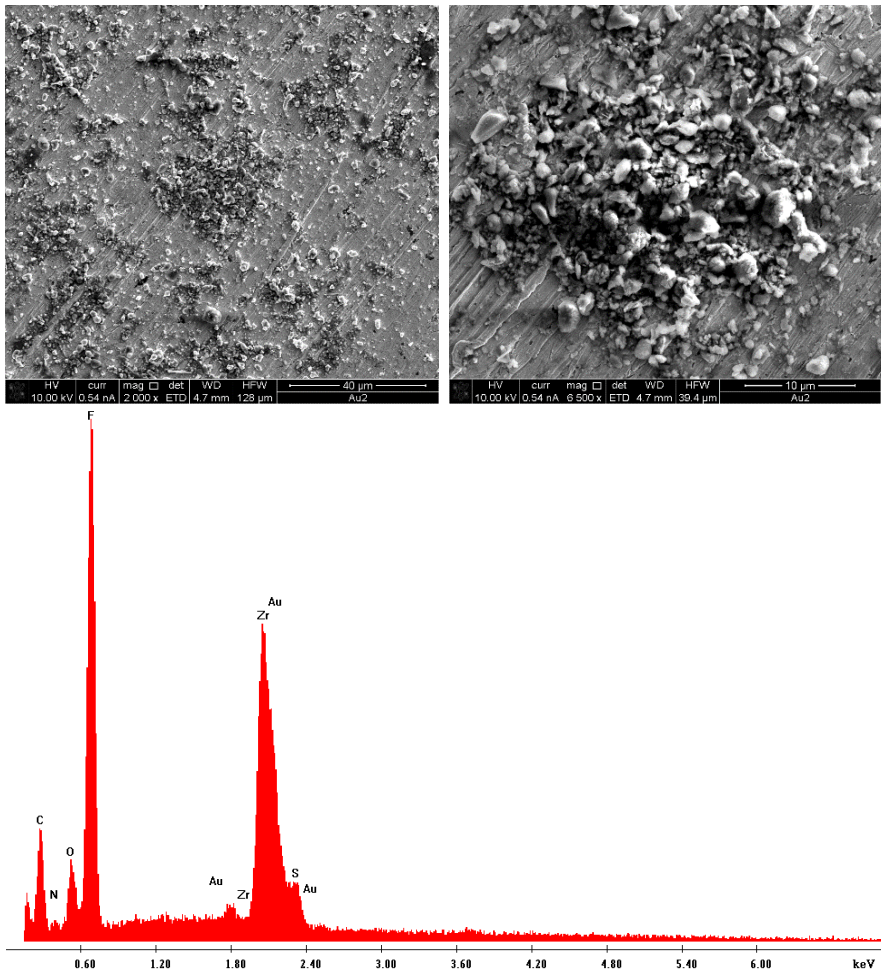

Figure 38: *SEM micrographs and EDX profiles of the deposit obtained at -1.85 V for 1 h at 125 °C on gold electrode in [BMP][TFSA] containing 0.25 M ZrF_4 and 0.25 M LiF.*

Moreover, a detailed study conducted on monocrystalline (111) gold electrode in pyrrolidinium based ionic liquid showed some characteristic peaks related to the strong interaction between the pyrrolinidium cations and the electrode surface [59].

Potentiostatic experiments were then performed to characterise the final reduction products, setting the potential at the peak values, determined in the cathodic scan of the cyclic voltammetries, for 1 h under stirring conditions. The samples obtained were characterized by SEM-EDX. SEM and EDX analyses revealed that Zr is not present on the surface of samples obtained at potential corresponding to the first cathodic peak. At potential values corresponding to -1.45 V, the SEM pattern shows the presence of a solid deposit: EDX analyses reveal the presence of Zr along with F, which may derive from ionic liquid trapped in the deposit (Figure 38).

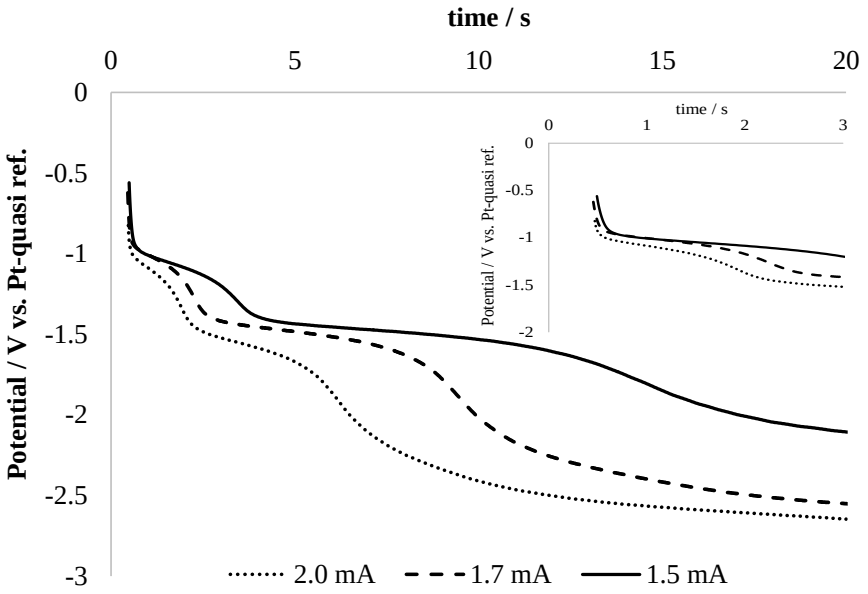

Figure 39: *Trend with time of potential measured during galvanostatic experiments at different values of imposed current density at gold electrode at 125 °C.*

To sketch a possible reaction path for the Zr deposition, a set of chronopotentiometries and potentiostatic experiments have been performed in this work. Figure 39 shows an example of

cronopotentiogram obtained at gold electrode: the experiments were carried out at different current intensity at 125°C.
Two plateaux can be observed at -1.0 V and -1.45 V corresponding to the peak potentials of the cyclic voltammograms at gold electrode, confirming that the electroreduction of Zr(IV) at gold electrode proceeds via two-step processes, and allow to establish that these steps are diffusion-controlled.

From the analysis of the transition times (τ_1 and τ_2) corresponding to the observed potential plateaux, it is possible to obtain information about the number of electrons exchanged in each step (Equation 2). For a two steps in-series electrochemical reaction, the first transition time (τ_1) can be correlated with the imposed current, the diffusivity and the concentration of the starting ion and the number of exchanged electrons (n_1) by the Sand equation [53]. The second transition time (τ_2) depends on the same parameters of the first; moreover it is correlated with the number of electrons exchanged in the second step (n_2), and with diffusivity and concentration of the electroactive species formed in the first step.

i (mA cm^{-2})	**τ_1 (s)**	**τ_2 (s)**	**τ_2/τ_1**
-2.50	3.2	10.4	3.25
-2.83	2.2	6.9	3.13
-3.33	1.45	4.13	2.84

Table 4: *Values of transition times at different electrode under different applied current densities.*

Table 4 reports the values of transition times obtained for each electrode under different applied current densities. The average τ_2/τ_1 value approaches 3, which is in agreement with the theoretical value obtainable with Equation 2 for $n_1 = n_2$. Taking into account the possible valence numbers of zirconium, the electrons exchanged in the two-steps reduction could be 1 or 2. Since metallic Zr was

obtained as final product of the reduction process, the results allow to establish the following reaction path:

Zr(IV) => Zr(II) => Zr

4.5. Electrochemical deposition of copper

4.5.1. Dissolution of pure copper metal

The electrochemical behaviour of copper ions was studied in the solution of ionic liquid prepared introducing copper cations into [BMP][TFSA] by anodic dissolution of pure copper metal.
The study of the electrochemical dissolution of copper electrode is presented in Figure 40: the steady-state curve, measured under stirring conditions at 125 °C, shows a single wave at ca. 0.1 V indicating that the dissolution of copper occurs through a single electrochemical step under the conditions adopted in this work.
In order to determine the oxidation state of copper species in [BMP][TFSA], the weight loss of the copper electrode and the charge passed during its anodic dissolution at a potential of 0.1 V were measured: a value of 49.14 C corresponding to a change in weight of 33 mg allows to confirm that the oxidation state of copper species is 1. This copper form may presumably be stabilized by the TFSA anion as CuTFSA. As reported in different works, Cu(I) species present high stability in ionic liquids such as 1-butyl-1-methylpyrrolidinium bis(trifluoromethylsulfonyl)amide [60] 1-ethyl-3-methylimidazolium tetrafluoroborate [61], and trimethyl-n-hexylammonium bis(trifluoromethylsulfonyl) amide [62]; the anodization of metallic copper in these ionic liquids always led to dissolved monovalent Cu.

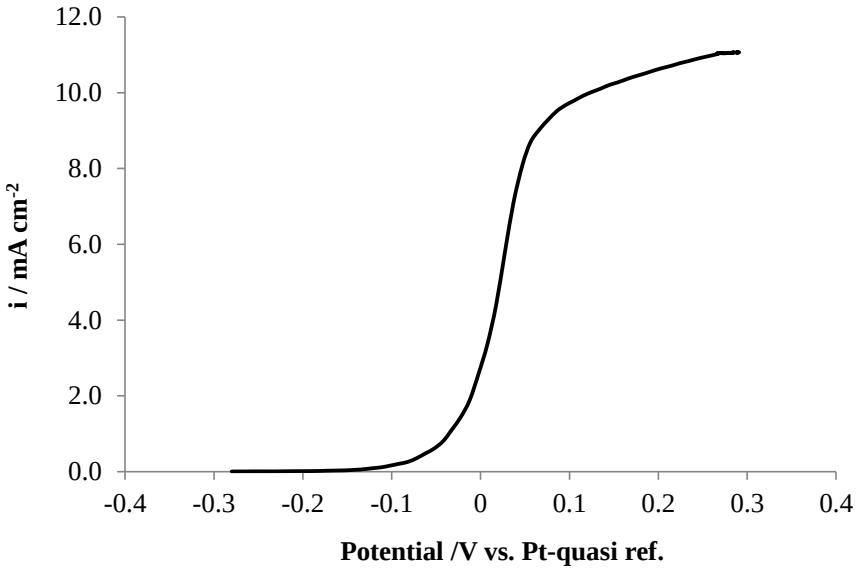

Figure 40: *Steady-state response recorded in [BMP][TFSA] at copper electrode at 125° C (scan rate 0.5 mV/s).*

4.5.2. Niobium substrate

Figure 41 shows the cyclic voltammograms obtained for Cu(I) species at niobium electrode at different scan rates in [BMP][TFSA] without adding LiF: the potential was scanned in the cathodic direction from the OCP to -1.4 V. As can be seen, all cyclic voltammograms exhibit the same general features with one cathodic peak and its corresponding anodic peak.

This behaviour is in agreement with the results obtained for the dissolution of copper: in the cathodic scan the reduction of Cu(I) to metallic copper occurs while in the reverse scan the stripping peak of the metal is visible. Moreover, when the potential scan is reversed after peak recorded at -0.8 V, a current loop is visible which is indicative of the nucleation process of copper on niobium surface [61].

As the effect of scan rate is concerned, it can be observed that, while the anodic peak is centred at -0.06 V, the cathodic peak shifts negatively with the scan rate from -0.62 to -0.87 V. In the examined range of scan rates the system shows then a quasi-reversible behaviour with a rate of electron transfer for copper deposition comparable to the rate of mass transfer.

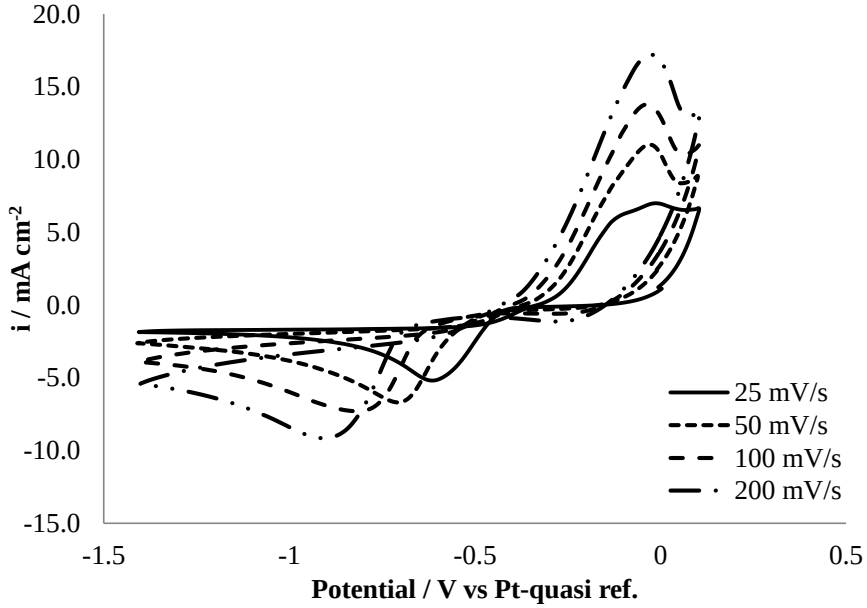

Figure 41: *Cyclic voltammograms of [BMP][TFSA] containing dissolved Cu at niobium electrode at 125 °C.*

Figure 42 reports the cyclic voltammogram obtained for Cu(I) species at niobium electrode: in this case the potential was scanned in the cathodic direction from the OCP to -1.4 V and the anodic stop potential has been increased up to 0.5 V.

After the stripping peak at -0.1 V the current density increases, and in the backward scan a new peak is present at ca. -0.3 V, indicating that Cu(II) species have been formed from the oxidation of Cu(I), which can be reduced by two one-electron steps in the cathodic sweep. Also in this case the current loop typical of a nucleation process is visible.

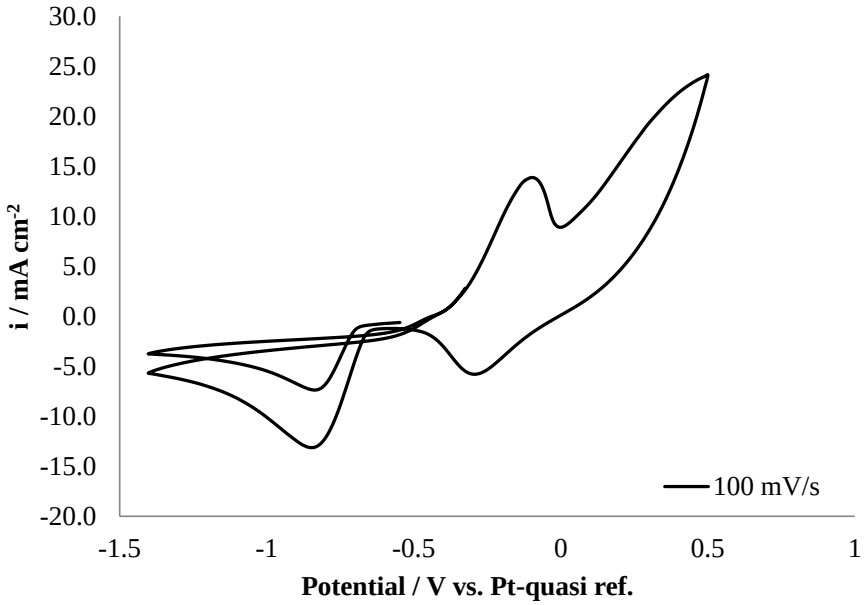

Figure 42: *Cyclic voltammogram of [BMP][TFSA] containing dissolved Cu at niobium electrode at 125° C (scan rate 100 mV/s).*

Experiments were also performed using [BMP][TFSA] with 0.25 M LiF in order to study the behaviour of copper in a solvent similar to that required for the refractory metals deposition.

As can be seen from Figure 43, the voltammetric behaviour significantly differs when LiF is added to the ionic liquid during the dissolution of copper: scanning the potential in the cathodic direction from the OCP to -1.4 V, two cathodic peaks are present and two not well-resolved anodic peaks are visible in the reverse scan. Moreover, the peak potentials are shifted to values more negative than the corresponding values obtained without LiF.

The presence of two reduction peaks in the first cathodic scan indicates that in the dissolution process both Cu(I) and Cu(II) are formed. However, the steady-state curves of dissolution of copper electrode along with the measurements of charge passed in the anodization vs. weight loss clearly indicate a one-electron process to form Cu(I). The presence of Cu(II) species in this solution can be

thus ascribed to the presence of fluoride ions in the solution: Cu(I) electrochemically produced could be stabilized by TFSA complex, but in presence of fluorides CuF_2 may be formed, allowing to a solution containing the two copper species [63].
The first cathodic peak in the voltammograms can be then attributed to the reduction of Cu(II) fluoride to Cu(I) at -0.5 V followed by the reduction wave of Cu(I) at -1.0 V, while a stripping peak in the reverse scan pertains to the electrochemical formation of Cu(I).

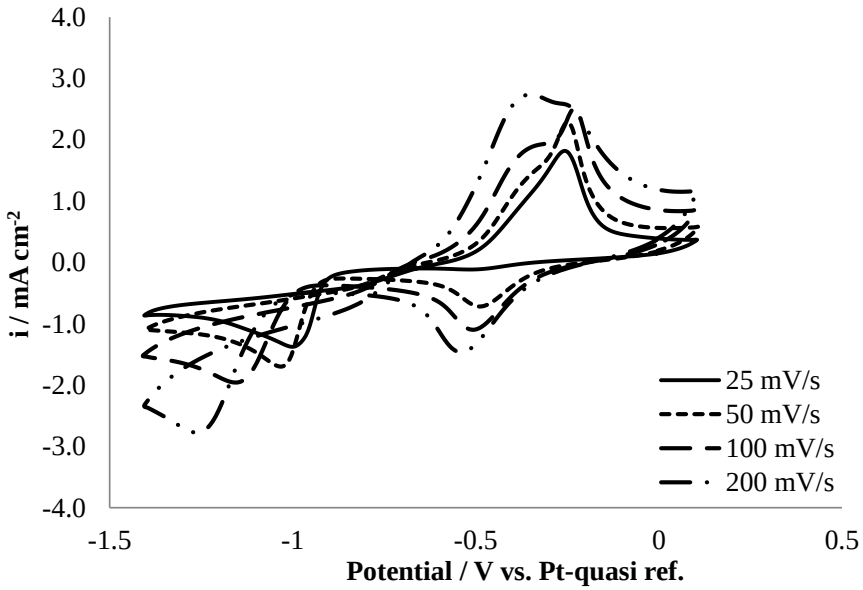

Figure 43: *Cyclic voltammograms of [BMP][TFSA] containing dissolved Cu and 0.25 M LiF at niobium electrode at 125° C.*

The deposition of copper on niobium electrode was achieved in the ionic liquid [BMP][TFSA] containing Cu(I) and 0.25 M LiF at 125 ◦C , at a fixed potential of -0.8 V for 1 h. Under these conditions, an adhesive red-brown deposit with metallic luster was visible on the electrode surface.

The SEM micrograph and EDX analyses in Figure 44 show the surface morphology of an electrodeposited copper layer on niobium substrate: the deposit is uniform and contains fine crystallites with average sizes of about 100 nm. EDX analyses in different points of the deposit indicate that Cu covers the whole Nb surface.

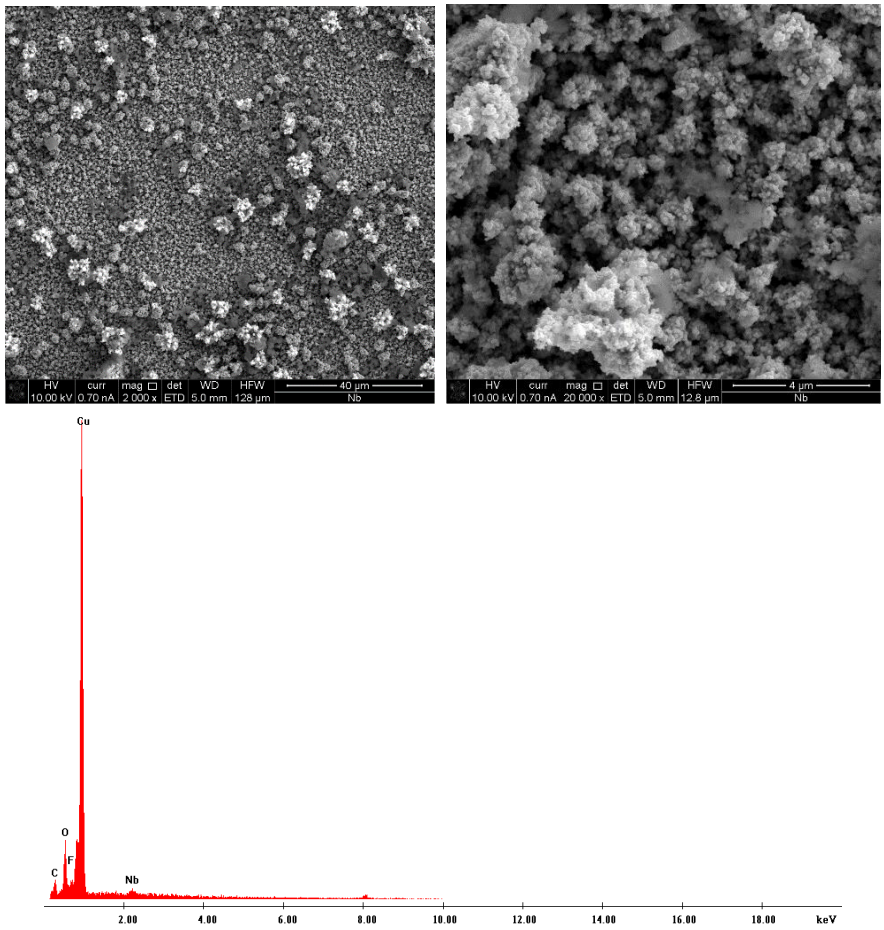

Figure 44: *SEM micrographs and EDX profile of the electrodeposit formed potentiostatically on niobium substrate from [BMP][TFSA] containing Cu and 0.25 M LiF at potential of -0.8 V for 1 h at 125° C.*

4.5.3. Tantalum substrate

Similar results were obtained using tantalum foils instead of niobium foils as working electrode.
Figure 45 reports the electrochemical behaviour of copper at tantalum substrate: one reduction peak at -0.8 V and the current loop typical of a nucleation process are visible in the voltammograms.
The potentiostatic deposition has been performed at a fixed potential of -0.8 V for 1 h: a red-brown deposit was visible on tantalum substrate also with naked eyes.
SEM micrograph and EDX analyses (Figure 46) reveal that the deposit is uniform and contains fine crystallites with average size ranging from 50 to 100 nm; EDX analyses indicate that copper covers almost completely the Ta surface.

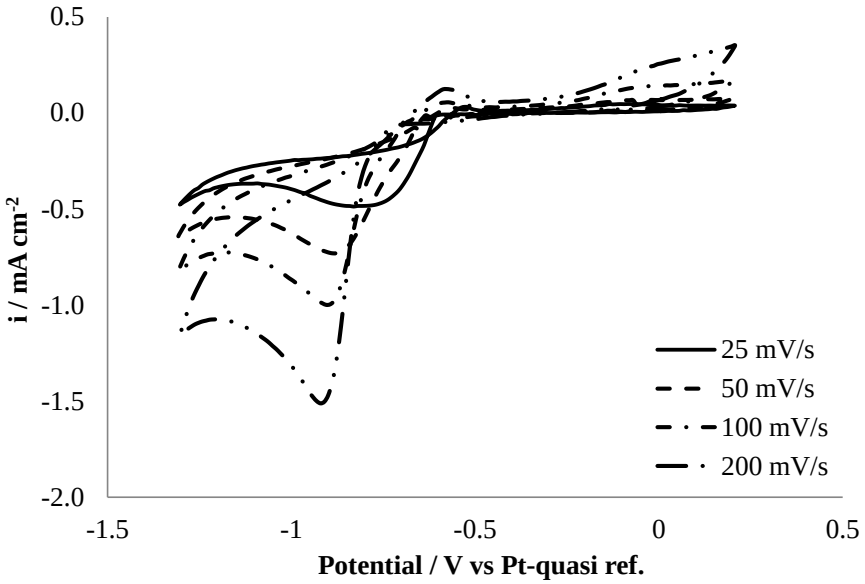

Figure 45: *Cyclic voltammograms of [BMP][TFSA] containing dissolved Cu and 0.25 M LiF at tantalum electrode at 125 °C.*

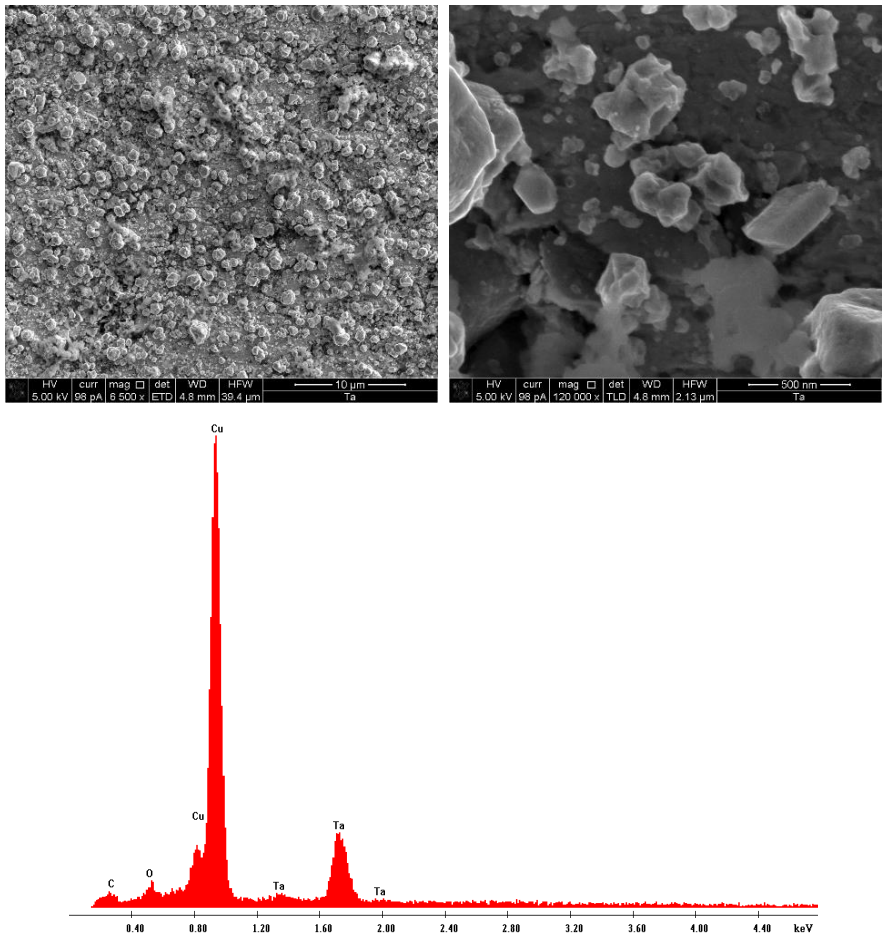

Figure 46: *SEM micrograph and EDX profile of the electrodeposit formed potentiostatically on tantalum electrode in [BMP][TFSA] containing dissolved Cu and 0.25 M LiF at potential of -0.8 V for 1 h at 125° C.*

4.6. Electrochemical deposition of composites

The mechanical properties of metallic multilayer composites have drawn world-wide attention in recent years. More specifically, fine-scale composites such as Cu/Nb and Cu/Ta have been the subject of many recent experimental and theoretical studies [64]. These fine

scale composite materials typically exhibit high yield strengths, which at room temperature can approach 1/2 to 1/3 of the theoretical strength.

Cu/Nb and Cu/Ta multilayer composites are immiscible systems and have been reported to exhibit length scale effect in some properties such as electrical resistivity and fracture properties [65].

4.6.1. Electrodepostion of Cu/Nb composites

Cu/Nb composites were prepared in dual bath using niobium foils as working electrode. A first deposit of copper was prepared at -0.8 V for 1800 s, followed by a niobium deposit obtained at -1.5 V for 3600 s. This procedure was repeated twice and the resulting sample was characterized by SEM-EDX analyses.
The results are reported in Figure 47 and Figure 48: the deposit is regular and the EDX analysis shows the presence of both copper and niobium. As it can be observed form the elemental maps, the last deposit of niobium is not uniform and copper is still visible.

Element	Wt%
C	5.46
O	13.92
F	4.13
Cu	44.15
Nb	32.33
Total	100

Table 5: *Semi quantitative EDX elemental analysis of the Cu/Nb composites obtained in dual bath mode on niobium electrode: first deposit of Cu prepared at -0.8 V for 1800 s, followed by Nb deposit obtained at -1.5 V for 3600 s. The procedure was repeated twice.*

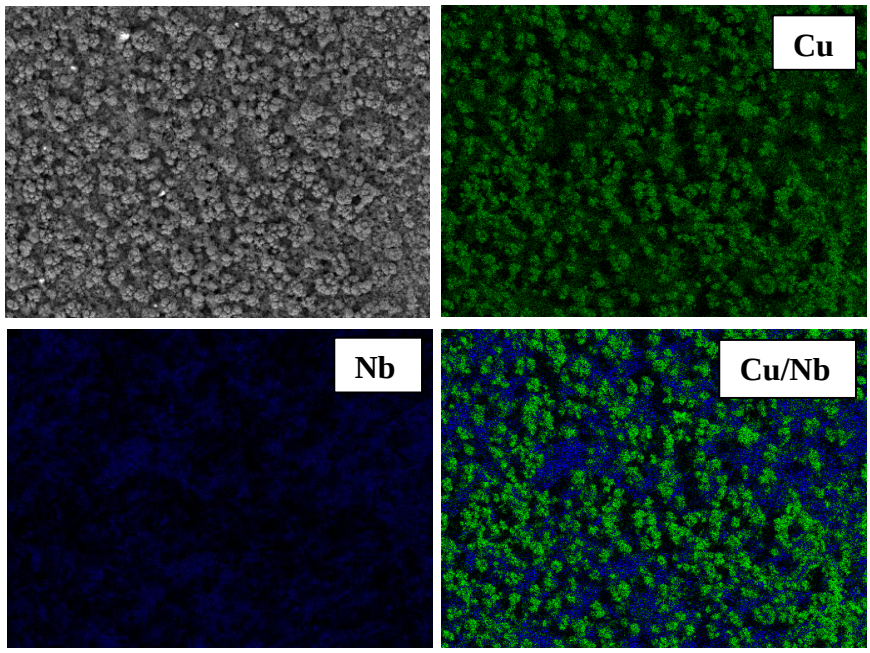

Figure 47: *SEM micrograph and elemental maps of the Cu/Nb electrodeposit obtained in dual bath mode on niobium electrode: first deposit of Cu prepared at -0.8 V for 1800 s, followed by Nb deposit obtained at -1.5 V for 3600 s. The procedure was repeated twice.*

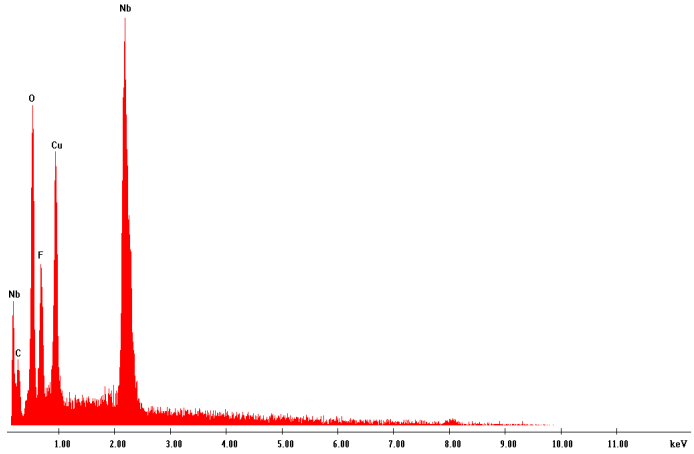

Figure 48: *EDX profile of the Cu/Nb electrodeposit obtained in dual bath mode on niobium electrode: first deposit of Cu prepared at -0.8 V for 1800 s, followed by Nb deposit obtained at -1.5 V for 3600 s. The procedure was repeated twice.*

The semiquantitative elemental analysis of the sample (Table 5) reports comparable amounts of niobium and copper: the presence of 14% of oxygen can be related to copper and niobium oxide formed at the surface of the sample exposed to air.
The FIB micrograph (Figure 49) of this sample shows that the first layer of copper is regular and dense, while the subsequent deposition of niobium presents a more porous structure. The further deposition of copper occurs on this porous surface, as well as the last niobium deposit.

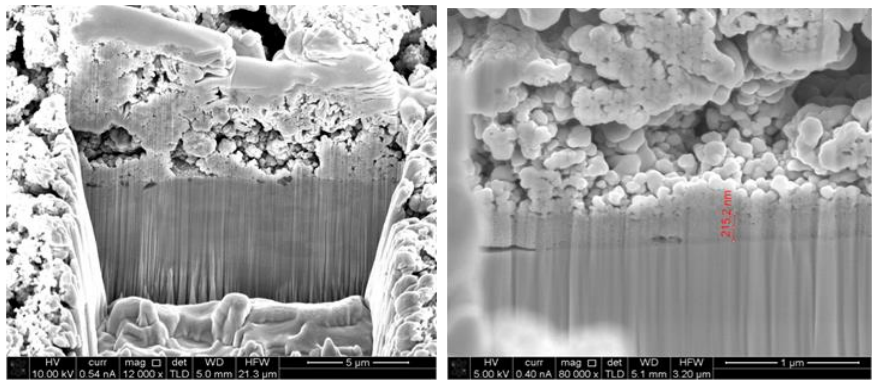

Figure 49: *SEM micrographs of the focused ion beam (FIB) cross section of the Cu/Nb electrodeposit obtained in dual bath mode on niobium electrode: first deposit of Cu prepared at -0.8 V for 1800 s, followed by Nb deposit obtained at -1.5 V for 3600 s. The procedure was repeated twice.*

4.6.2. Electrodepostion of Cu/Ta composites

The electrodeposition of Cu/Ta composites has been carried out in dual bath using either BDD substrate (Figure 50 and Figure 51) or tantalum foils (Figure 52) as working electrode. The first layer of copper was realized fixing the potential at -0.8 V for 1800 s, followed by a tantalum deposit obtained at -1.8 V for 3600 s. Before the electrodeposition of tantalum, the sample, coated with the copper layer, was washed in isopropanol in order to avoid the contamination

of the solution of IL containing LiF and TaF_5. The procedure was repeated twice.

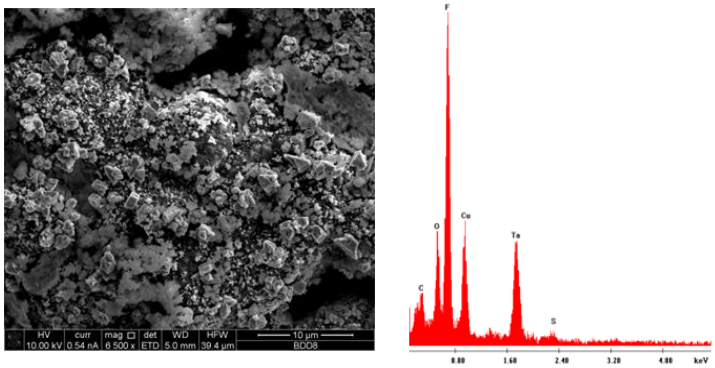

Figure 50: *SEM micrograph and EDX profile of the Cu/Ta electrodeposit obtained in dual bath mode on BDD electrode: first deposit of Cu prepared at -0.8 V for 1800 s, followed by Ta deposit obtained at -1.8 V for 3600 s.*

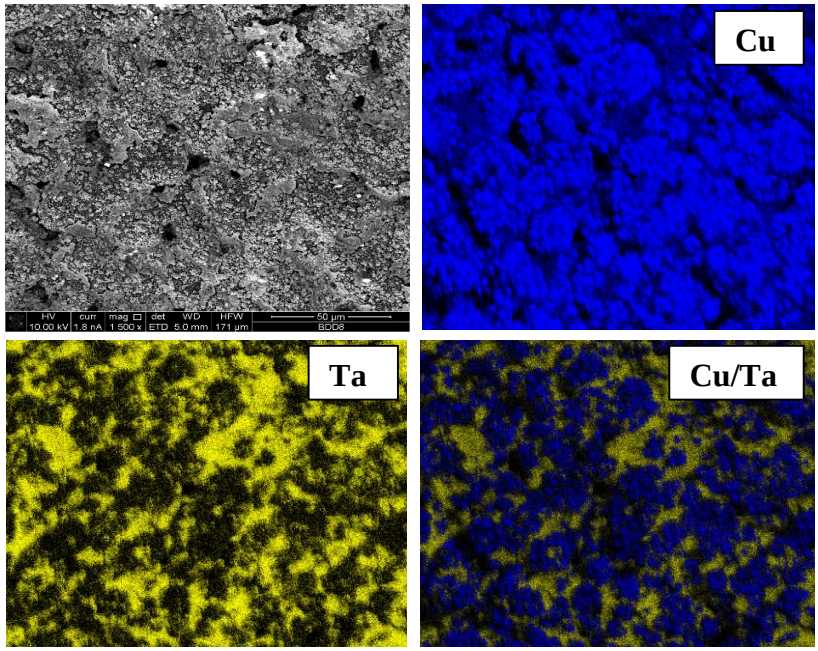

Figure 51: *SEM micrograph and elemental maps of the Cu/Ta electrodeposit obtained in dual bath mode on BDD electrode: first deposit of Cu prepared at -0.8 V for 1800 s, followed by Ta deposit obtained at -1.8 V for 3600 s.*

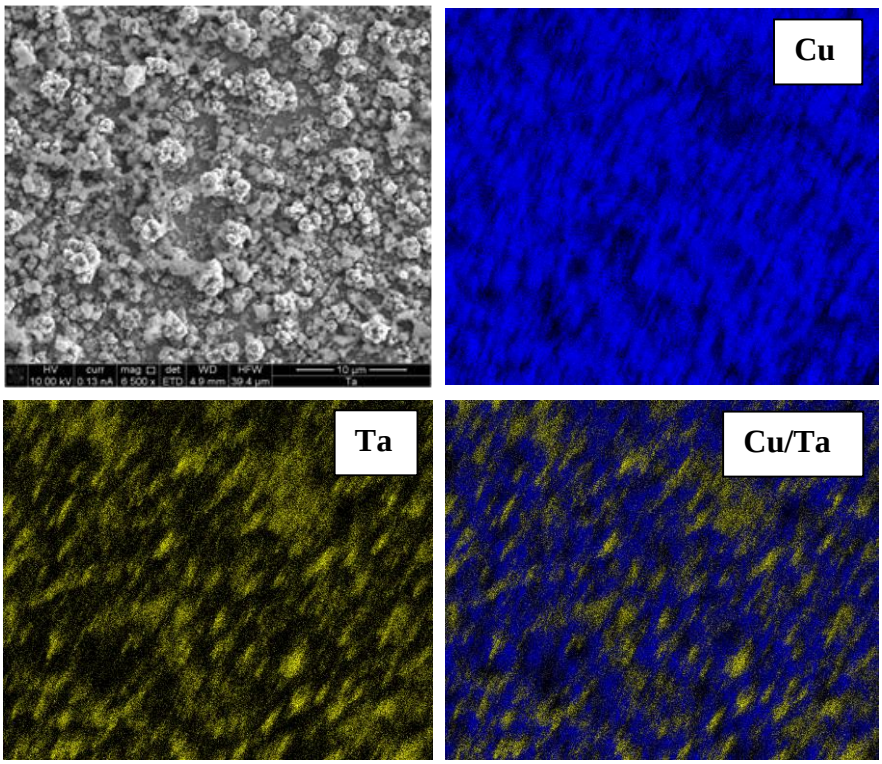

Figure 52: *SEM micrograph and elemental maps of the Cu/Ta electrodeposit obtained in dual bath mode on tantalum electrode: first deposit of Cu prepared at -0.8 V for 1800 s, followed by Ta deposit obtained at -1.8 V for 3600 s.*

The FIB micrograph of the composite realized on tantalum substrate (Figure 53) shows that the first layer of copper is almost regular with average size of 50 nm, while the subsequent deposition of tantalum presents a more porous structure. The further deposition of copper and tantalum occurs on this porous surface.

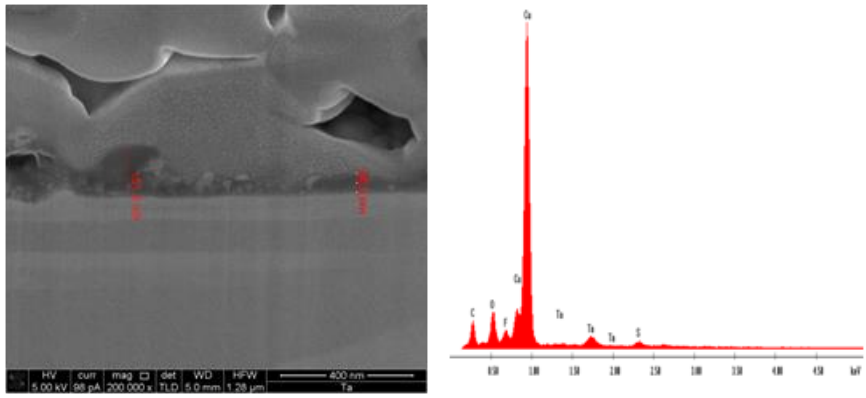

Figure 53: *SEM micrograph and EDX analysis of the focused ion beam (FIB) cross section of the Cu/Ta electrodeposit obtained in dual bath mode on tantalum electrode: first deposit of copper prepared at -0.8 V for 1800 s, followed by tantalum deposit obtained at -1.8 V for 3600 s.*

Chapter 5

Conclusions

In this Chapter conclusions are given.

Based on the objectives introduced at the beginning of this thesis, several conclusions can be drawn from this study.

The pre-electrolysis process implemented in this study was shown to be effective in removing impurities from the as-received ionic liquid.

The electroreduction of NbF_5, TaF_5, ZrF_4 was investigated in the purified ionic liquid, 1-butyl-1-methyl-pyrrolidinium bis(trifluoromethylsulfonyl)imide at 125 °C.
The copper solutions were obtained by dissolution of metallic copper: cyclic and linear sweep voltammetries showed that both Cu(I) and Cu(II) may be present, depending on the electrolyte composition.

Under potentionstatic conditions thin coatings of Nb, Ta, Zr and Cu were obtained in the presence of LiF; however further electrochemical experiments are required to improve the electrochemical parameters in order for a uniform, adherent layer of metals to be obtained.

The samples were characterized by SEM-EDX and XRD analyses.

SEM images reveal that a deposit of niobium can be obtained at -1.5 V, while at -0.7 V and -2.4 V niobium is not present on the BDD surface; the XRD pattern shows that metallic Nb is the dominant crystalline phase over the background mostly due to the B-doped C diamond phase used as the conductive substrate during the electrochemical deposition process. Also using a metal substrate, a deposit of niobium was observed at -1.5 V at 125°C.

On the electrodeposition of tantalum is concerned, only when a potential of -1.8 V is applied a dark-brown solid was obtained on BDD, gold and copper substrates.

Metallic zirconium was obtained fixing the potential at the value corresponding to the more negative reduction peak that appears in the voltammograms recorded using different substrates.

The EDX analyses show the presence of the metal of interest along with F, O and C; in some cases also sulphur was detected. One assumption is that sulphur and some of the oxygen may result from the ionic liquid trapped in the crackle layer during the growth of the deposit.

Copper-niobium and copper-tantalum nanometric composites were prepared in dual bath using different working electrodes.

The deposits were characterised by SEM-EDX analyses revealing that both Cu/Nb and Cu/Ta composites are characterised by fine crystallites with average sizes in the range 50-100 nm. Although the results are promising, further studies are requested to improve the morphological properties of the resulting composites.

The present work has shown that it is possible to deposit a layer of niobium, tantalum, zirconium and copper from an ionic liquid which underwent a specialised pre-electrolysis process. However, further work is recommended in improving the adherence and uniformity of the layers on the substrates.

Appendix

Electrochemical background and techniques

This chapter is focused on the electrochemical processes taking place at electrode surface and electrochemical techniques used to investigate the electrochemical behaviour of electrode materials.

A.1. Electrochemical processes

Electrochemical reactions are heterogeneous chemical processes which involve the transfer of charge in a ionic conductor (electrolyte) to or from a surface (electrode), generally a metal or a semiconductor. Charge is transported through the electrode by the movement of electrons. In the electrolyte phase, charge is provided by the movement of ions. Electrochemical cells are defined most generally as two electrodes (anode and cathode) separated by at least one electrolyte phase.

The electrochemical reaction taking place in a cell is the result of two independent half-reactions, which describe the real chemical changes at the two electrodes. The reaction that take place at the electrode of interest (working electrode) can be studied by using a second electrode (counter electrode). The potential of the working electrode can be controlled with respect to the reference electrode; since reference electrode has a fixed potential it is possible to relate any changes in the cell to the working electrode.

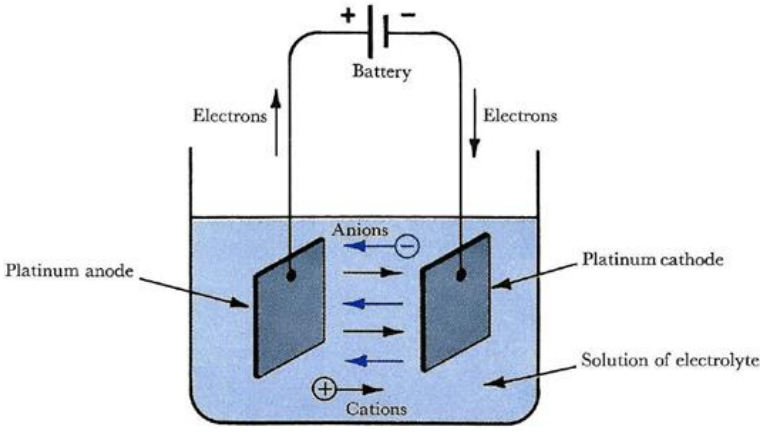

Figure 54: *Schematic diagram of an electrochemical cell.*

In a typical electrochemical experiment were a working and a reference electrode are immersed in a solution, the variation of the potential, E, by means of an external power supply, can produce a current flow in the external circuit because, as reactions occur, electrons cross the electrode/solution interfaces.
Moreover, when electrolysis occurs, in addition to electron transfer at the anode and cathode surfaces, ions must pass through the solution between the electrodes and electrons though the wires externally interconnecting the two electrodes (in order to maintain electrical neutrality at all points in the system).
Hence the current through the external circuit, *I*, given by

$$I = A\, i$$

(when *A* is the electrode area and *i* the current density), is a convenient measure of the rate of the cell reaction.
The number of electrons that cross an interface is measured in terms of the total charge, *Q*, passed in the circuit. Moreover, the current through the external circuit is a measure of the rate of the cell reaction.
The relationship between charge and amount of product formed is given by Faraday's law.

$$Q = \int_0^t I\, dt = mnF$$

where *Q* is the charge, passed during a period *t*, required to convert *m* moles of starting material to product in an electrode reaction involving the transfer of *n* electrons/molecule; *F* is 96485.4 C.
Two types of processes occur at electrodes: one kind involves processes in which charges are transferred across the electrode-solution interface. Since such reactions are governed by Faraday's law they are called faradaic processes. Electrodes at which faradaic

processes occur are sometimes called charge transfer electrodes. Under some conditions, a given electrode-solution interface will show a range of potentials where no charge-transfer reactions occur because such reactions are thermodynamically or kinetically unfavourable. However, processes such as adsorption and desorption can occur, and the structure of the electrode-solution interface can change with changing potential or solution composition. These processes are called nonfaradaic processes. Although charge does not cross the interface, external currents can flow (at least transiently) when the potential, electrode area, or solution composition change. Both faradaic and nonfaradaic processes occur when electrode reactions take place. Although the faradaic processes are usually of primary interest in the investigation of an electrode reaction, the effects of the nonfaradaic processes must be taken into account in using electrochemical data to obtain information about the charge transfer and associated reactions.

A.1.1. Nonfaradaic processes

An electrode at which no charge transfer can occur across the metal-solution interface, is called an ideal polarized electrode (IPE). While no real electrode can behave as an IPE over the whole potential range available in a solution, some electrode-solution systems can approach ideal polarizability over limited potential ranges [53].

At any interface between two phases and particularly between an electrode and an electrolyte solution, there exists a segregation of positive and negative charge in a direction normal to the phase boundary. These charges may be associated in the form of dipolar molecules or polarised atoms, or they may be free as holes, electrons, or ions. The charge segregation may occur through the preferential adsorption of either positive or negative ions at the interface, through the transfer of charge across the interface, or through the deformation of polarisable molecules by the asymmetrical force field at the interface. The theory of the electrical double layer is concerned with

the charge distribution and electrical potentials that arise as a consequence of this charge separation [52].

The study of the electrical double layer is intimately concerned with the concept of the ideally polarisable electrode; since, at ideally polarisable electrode, charge does not cross the interface during potential changes, the interface behaves like a capacitor. For a given applied potential, charge is stored in equal measure on the electrode and in the solution. In the case of a metallic electrode, the excess or deficiency of electrons is limited to a very thin surface layer, while the charge in solution is distributed in the proximity of the electrode surface. This charge distribution at the interface is called double layer with which a double-layer capacitance (C_{dl}) is associated.

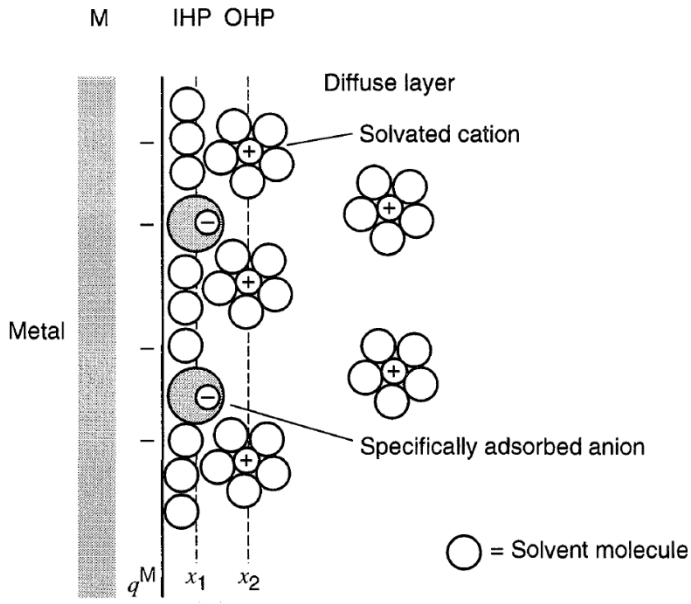

Figure 55: *Proposed model of the double-layer region under conditions where anions are specifically adsorbed.*

The solution side of the double layer is constituted of several "layers". That closest to the electrode, the inner layer, called also the Helmholtz layer, contains solvent molecules and sometimes other

species (ions or molecules). The locus of the electrical centres of the specifically adsorbed ions is called the inner Helmholtz plane (IHP), which is at a distance x_1. Solvated ions can approach the metal only to a distance x_2; the locus of centres of these nearest solvated ions is called the outer Helmholtz plane (OHP). The interaction of the solvated ions with the charged metal involves only long-range electrostatic forces, so that their interaction is essentially independent of the chemical properties of the ions. These ions are said to be nonspecifically adsorbed. Because of thermal agitation in the solution, the nonspecifically adsorbed ions are distributed in a three dimensional region called the diffuse layer, which extends from the OHP into the bulk of the solution. The structure of the double layer can affect the rates of electrode processes [53].

A.1.2. Faradaic processes

Electrochemical cells in which faradaic currents are flowing are classified as either galvanic or electrolytic cells. A galvanic cell is one in which reactions occur spontaneously at the electrodes when they are connected externally by a conductor.
Considering a general electrode reaction such as $O + ne^- \leftrightarrow R$, it is possible to consider that the current (or electrode reaction rate) is governed by the rates of processes such as:

- Mass transfer to the electrode surface and vice versa
- Electron transfer at the electrode surface
- Homogeneous or heterogeneous chemical reactions on the electrode surface
- Other surface reactions, such as adsorption, desorption, or crystallization (electrodeposition).

The rate constants for some of these processes depend on the potential. The simplest reaction only involves mass transfer and electron transfer steps, however, chemical reactions and adsorption/desorption processes are taking place in some reactions.

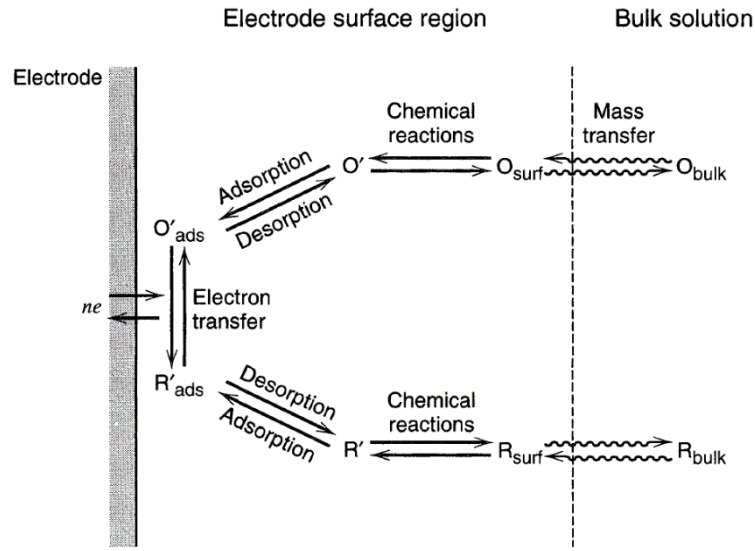

Figure 56: *Pathway of a general electrode reaction.*

The response of the electrode to the current flow corresponds to an overpotential that is the sum of different terms associated with the reaction steps occurring with a finite rate in the electrochemical cell: η_{mt} (the mass-transfer overpotential), η_{ct} (the charge-transfer overpotential), η_{rxn} (the overpotential associated with a preceding reaction), etc. The electrode reaction can then be represented by a resistance, R, composed of a series of resistances (or more exactly, impedances) representing the various steps: R_m, R_{ct}, etc.

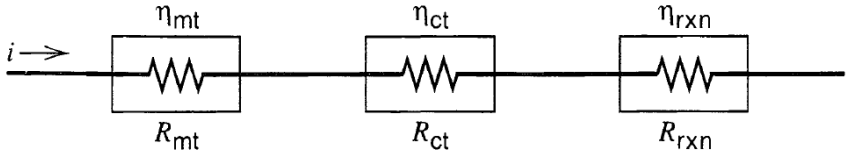

Figure 57: *Processes in an electrode reaction represented as resistances.*

A fast reaction step is characterized by a small resistance (or impedance), while a slow step is represented by a high resistance [53].

The kinetic of a system is strongly influenced by the applied potential, the nature and the structure of the reacting species, the solvent, the electrode material and adsorbed layers on the electrode.

A.1.3. The Butler-Volmer equation [52]

As reported above the potential of an electrode strongly affects the kinetics of reactions occurring on its surface. The phenomenological model of Butler-Volmer is able to relate the reaction rate (current density) with the applied electrode potential.
The simplest electrode process can be represented as one electron process:

$$O + e^- \leftrightarrow R$$

It is necessary to consider the thermodynamics and the kinetics of the electron transfer process. If the kinetics of electron transfer are rapid, the concentrations of *O* and *R* at the electrode surface can be assumed to be at equilibrium with the electrode potential, as governed by the Nernst equation:

$$E_{eq} = E^0 + \frac{RT}{nF}\ln\left(\frac{c_O^\sigma}{c_R^\sigma}\right)$$

where the equilibrium potential is related to the standard potential of the couple *O/R*, E^0, and the surface concentration of *O* and *R*. The standard potential clearly represents the particular equilibrium potential when the surface concentrations of *O* and *R* are equal. If no current passes through the cell no chemical change can occur; the surface concentrations must therefore be equal to the bulk concentrations c_O^∞ and c_R^∞. While no net current is flowing and there is no overall chemical change in the cell, there must be a dynamic equilibrium at the working electrode surface, for example the reduction of *O* and the oxidation of *R* are both occurring, but the processes are of equal rate:

$$i_0 = -\vec{\imath} = \overleftarrow{\imath}$$

where I_0 is the exchange current density, and $\vec{I}$ and $\overleftarrow{I}$ are the partial current densities for the forward and backward reactions.
The magnitude of the current flowing at any potential depends on the kinetics of electron transfer. At any potential the measured current density in given by

$$i = \vec{\imath} + \overleftarrow{\imath}$$

(where $\vec{\imath}$ is negative); the current density is dependent on a rate constant and the concentration of the electroactive species at the site of the electron transfer, the electrode surface, i.e.

$$\vec{\imath} = -nF\vec{k}c_O^{\sigma} \qquad and \qquad \overleftarrow{\imath} = -nF\overleftarrow{k}c_R^{\sigma}$$

The rate constant vary with the applied electron potential according to the equations of the form

$$\overrightarrow{k_c} = \overrightarrow{k_0}\exp\left(-\frac{\alpha_c n\,F}{R\,T}E\right) \qquad and \qquad \overleftarrow{k_a} = \overleftarrow{k_0}\exp\left(\frac{\alpha_a n\,F}{R\,T}E\right)$$

where α_a e α_c are constants (between 0 e 1 and generally approximately 0.5) known as the transfer coefficients for the anodic and cathodic reactions, respectively. For a simple electron transfer reaction $\alpha_a + \alpha_c = 1$, so that one transfer coefficient may be eliminated from any equation; $\overrightarrow{k_c}$ and $\overleftarrow{k_a}$ represent the heterogeneous rate constant of the reduction and oxidation reaction, respectively.

At equilibrium ($E=E_{eq}$) the net current density is zero and the potential of the working electrode is given by the Nernst equation.

Taking these information into account it is possible define the overpotential as the deviation of the potential from the equilibrium value:

$$\eta = E - E_{eq}$$

Taking into account the definition of the exchange current density, $i_0 = -\vec{\imath} = \overleftarrow{\imath}$ at $\eta=0$ it is possible to obtain the Butler-Volmer equation:

$$i = i_0 \left[\exp\left(\frac{\alpha_a nF}{RT}\eta\right) - exp\left(\frac{\alpha_c nF}{RT}\eta\right)\right]$$

It is possible to observe how current density varies with exchange current density, overpotential, and the transfer coefficients.
Depending on the overpotential value, three cases can be distinguished: the first two applying an high overpotential value, while the third applying a very low overpotential:

- $|\overleftarrow{\imath}| \gg |\vec{\imath}|$
  $logi = logi_0 + \frac{\alpha_a nF}{2.3\ RT}\eta$

- $|\vec{\imath}| \gg |\overleftarrow{\imath}|$
  $log - i = logi_0 - \frac{\alpha_c nF}{2.3\ RT}\eta$

- $\eta \ll RT/\alpha_c nF$ and $\eta \ll RT/\alpha_a nF$
  $i = i_0 \frac{nF}{RT}\eta$

The first two cases are known as the Tafel equations and are the basis of a simple method of determining the exchange current density and a transfer coefficient.

As shown in Figure 58, both linear segments extrapolate to an intercept of $logi_0$. The plots deviate sharply from linear behaviour as

η approaches zero, because the back reactions can no longer be regarded as negligible.

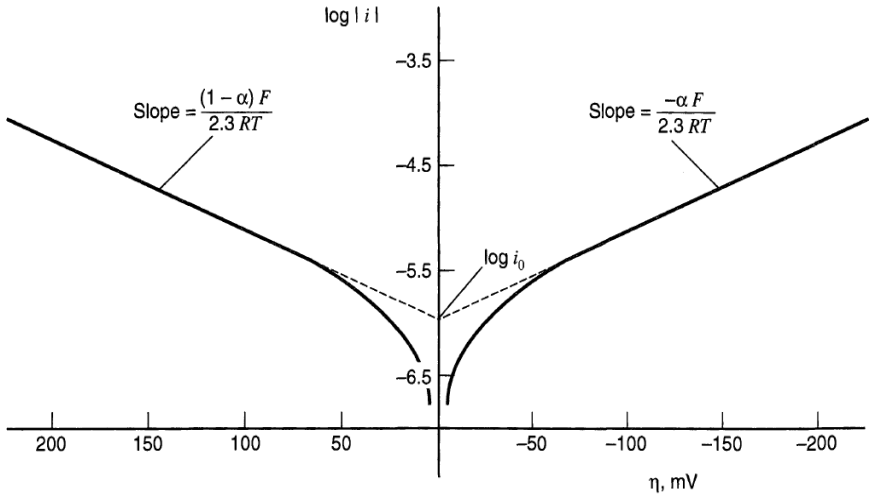

Figure 58: *Tafel plots for anodic and cathodic branches of the current-overpotential curve for O + e *= R with a = 0.5, T = 298 K.*

A.2. Electrochemical techniques [52]

A.2.1. Potential sweep techniques and cyclic voltammetry

The electrochemical behaviour of a system can be obtained through a series of steps to different potentials with recording of the current-time curves. Potential sweep techniques, such as cyclic voltammetry, are widely used to determine the kinetic parameters for a large variety of mechanisms. This technique permits to obtain the potentials at which processes occur and to identify the presence of coupled homogeneous reactions. Although better techniques probably exist for the determination of precise kinetic data, cyclic voltammetry is the technique of choice when studying a system for the first time.

Figure 59 shows the potential-time waveforms used for sweep measurements.

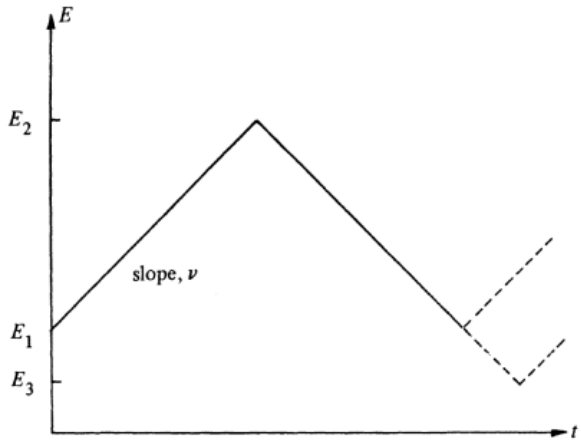

Figure 59: *Potential-time profiles for sweep-voltammetry.*

Cyclic voltammetry (CV) involves sweeping the electrode potential between limits E_1 and E_2 at a known sweep rate, v; on reaching the potential E_2 the sweep is reversed. On again reaching the initial potential, E_1, there are several possibilities. The potential sweep may be halted, again reversed, or alternatively continued further to a value E_3. The linear sweep voltammetry (LSV) involves sweeping the electrode potential between limits E_1 and E_2 at a known sweep rate, v. In both CV and LSV experiments the cell current is recorded as a function of the applied potential. Cyclic voltammetry techniques are used to study a system for the first time: it is usual to start by carrying out qualitative experiments before proceeding to semi-quantitative and finally quantitative ones from which kinetic parameters may be calculated.

Voltammograms are recorded over a wide range of sweep rates and for various values of E_1, E_2 and E_3; observing how peaks appear and disappear as the potential limits and sweep rate are varied it is possible to determine how the processes represented by the peaks are related. At the same time, from the sweep rate dependence of the peak

amplitudes the role of adsorption, diffusion, and coupled homogeneous chemical reactions may be identified.

A.2.2. Reversible reactions

For a simple reversible reaction where only O is initially present in solution

$$O + e^- \leftrightarrow R$$

it is possible to record a voltammogram that appear like a steady-state *I* vs *E* curve when a very slow linear potential sweep is applied to such a system. Figure 60 shows a typical cyclic voltammogram where it is possible observe that the charge associated with the anodic process is low compared to the forward reduction process.

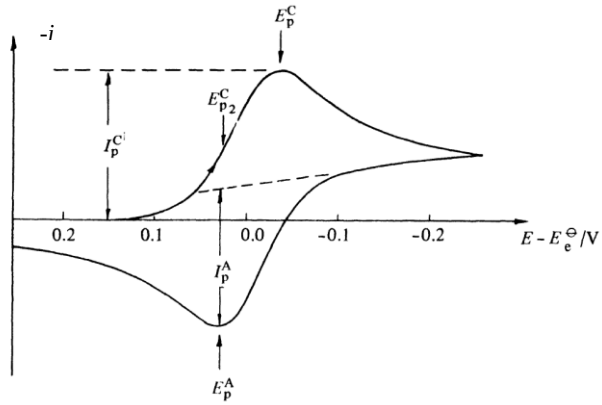

Figure 60: *Cyclic voltammogram for a reversible process; Initially only O is present in solution.*

This is because throughout most of the experiment, there is a concentration difference driving *R* away from the electrode; most of the product, *R*, therefore diffuses into the bulk solution and cannot be reoxidised on the timescale of a cyclic voltammetric experiment.

The peak current density has been found to be proportional to the concentration of electroactive species and to the square roots of the sweep rate and diffusion coefficient for a planar diffusion:

$$i_p = -0.4463\, nF \left(\frac{nF}{RT}\right)^{1/2} c_O^{\infty} D^{1/2} \nu^{1/2}$$

This is called the Randles-Sevčik equation and at 25°C this reduces to the form

$$i_p = -(2.69 \times 10^5) n^{3/2} c_O^{\infty} D^{1/2} \nu^{1/2}$$

where i_p, the peak current density is in A cm^{-2}, D is in cm^2 s^{-1}, ν is in V s^{-1}, and c_O^{∞} is in mol cm^{-3}.

The reversibility of the system can be tested checking whether a plot of i_p as a function of $\nu^{1/2}$ is both linear and passes through the origin (or alternatively whether $i_p/\nu^{1/2}$ is a constant). If this is found to be true further diagnostic tests can be applied, all of which should be satisfied by a reversible system.

The test of reversibility has to be applied over a wide range of sweep rates or false conclusions may be reached. A reversible cyclic voltammogram can only be observed if both *O* and *R* are stable and the kinetics of the electron transfer process are fast so that at all potentials and potential scan rates the electron transfer process on the surface is in equilibrium so that surface concentrations follow the Nernst equation.

The following experimental parameter values can be useful to characterize the cyclic voltammogram of a reversible process at 25°C:

- $\Delta E_p = E_p^A - E_p^C = {}^{59}/_{n}\ mV$
- $\left|E_p - E_{p/2}\right| = {}^{59}/_{n}\ mV$
- $\left|i_p^A / i_p^C\right| = 1$
- $i_p \propto \nu^{1/2}$

- E_p is independent of ν
- At potentials beyond E_p, $i^{-2} \propto t$

A.2.3. Irreversible systems

In the case of the reversible system discussed above, the electron transfer rates at all potentials are significantly greater than the rate of mass transport, and therefore Nernstian equilibrium is always maintained at the electrode surface. When the rate of electron transfer is insufficient to maintain this surface equilibrium then the shape of the cyclic voltammogram changes. For such a system at low potential scan rates the rate of electron transfer is greater than that of mass transfer, and a reversible cyclic voltammogram can be recorded; however, the rate of mass transport increases with increasing scan rates and becomes comparable to the rate of electron transfer leading to increase the peak separation. Furthermore the peak height is slightly reduced from that for a reversible system.

For irreversible systems the peak current density can be calculated by:

$$i_p = -(2.99 \times 10^5) n (\alpha_C n_\alpha)^{1/2} c_O^\infty D_O^{1/2} \nu^{1/2}$$

where n_α is the number of electrons transferred up to, and including, the rate determining step. The peak current density is proportional not only to the concentration and to the square root of the sweep rate, as in the case of reversible system, but also to the square root of the transfer coefficient. For an irreversible system, $E_p{}^c$ is found to vary with the sweep rate as shown below:

$$E_p^C = K - \frac{2.3\ RT}{2\alpha_C n_\alpha F} log\nu$$

where

$$K = E^0 - \frac{RT}{\alpha_C n_\alpha F}\left[0.78 - \frac{2.3}{2} log\left(\frac{\alpha_C n_\alpha F D}{k_0^2 RT}\right)\right]$$

The shape factor $\left|E_p - E_{p/2}\right|$ is different for the irreversible case and is given by

$$\left|E_p - E_{p/2}\right| = \frac{48}{\alpha_C n_\alpha}\, mV\ at\ 25°C$$

From this equation it is possible to estimate the factor $\alpha_C n_\alpha$ required for the estimation of *D* and k^0.

The following experimental parameter values can be useful to characterize the cyclic voltammogram of an irreversible process at 25°C:

- No reverse peak
- $i_p^C \propto \nu^{1/2}$
- E_p^C shifts $-30/\alpha_C n_\alpha\, mV$ for each decade increase in ν
- $\left|E_p - E_{p/2}\right| = 48/\alpha_C n_\alpha\ mV$

A.2.4. Quasi reversible systems

It is quite common for a process that is reversible at low sweep rates to become irreversible at higher ones after having passed through a region known as quasi-reversible at intermediate values. This transition from reversibility occurs when the relative rate of the electron transfer with respect to that of mass transport is insufficient to maintain Nernstian equilibrium at the electrode surface. This change from reversible, to quasi-reversible and finally irreversible behaviour can readily be seen from a plot of i_p as a function of $v^{1/2}$ as shown in Figure 61.

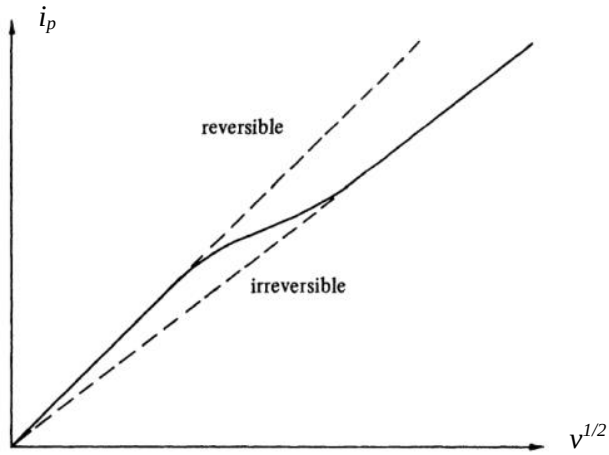

Figure 61: *Plot of the dependence of the peak current density on the square root of the potential sweep rate, showing the transition from reversible to irreversible behaviour with increasing sweep rate* α_c*= 0.5.*

The following experimental parameter values can be useful to characterize the cyclic voltammogram of a quasi-reversible process:

- $|i_p|$ increases with $v^{1/2}$ but is not proportional to it
- $|i_p^A/i_p^C| = 1$ provided $\alpha_A = \alpha_C = 0.5$
- ΔE_p is greater than $59/n$ mV and increases with increasing v
- E_p^C shifts negatively with increasing v

A.3. Potential step techniques [52]

A complete analysis of any electrochemical process requires the identification of all the individual steps and, where possible, their quantification. Such a description requires at least the determination of the standard rate constant, k_0, and the transfer coefficients, α_A and α_C, for the electron transfer step, the determination of the number of electrons involved and of the diffusion coefficients of the oxidised

and reduced species (if they are soluble in either the solution or the electrode).
For an electrode reaction where only *O* is initially present in the solution

$$O + e^- \leftrightarrow R$$

the potential-time profile (Figure 62) can be obtained choosing a potential E_1 such that no reduction of *O*, or indeed any other electrode reaction, occurs.

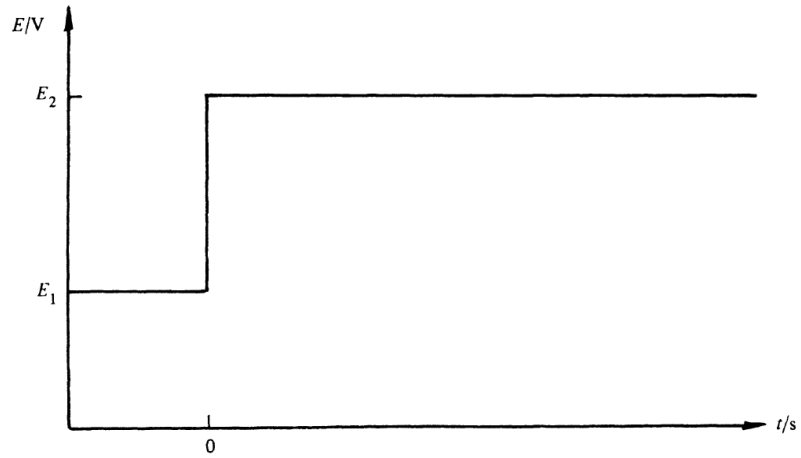

Figure 62: *The potential-time profile for a single potential step chronoamperometric experiment.*

Then at time $t = 0$ the potential is instantaneously changed to a new value E_2, where the reduction of *O* occurs at a diffusion controlled rate. Solving the Fick's 2nd Law with the appropriate boundary conditions for a planar electrode it is possible to obtain the Cottrell equation:

$$|i| = \frac{nFD^{1/2}c_O^{\infty}}{\pi^{1/2}t^{1/2}}$$

It is possible to observe in Figure 63 (curve a) that the current falls as $t^{-1/2}$. A plot of *i* vs $t^{-1/2}$ should therefore be linear and should pass through the origin, and the diffusion coefficient of species *O* can be found from the gradient of the straight line.

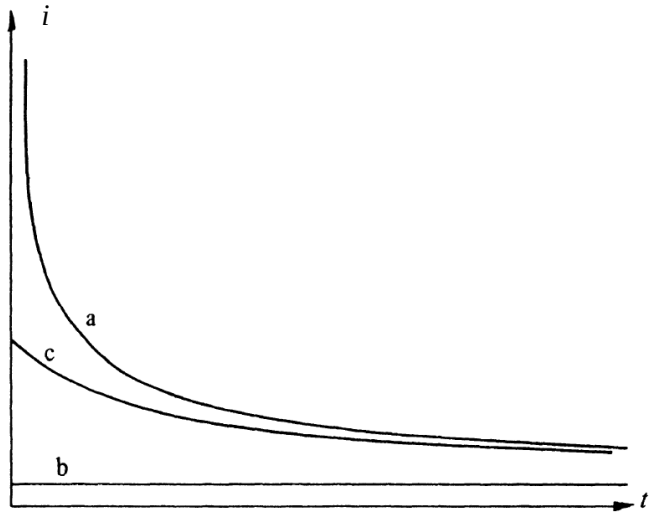

Figure 63: *I-t responses for a potential step experiment. The potential E_2 is chosen so that a: the reaction is diffusion controlled, b: the reaction is kinetically controlled, and c: there is mixed control.*

If the standard rate constant for the reaction described above is very small (or E_2 corresponds to a low overpotential for the reaction), a current time transient of the type shown by curve *b* of Figure 63 will be observed. This is because the surface concentration of *O* does not change significantly (<1%) due to the imposition of the pulse, and therefore diffusion does not play a significant role in determining the rate. The measurement is essentially a steady state one. For the intermediate situation, where the rates of diffusion and electron transfer are comparable, the *i* vs *t* transient has the form shown by curve *c* of Figure 63; the current falls with time but less steeply than for the diffusion controlled case. Under these conditions the system is said to exhibit mixed control.

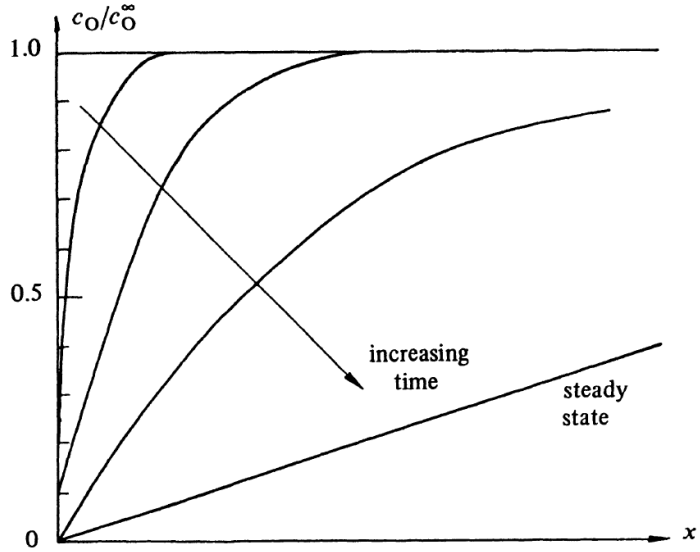

Figure 64: *A schematic diagram of the time evolution of the concentration profiles for a species O undergoing reduction under conditions of mixed control.*

The time evolution of the concentration profile for species *O* under mixed control is shown in Figure 64. The flux of *O* at the surface is simply given by Fick 's 1st Law:

$$J = -D(\partial c_O/\partial x)_{x=0}$$

From Figure 64 it can be seen that this flux is greatest at short times. Indeed at time *t=0,* i.e. immediately after the potential step is applied, the flux would be infinite and therefore the current density at time *t=0* ($i_{t=0}$) would be kinetically controlled, and from its value the rate constant for the electrode reaction could be found. Unfortunately, for a number of reasons, the value of $i_{t=0}$ cannot be directly measured.
Since $i_{t=0}$ cannot be measured directly it is necessary to resort to an extrapolation procedure to obtain its value, and whilst direct extrapolation of an *i* vs *t* transient is occasionally possible, a linear extrapolation is always preferable. In order to see how this should be done we must first solve Fick's 2nd Law for a potential step

experiment under the conditions of mixed control. The differential equations to be solved are

$$\frac{\partial c_O}{\partial t} = D_O \frac{\partial^2 c_O}{\partial x^2}$$
$$\frac{\partial c_R}{\partial t} = D_R \frac{\partial^2 c_R}{\partial x^2}$$

and for the case where both *O* and *R* are present in the solution prepared for the experiment, and the potential is stepped to negative overpotentials, these must be solved subject to specific initial and boundary conditions appropriate to mixed control. It has been found that at short times a plot of i vs $t^{1/2}$ should be a straight line of intercept $i_{t=0}$ given by

$$i_{t=0} = -nF\vec{k}c_O^{\infty}$$

from which the potential dependent rate constant *k* can be obtained.

An analysis of experimental transient data can be made in the following manner: $it^{1/2}$ is first plotted as a function of $t^{1/2}$ as shown in Figure 65.

The horizontal region at large values of $t^{1/2}$ corresponds to the diffusion controlled region, whereas the short time data are affected by kinetics.

With all determinations of reaction kinetics it is usual to perform experiments over a range of potentials, thus obtaining a range of potential dependent rate constants.

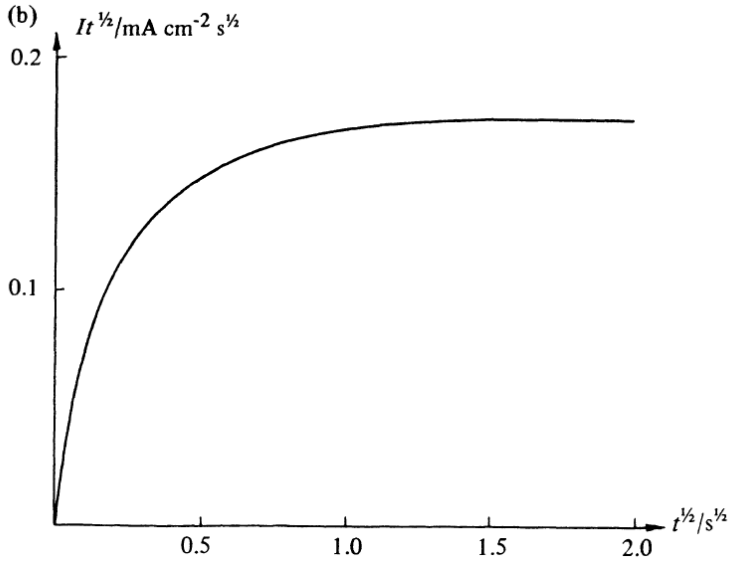

Figure 65: *Analysis of i-t data from a chronoamperometric experiment corresponding to* $\vec{k}$ *= 10^{-2} cm s^{-1}, D = 10^{-5} cm^2 s^{-1}, and* c_O^{∞}*=10^{-6} molcm^{-3}; it$^{1/2}$ plotted as a function of t$^{1/2}$*

$$\vec{k} = k^0 exp\left(-\frac{\alpha_C nF\left(E - E_{eq}^0\right)}{RT}\right)$$

$$\overleftarrow{k} = k^0 exp\left(-\frac{\alpha_A nF\left(E - E_{eq}^0\right)}{RT}\right)$$

Plots of $log\vec{k}$ or $log\overleftarrow{k}$ as a function of *E* should therefore be linear, and from the gradient of these straight lines the values of the transfer coefficient α_A and α_B may be obtained. If $log\vec{k}$ (or $log\overleftarrow{k}$) is not a linear function of *E* it is probable that the reaction mechanism is more complex than had been assumed.

Bibliography

[1] S. Menezes and D. Anderson, «Wavelength-Property Correlation in Electrodeposited Ultrastructured Cu-Ni Multilayers» *Journal of the Electrochemical Society,* p. 440–444, 1990.

[2] B. Huang, K. Ishihara and P. Shingu, «Preparation of high strength bulk nano-scale Fe/Cu multilayers by repeated pressing-rolling» *Journal of Materials Science Letters,* vol. 20, p. 1669–1670, 2001.

[3] A. Misra, M. Verdier, Y. Lu, H. Kung, T. Mitchell, M. Nastasi and J. Embury, «Structure and mechanical properties of Cu-X (X= Nb, Cr, Ni) nanolayered composites» *Scripta Materialia,* vol. 39, pp. 555-560, 1998.

[4] M. Demkowicz and R. Hoagland, «Structure of Kurdjumov–Sachs interfaces in simulations of a copper–niobium bilayer» *Journal of Nuclear Materials,* vol. 372, pp. 45-52, 2008.

[5] T. Hochbauer, A. Misra, K. Hattar and R. Hoagland, «Influence of interfaces on the storage of ion-implanted He in multilayered metallic Composites» *Journal of Applied Physics,* vol. 98, pp. 123516-123517, 2005.

[6] H. L. Chum, V. R. Koch, L. L. Miller and R. A. Osteryoung, «An Electrochemical Scrutiny of Organometallic Iron Complexes and Hexamethylbenzene in a Room Temperature Molten Salt» *Journal of the American Chemical Society,* vol. 97, pp. 3264-3265, 1975.

[7] J. Robinson and R. A. Osteryoung, «An electrochemical and spectroscopic study of some aromatic hydrocarbons in the room temperature molten salt system aluminum chloride-n-butylpyridinium chloride» *Journal of the American Chemical Society,* vol. 101, pp. 323-327, 1979.

[8] T. B. Scheffler, C. L. Hussey, K. R. Seddon, C. M. Kear and P. D. Armitage, «Molybdenum chloro complexes in room-temperature chloroaluminate ionic liquids: stabilization of hexachloromolybdate(2-) and hexachloromolybdate(3-)» *Inorganic Chemistry,* vol. 22, pp. 2099-2100, 1983.

[9] D. Appleby, C. L. Hussey, K. R. Seddon and J. E. Turp, «Room-temperature ionic liquids as solvents for electronic absorption spectroscopy of halide complexes» *Nature,* vol. 323, pp. 614-616, 1986.

[10] C. L. Hussey, «Room-temperature molten salt systems,» *Advances in Molten Salt Chemistry,* vol. 5, pp. 185-229, 1983.

[11] J. S. Wilkes and M. J. Zaworotko, «Air and water stable 1-ethyl-3-methylimidazolium based ionic liquids» *Journal of the Chemical Society, Chemical Communications,* vol. 14, pp. 965-967, 1992.

[12] D. R. MacFarlane, P. Meakin, J. Sun, N. Amini and M. Forsyth, «Pyrrolidinium Imides: A New Family of Molten Salts and Conductive Plastic Crystal Phases» *The Journal of Physical Chemistry B,* vol. 103, pp. 4164-4170, 1999.

[13] M. Gaune-Escard and K. R. Seddon, Molten Salts and Ionic Liquids: Never the Twain?, John Wiley & Sons, 2010.

[14] F. Endres and S. Zein El Abedin, «Air and water stable ionic liquids in physical chemistry» *Physical Chemistry Chemical Physics,* vol. 8, pp. 2101-2116, 2006.

[15] F. H. Hurley and T. Wler Jr., «The Electrodeposition of Aluminum from Nonaqueous Solutions at Room Temperature» *Journal of the Electrochemical Society,* vol. 98, pp. 207-212, 1951.

[16] O. Hiroyuki, Electrochemical Aspects, Hoboken, New Jersey: John Wiley & Sons, Inc., 2005.

[17] F. Endres, «Ionic Liquids: Solvents for the Electrodeposition of Metals and Semiconductors» *A European journal of Chemical Physics and Physical Chemistry,* vol. 3, p. 144–154, 2002.

[18] A. Abbott and K.J. McKenzie, «Application of ionic liquids to the electrodeposition of metals» *Physical Chemistry Chemical Physics,* vol. 8, pp. 4265-4279, 2006.

[19] S. Majumdar, P. Sengupta, G. Kale and I. Sharma, «Development of multilayer oxidation resistant coatings on niobium and tantalum» *Surface & Coatings Technology,* vol. 200, pp. 3713-3718, 2006.

[20] M. Zhang, Y. Zhang, P. Rack, M. Miller and T. Nieh, «Nanocrystalline tetragonal tantalum thin films» *Scripta Materialia,* vol. 57, p. 1032–1035, 2007.

[21] N. Borisenko, A. Ispas, E. Zschippang, Q. Liu, S. Zein El Abedin, A. Bund and F. Endres, «In situ STM and EQCM studies of tantalum electrodeposition from TaF_5 in the air- and water-stable ionic liquid 1-butyl-1-methylpyrrolidinium

bis(trifluoromethylsulfonyl)amide» *Electrochimica Acta* , vol. 54, pp. 122-128, 2009.

[22] V. Grinevitch, S. Kuznetsov, A. Arakcheeva, T. Olyunina, A. Schonleber and M. Gaune-Escard, «Electrode and chemical reactions during electrodeposition of tantalum products in CsCl melt» *Electrochimica Acta,* vol. 51, pp. 6563-6571, 2006.

[23] A. Jiang, T. A. Tyson and L. Axe, «The stability of the β phase of tantalum: a molecular dynamics study» *Journal of Physics: Condensed Matter* , vol. 17, pp. 1841-1850. , 2005.

[24] L. Gladczuk, A. Patel, C. Paur and M. Sosnowski, «Tantalum films for protective coatings of steel,» *Thin solid films,* vol. 467, pp. 150-157, 2004.

[25] H. Li, H. Nersisyan, K. Park, S. Park, J. Kim, J. Lee and J.H. Lee, «Nuclear-grade zirconium prepared by combining combustion synthesis with molten-salt electrorefining technique» *Journal of Nuclear Materials,* vol. 413, pp. 107-113, 2001.

[26] S. Senderoff and G. W. Mellors, «Coherent Coatings of Refractory Metal» *Science,* vol. 153, pp. 1475-1481, 1966.

[27] D. Inman and S.H. White, «The production of refractory metals by the electrolysis of molten salts; design factors and limitations» *Journal of applied electrochemistry,* vol. 8, pp. 375-390, 1978.

[28] A. Girginov, T. Tzvetkoff and M. Bojinov, «Electrodeposition of refractory metals (Ti, Zr, Nb, Ta) from molten salts electrolytes» *Journal of applied electrochemistry,* vol. 25, pp. 993-1003, 1995.

[29] S. Senderoff, G. Mellors and W. Reinhart, «The electrodeposition of coherent deposits of refractory metals» *Journal of Electrochemical Society,* vol. 112, pp. 840-845, 1965.

[30] V. Van, J. Madejovà, A. Silny and V. Danek, «Niobium Complexes in Fluoride Melts» *Chemical Papers,* vol. 54, pp. 137-143, 2000.

[31] B. Gillesberg, J. Von Barner, N. Bjerrum and F. Lantelme, «Niobium plating processes in alkali chloride melts» *Journal of Applied Electrochemistry,* vol. 29, pp. 939-949, 1999.

[32] L. Polyakova, E. Polyakov, F. Matthiesen, E. Christensen and N. Bjerrum, «Electrochemical study of tantalum in fluoride and oxofluoride melts» *Journal of Electrochemical Society,* vol. 141, pp. 2982-2988, 1994.

[33] P. Chamelot, P. Palau, L. Massot, A. Savall and P. Taxil, « Electrodeposition processes of tantalum(V) species in molten fluorides containing oxide ions» *Electrochimica Acta,* vol. 47, pp. 3423-3429, 2002.

[34] C. Guang-Sen, M. Okido and T. Oki, «Electrochemical studies of zirconium and hafnium in alkali chloride and alkali fluoride-chloride molten salts» *Journal of applied electrochemistry,* vol. 20, pp. 77-84, 1990.

[35] M. Kawase and Y. Ito, «The electroformation of Zr metal, Zr–Al alloy and carbon films on ceramic» *Journal of applied electrochemistry,* vol. 33, pp. 785-793, 2003.

[36] Z. Chen, Y. Li and S. Li, «Electrochemical behavior of zirconium in the LiCl–KCl molten salt at Mo electrode»

Journal of Alloys and Compounds, vol. 509, pp. 5958-5961, 2011.

[37] Y. Wu, Z. Xu, S. Chen, L. Wang and G. Li, «Electrochemical behavior of zirconium in molten NaCl-KCl-K_2ZrF_6 system» *Rare Metals,* vol. 30, pp. 8-13, 2011.

[38] H. Groult, A. Barhoun, H. El Gallali, S. Borensztjan and F. Lantelme, «Study of the electrochemical reduction of Zr^{4+} ions in molten alkali fluorides» *Journal of Electrochemical Society,* vol. 155, pp. 19-25, 2008.

[39] M. Gibilaro, L. Massot, P. Chamelot, L. Cassayre and P. Taxil, «Investigation of Zr(IV) in LiF–CaF_2: Stability with oxide ions and electroreduction pathway on inert and reactive electrodes» *Electrochimica Acta,* vol. 95, pp. 185-191, 2013.

[40] O. Babushkina, E. O. Lomako and W. Freyland, «Electrochemistry and Raman spectroscopy of niobium reduction in basic and acidic pyrrolidinium based ionic liquids. Part I: 1-Butyl-1-methylpyrrolidinium chloride with $NbCl_5$» *Electrochimica Acta,* vol. 62, p. 234–241, 2012.

[41] S. Zein El Abedin, H. Farag, E. Moustafa, U. Welz-Biermann and F. Endres, «Electroreduction of tantalum fluoride in a room temperature ionic liquid at variable temperatures» *Physical Chemistry Chemical Physics,* vol. 7, pp. 2333-2339, 2005.

[42] O. B. Babushkina and S. Ekres, «Spectroscopic study of the electrochemical behaviour of tantalum(V) chloride and oxochloride species in 1-butyl-1-methylpyrrolidinium chloride» *Electrochimica Acta,* vol. 56, pp. 867-877, 2010.

[43] T. Tsuda, C. Hussey, G. Stafford and O. Kongstein, «Electrodeposition of Al-Zr alloys from lewis acidic aluminum

chloride-1-ethyl-3-methylimidazolium chloride melt» *Journal of the electrochemical society,* vol. 151, pp. 447-454, 2004.

[44] C. Fu, L. Aldous, N. Manan and R. Compton, «Electrochemistry of zirconium tetrachloride in the ionic liquid N-butyl-N-methylpyrrolidinium bis(trifluoromethylsulfonyl) imide: formation of Zr(III) and exploitation of $ZrCl_4$ as a facile ionic liquid drying agent» *Electroanalysis,* vol. 24, pp. 210-213, 2012.

[45] L. Lutterotti, R. Ceccato, R. Dal Maschio and E. Pagani, «Quantitative analysis of silicate glass in ceramic materials» *Materials Science Forum,* vol. 87, pp. 278-281, 1998.

[46] S. Kuznetsov, «Electrochemistry of refractory metals in molten salts: Application for the creation of new and functional materials» *Pure and Applied Chemistry,* vol. 81, p. 1423–1439, 2009.

[47] F. Lantelme, A. Salmi, B. Coffin, J. Claverie and. Y. Le Petitcorps, «Electrochemical deposition of niobium on vitreous carbon and silicon carbide fibres in fused alkali chlorides» *Materials science & engineering. B, Solid-state materials for advanced technology,* vol. 39, pp. 202-207, 1996.

[48] J. Von Barner, E. Christensen, N. Bjerrum and B. Gilbert, «Vibrational spectra of niobium(V) fluoro and oxo fluoro complexes formed in alkali-metal fluoride melts» *Inorganic Chemistry,* vol. 30, pp. 561-566, 1991.

[49] Z. Alimova, E. Polyakov, L. Polyakova and V. Kremenetskiy, «The role of fluoride ions in reduction-oxidation equilibria in

CsCl-KCl-NaCl-K_2NbF_7 melts» *Journal of Fluorine Chemistry*, vol. 59, p. 203–210, 1992.

[50] S. Zein El Abedin and F. Endres, «Ionic liquids: the link to high-temperature molten salts?» *Accounts of Chemical Research*, vol. 40, pp. 1106-1113, 2007.

[51] A. Ispas, B. Adolphi, A. Bund and F. Endres, «On the electrodeposition of tantalum from three different Ionic Liquids with the bis(trifluoromethyl sulfonyl) amide ion» *Physical Chemistry Chemical Physics*, vol. 12, pp. 1793 -1803, 2010.

[52] D. Pletcher, R. Greff, R. Peat, L. Peter and J. Robinson, Instrumental Methods in Electrochemistry, Cambridge: Woodhead Publishing, 2001.

[53] A. Bard and L. Faulkner, Electrochemical methods, Hoboken: John Wiley & Sons, 2001.

[54] S. Randstrom, G. Appetecchi, C. Lagergren, A. Moreno and S. Passerini, «The influence of air and its components on the cathodic stability of N-butyl-N-methylpyrrolidinium bis(trifluoromethanesulfonyl)imide» *Electrochimica Acta* , vol. 53, pp. 1837-1842, 2007.

[55] R. Randstrom, M. Montanino, G. Appetecchi, C. Lagergren, A. Moreno and S. Passerini, «Effect of water and oxygen traces on the cathodic stability of N-alkyl-N-methylpyrrolidinium bis(trifluoromethanesulfonyl)imide» *Electrochimica Acta*, vol. 53, pp. 6397-64, 2008.

[56] M. Eshed, S. Pol, A. Gedanken and M. Balasubramanian, «Zirconium nanoparticles prepared by the reduction of

zirconium oxide using the RAPET method» *Beilstein Journal of Nanotechnology,* vol. 2, p. 198–203, 2011.

[57] Z. Chen, Y. Li and S. Li, «Electrochemical behavior of zirconium in the LiCl–KCl molten salt at Mo electrode» *Journal of Alloys and Compounds* , vol. 509, pp. 5958-5961, 2011.

[58] Y. Wu, Z. Xu, S. Chen, L. Wang and G. Li, «Electrochemical behavior of zirconium in molten NaCl-KCl-K_2ZrF_6 system» *Rare Metals* , vol. 30, pp. 8-13, 2011.

[59] M. Druschler, N. Borisenko, J. Wallauer, C. Winter, B. Huber, F. Endres and B. Roling, «New insights into the interface between a single-crystalline metal electrode and an extremely pure ionic liquid: slow interfacial processes and the influence of temperature on interfacial dynamics» *Physical Chemistry Chemical Physics,* vol. 14, pp. 5090-5099, 2012.

[60] S. Zein El Abedin, A. Saad, H. Farag, N. Borisenko, Q. Liu and F. Endres, «Electrodeposition of selenium, indium and copper in an air- and water-stable ionic liquid at variable temperatures,» *Electrochimica Acta,* vol. 52, pp. 2746-2754, 2007.

[61] P. Chen and I. Sun, «Electrochemical study of copper in a basic 1-ethyl-3 methylimidazolium tetrafluoroborate room temperature molten salt» *Electrochimica Acta,* vol. 45, pp. 441-450, 1999.

[62] K. Murase, K. Nitta, T. Hyrato and Y. Awakura, «Electrochemical behaviour of copper in trimethyl-n-hexylammonium bis((trifluoromethyl)sulfonyl)amide, an

ammonium imide-type room temperature molten salt» *Journal Applied Electrochemistry,* vol. 31, pp. 1089-1094, 2001.

[63] A. Ismail, S. Zein El Abedin, O. Höfft and F. Endres, «Unexpected decomposition of the bis (trifluoromethylsulfonyl) amide anion during electrochemical copper oxidation in an ionic liquid» *Electrochemistry Communications* , vol. 12, pp. 909-911, 2010.

[64] A. Misra, M. Verdier, Y. Lu, H. Kung, T. Mitchell, M. Nastasi and J. Embury, «Structure and mechanical properties of Cu-X (X = Nb,Cr,Ni) nanolayered composites,» *Scripta Materialia,* vol. 39, p. 555–560, 1998.

[65] M. Wei, Z. Cao, J. Shi, G. Pan, L. Xu and X. Meng, «Anomalous plastic deformation in nanoscale Cu/Ta multilayers» *Materials Science & Engineering A,* vol. 598, p. 355–359, 2014.

[66] C. Guang-Sen, M. Okido and T. Oki, «Electrochemical studies of zirconium and hafnium in alkali chloride and alkali fluoride-chloride molten salts,» *Journal of applied electrochemistry,* vol. 20, pp. 77-84, 1990.

[67] P. Chen and I. Sun, «Electrochemical study of copper in a basic 1-ethyl-3 methylimidazolium tetrafluoroborate room temperature molten salt» *Electrochimica Acta,* vol. 45, pp. 441-450, 1999.

Table of symbols

Roman symbols

A	Surface area	cm^2
c_i^{∞}	Concentration of the species *i* in the bulk solution	mol cm^{-3}
c_i^{σ}	Concentration of the species *i* at the electrode surface	mol cm^{-3}
C_{dl}	Double layer capacitance	F cm^{-2}
D	Diffusion coefficient	cm^2 s^{-1}
E	Potential of an electrode vs a reference	V
E^0	Standard potential	V
E_{eq}	Equilibrium potential	V
F	Faraday's constant	C mol^{-1}
i	Current density	A cm^{-2}
i_0	Exchange current density	A cm^{-2}
i_p	Peak current density	A cm^{-2}
I	Current intensity	A
I(Q)	Scattered intensity	-
J_i	Flux of species i	mol cm^{-2} s^{-1}
k	Rate constant for a chemical reaction	cm s^{-1}

k_0	Standard rate constant	cm s^{-1}
K	Equilibrium constant	
m	Moles of electroactive species in electrolysis cell	mol
M	Molar	mol/L
n	Electron numbers	-
Q	Charge	C
Q	Scattered wave vector	-
R	Gas constant	J mol^{-1} K^{-1}
R	Resistance	Ω
t	Time	s
T	Absolute temperature	K
x	Distance perpendicular to the electrode surface	cm

Greek symbols

α	Transfer coefficient	-
η	Overpotential	V
θ	Scattering angle	°
λ	X-ray wave length	-
ν	Potential scan rate	V s^{-1}
τ	Transition time	s

Acronims

Ag	Silver
AgCl	Silver chloride
Al	Aluminium
$AlCl_3$:	Aluminium chloride
Au(111)	Monocrystalline gold
BDD	Boron Doped Diamond
[BMP] [TFSA]	1-butyl-1-methylpyrrolidinium bis(trifluoromethylsulfonyl)imide
C	Carbon
CaF_2	Calcium fluoride
Cu	Copper
CuF_2	Copper(II) fluoride
CV	Cyclic Voltammetry
EDX	Energy Dispersive X-ray
F	Fluorine
F^-	Fluoride ion
FIB	Focused ion beam
FLINAK	Eutectic mixture of LiF-NaF-KF
IHP	Inner Helmholtz Plane
IL	Ionic Liquid
IPE	Ideal Polarized Electrode
K^+	Potassium ion
KCl	Potassium chloride

KF	Potassium fluoride
K_2NbF_7	Potassium heptafluoroniobate
K_2TaF_7	Potassium heptafluorotantalate
K_2ZrF_6	Potassium hexafluorozirconate
Li^+	Lithium ion
LiCl	Lithium chloride
LiF	Lithium fluoride
LSV	Linear Sweep Voltammetry
Na^+	Sodium ion
NaCl	Sodium chloride
NaF	Sodium fluoride
Nb	Niobium
NbC	Niobium carbide
Nb_2C	Niobium carbide
Nb_6C_5	Niobium carbide
$NbCl_5$	Niobium(V) chloride
NbF_5	Niobium(V) fluoride
NbF_7^{2-}	Heptafluoroniobate anion
NbF_7^{3-}	Heptafluoroniobate anion
Ni	Nickel
O	Oxygen
OCP	Open circuit potential
OHP	Outer Helmholtz Plane
ppm	parts per million

Pt	Platinum
[Py1,4] TFSA	1-butyl-1-methylpyrrolidinium bis(trifluoromethylsulfonyl)imide
Pyr_{14} Cl	1-butyl-1-methylpyrrolidinium chloride
R.T.	Room temperature
RTIL	Room Temperature Ionic Liquid
S	Sulphur
Se	Selenium
SEM	Scanning Electron Microscopy
Si/BDD	Silicon coated with boron doped diamond
Ta	Tantalum
TaF_3	Tantalum(III) fluoride
TaF_5	Tantalum(V) fluoride
TaF_7^{2-}	Heptafluorotantalate anion
Ti	Titanium
V	Vanadium
XRD	X-ray diffraction
Zr	Zirconium
$ZrCl_3$	Zirconium(III) chloride
ZrCl4	Zirconium(IV) chloride
$ZrCl_2O$	Zirconium chloride oxide
ZrF_4	Zirconium(IV) fluoride

List of figures[1]

[1] **a** Figures from "On the Electrodeposition of Niobium from 1-Butyl-1-Methylpyrrolidinium Bis(trifluoromethylsulfonyl)imide at Conductive Diamond Substrates", Electrocatalysis (2014) 5: 16-22, Permission requested.

b Figures from Electrochemical deposition of Cu and Nb from pyrrolidinium based ionic liquid, Thin solid films (2014) 571: 325-331, Permission requested.